MODERN LASER PHYSICS AND LASER-INFORMATION TECHNOLOGIES FOR SCIENCE AND MANUFACTURE

1st INTERNATIONAL RUSSIAN-CHINESE CONFERENCE / YOUTH SCHOOL-WORKSHOP

September 23 – 28, 2011

Suzdal / Vladimir (Russia)

Program

Book of Abstracts

Министерство образования и науки Российской Федерации

Государственное образовательное учреждение
высшего профессионального образования
«Владимирский государственный университет
имени Александра Григорьевича и Николая Григорьевича Столетовых»

СОВРЕМЕННЫЕ ЛАЗЕРНАЯ ФИЗИКА И ЛАЗЕРНЫЕ ИНФОРМАЦИОННЫЕ ТЕХНОЛОГИИ ДЛЯ НАУКИ И ПРОИЗВОДСТВА

(MODERN LASER PHYSICS AND LASER-INFORMATION TECHNOLOGIES FOR SCIENCE AND MANUFACTURE)

ПРОГРАММА И ТЕЗИСЫ ДОКЛАДОВ ПЕРВОЙ МЕЖДУНАРОДНОЙ РОССИЙСКО-КИТАЙСКОЙ КОНФЕРЕНЦИИ / МОЛОДЁЖНОЙ ШКОЛЫ-СЕМИНАРА

23 – 28 сентября 2011 г.
Суздаль / Владимир

Владимир 2011

УДК 535.14:621.373.826:681.7
ББК 22.34
С56

Редакционная коллегия:
С.М. Аракелян (ответственный редактор) – доктор физ.-мат. наук, профессор
А.П. Алоджанц – доктор физ.-мат. наук
А.О. Кучерик – кандидат физ.-мат. наук
А.Ю. Лексин – кандидат физ.-мат. наук, доцент
А.В. Осипов

Сборник содержит программу и тезисы докладов участников Первой международной Российско-Китайской конференции / молодёжной школы-семинара "Современные лазерная физика и лазерные информационные технологии для науки и производства" (Суздаль/Владимир, 23-28 сентября 2011 г.). Представлены результаты теоретических работ и практических приложений лазеров в различных областях науки и промышленности. Работы выполнены как ведущими учеными, так и молодыми научными сотрудниками, аспирантами, студентами. Конференция поддержана Российским фондом фундаментальных исследований (грант №11-02-06143-г) и ФЦП «Научные и научно-педагогические кадры инновационной России (2009-2013 годы)» (госконтракт №14.741.12.0184).

ISBN 978-5-9984-0215-9

© Владимирский государственный университет, 2011

MODERN LASER PHYSICS AND LASER-INFORMATION TECHNOLOGIES FOR SCIENCE AND MANUFACTURE

1st INTERNATIONAL RUSSIAN-CHINESE CONFERENCE / YOUTH SCHOOL-WORKSHOP

September 23 – 28, 2011, Suzdal / Vladimir (Russia)

СОВРЕМЕННЫЕ ЛАЗЕРНАЯ ФИЗИКА И ЛАЗЕРНЫЕ ИНФОРМАЦИОННЫЕ ТЕХНОЛОГИИ ДЛЯ НАУКИ И ПРОИЗВОДСТВА

ПЕРВАЯ МЕЖДУНАРОДНАЯ РОССИЙСКО-КИТАЙСКАЯ КОНФЕРЕНЦИЯ / МОЛОДЁЖНАЯ ШКОЛА-СЕМИНАР

23 – 28 сентября 2011 г., Суздаль / Владимир

第一届中俄国际会议/青年暑期论坛

用于科学研究与制造业的现代激光物理和激光信息技术

2011年 9月 23日 – 28日， 俄罗斯，弗拉基米尔-苏兹达里

SPONSORED BY

Ministry of Education & Science
of the Russian Federation

Russian Academy of Sciences

Chinese Academy of Sciences

Russian Foundation for Basic Research

National Natural Science Foundation of China

NT-MDT Co.

Avesta Ltd.

Nankai University

INFORMATION SPONSOR

“Poisk”, The Newspaper of Scientific Community

Program

ORGANIZERS

M.V. Lomonosov Moscow State University, Moscow

Institute on Laser and Information Technologies, RAS, Shatura, Moscow Region

Institute of Laser Physics, the RAS Siberian Branch, Novosibirsk

Institute of Spectroscopy, RAS, Troitsk, Moscow Region,

A.G. & N.G. Stoletovs Vladimir State University, Vladimir

Tianjin University, Tianjin

Nankai University, Tianjin

Shandong University, Jinan

Technical Institute of Physics and Chemistry, Beijing

Shanghai Institute of Ceramics, Shanghai

South China University of Technology

Guangzhou Research Institute of Non-Ferrous Metals.

SUPPORTED BY

Ministry of Education and Science of the Russian Federation

Russian Academy of Sciences

Russian Foundation for Basic Research

Chinese Academy of Sciences

National Natural Science Foundation of China

Nankai University, Tianjin.

CO-CHAIRS OF THE CONFERENCE

Sergey N. Bagayev, *RAS Academician, Director of SB RAS Institute of Laser Physics*

Vladislav Ya. Panchenko, *RAS Academician, Director of RAS Institute on Laser and Information Technologies*

Jianquan Yao, *CASS Academician, Tianjin University*

ORGANIZING COMMITTEE CHAIR

Valentin V. Morozov, *Professor, Rector of A.G. & N.G. Stoletovs Vladimir State University*

PROGRAM COMMITTEE

Sergey N. Bagayev, *Academician, Institute of Laser Physics, SB RAS*

Vladislav Ya. Panchenko, *Academician, Institute on Laser and Information Technologies, RAS*

Yevgeniy A. Vinogradov, *Institute of Spectroscopy, RAS*

Ivan A. Shcherbakov, *A.M. Prokhorov Institute of General Physics of RAS*

Vladimir A. Makarov, *International Laser Center, M.V.Lomonosov Moscow State University*

Sergey M. Arakelyan, *A.G. & N.G. Stoletovs Vladimir State University*

Alexander P. Alodjants, *A.G. & N.G. Stoletovs Vladimir State University*

Sergei V. Garnov, *A.M. Prokhorov Institute of General Physics of RAS*

Valery G. Prokoshev, *A.G. & N.G. Stoletovs Vladimir State University*

Victor N. Zadkov, *Department of Physics, M.V.Lomonosov Moscow State University*

Jianquan Yao, *Academician, Tianjin University, Tianjin*

Huitian Wang, *Nankai University, Tianjin*

Feng Song, *Nankai University, Tianjin*

Huaijin Zhang, *Shandong University, Jinan*

Zhaojun Liu, *Shandong University, Jinan*

Qinjun Peng, *Technical Institute of Physics and Chemistry, Beijin*

Zhiming Wang, *Technical Institute of Physics and Chemistry, Beijin*

Yubai Pan, *Shanghai Institute of Ceramics, Shanghai*

Prof. Jun Xu, *Shanghai Institute for Ceramics, Shanghai*

Prof. Yang Yongqiang, *Institute of Welding Technology, Guangdong General Reseach Institute for Industrial Technology*

Prof. Qiu Xianyang, *Guangzhou Research Institute of Non-ferrous Metals*

CONTACTS

Prof. Sergey Arakelyan,
Vice-chair of the Organizing Committee,

A.G. & N.G. Stoletovs Vladimir State University,
Gorky str., 87, Vladimir 600000, Russia
Ph./fax: (4922)533358, fax: (4922) 333369
e-mail: arak@vlsu.ru, laser@vlsu.ru

Dr. Alexey Kucherik,
Scientific Secretary of the Orginizing Committee

A.G. & N.G. Stoletovs Vladimir State University,
Gorky str., 87, Vladimir 600000, Russia
Ph./fax: (4922)479621, fax: (4922) 333369
e-mail: kucherik@vlsu.ru, laser@vlsu.ru

GOAL OF THE CONFERENCE

The Conference is aimed at involvement of young scientists (students, post-graduates, post-docs) in discussing pressing problems in the fields of laser physics and its applications, as well as in establishing contacts between participants from Russia and China, having common interests in research and innovations.

SCOPE OF THE CONFERENCE

- Nano- and femto-photonics: Foundations and applications
- Quantum and atom optics; quantum information science
- Physics of terahertz radiation: Generation and future applications
- Modern tendency and advantages in solid-state lasers and laser systems: development in new laser and nonlinear optical crystals
- New laser technologies in biomedicine, ecology and industry: Bio- imaging, laser-plasma technologies, laser prototyping, etc.
- Laser-information systems: Big machines and mobile/space, atmospheric-, water- and land-based systems.

FORMAT OF THE CONFERENCE

Participation of the leading Russian and Chinese scientists who will deliver lectures for the participants.

Official language of the Conference is English.

Supported by grant #11-02-06143-г of the Russian Foundation for Basic Research and by Federal Special-Purpose Program "Scientific and scientific-padagogical personnel of innovative Russia (2009-2013)".

LOCATION

Suzdal and Vladimir are the oldest Russian towns, located in the very center of the European part of the country, in the Heart of Golden Ring of Russia.

Vladimir (180 km Easter from Moscow) was founded in the Xth century by Saint Vladimir on the high bank of the Klyazma river. Its history is rich in great and tragic periods of Russia. Vladimir was the capital of Northern-East Russia and the main Russian town in XII-XIIIth centuries. In the XIII century it was destroyed by the hordes of Mongols. Nevertheless, it held the leadership among Russian towns and remained as the cultural and spiritual center of Russia until the end of XIVth century when the Moscow tzars united the Russian lands. Nowadays, it is a beautiful green town, where the modern buildings are adjacent to the pearls of ancient Russian architecture.

Suzdal is a wonderful ancient Russian town with fantastic architectural monuments of the past, located in the Golden Ring area north from Vladimir (30 km). In the XII-XIVth centuries Suzdal was one of the most powerful towns of the ancient Russ. In Suzdal/Vladimir, and in the neighboring territories an architectural style that is characterized by sophisticated proportions and fine design of facades with the arc belt was established. The major monuments representing this architectural style are still with us.

Central part of Vladimir

Suzdal

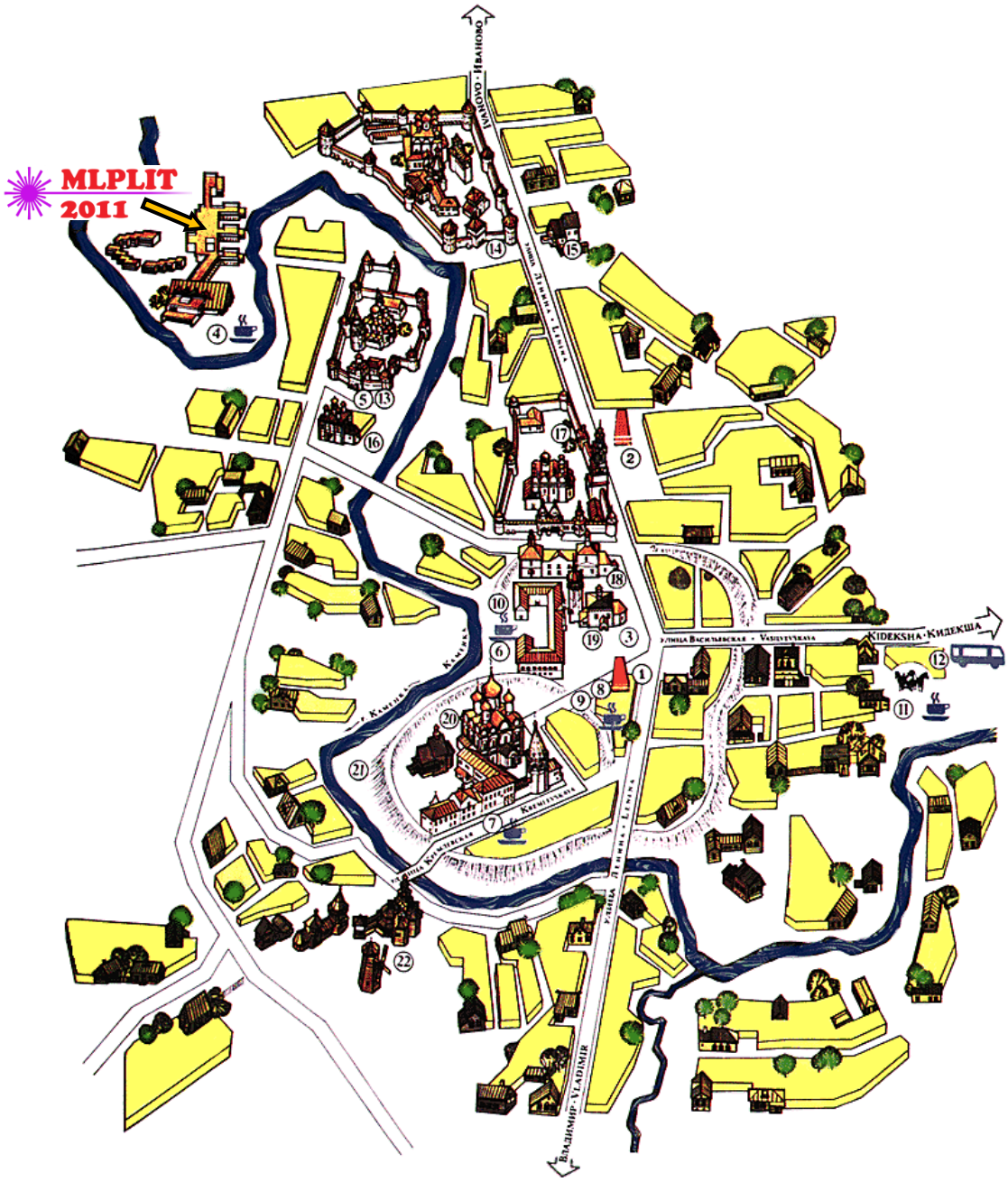

2. Suzdal City Council, Lenin monument
3. Monument to those fallen in World War II
4. Suzdal Tourist Centre. Hotel, motel, restaurant
5. Hotel on the grounds of the former Convent of the Intercession. The former convent refectory houses the restaurant Trapeznaya
6. Restaurant Gostiny Dvor
7. Restaurant Trapeznaya in Suzdal Kremlin
8. Restaurant Pogrebok (cellar)
9. Souvenirs' store Suzdalskaya Lavka
10. Arcade of shops (19th century)
11. Coachman's Inn
12. Bus station
13. The Convent of the Intercession (16th-18th cent.) Expositions: "From the History of the Convent", "Articles of Needlework", "Interior of the 17th-century Chancellor's House"
14. The Spaso-Yevfimievsky Monastery (16th-17th cent.) Museum of the Amateur Works of Art of the Peoples of the Russian Federation. Exposition: Gold Treasure Trove
15. The 17th-century townsman' house. The Interiors of Living Home Exposition.
16. The Church of St Peter and St Paul (17th century) Wood Painting Exposition
17. The Monastery of the Deposition of the Robe (16th-19th cent.)
18. The Church of St Nicholas and the Holy Cross (18th century). Peasant Clothing Exhibition
19. The Church of the Resurrection (18th century) Exposition: Folk Wood Carving
20. Suzdal Kremlin (13th-18th cent.). Expositions: "Leninist Policy of Protecting the Monuments of History and Culture", "Early Russian Painting", "The Cross Chamber Interior"
21. The earthen rampart surrounding the Kremlin (12th cent.)
22. The open-air Museum of Wooden Architecture and Peasants' Everyday Life.

AGENDA OF THE CONFERENCE

- **Plenary Session Topics (60 min)**
  - **S1.** Nano- and Femtophotonics: Foundations and Applications
  - **S2.** Nonlinear and Atom Optics; High Precision Measurements and Quantum Information Science
  - **S3.** Physics of Terahertz Radiation: Generation and Future Applications
  - **S4.** Modern tendency and Advantages in Lasers; Development in New Laser Materials
  - **S5.** New Laser Technologies in Biomedicine, Ecology and Industry: Bio- imaging, Laser-plasma technologies, Laser Prototyping, etc.
- **Keynote talks (45 min)**
- **Oral talks (30 min)**
- **Oral talks – Young scientists (20 min)**
- **Posters**

September 22, Thursday
(Suzdal Tourist Center)

	Arrival to Suzdal. **Accomodation in the Suzdal Tourist Center**

September 23, Friday
(Suzdal Tourist Center)

09.00 – 10.30	**Registration**
10.30 – 11.00	**Opening Ceremony**
Chairmen: I.A. Shcherbakov / Feng Song	
11.00 – 12.00	***S3. Jianquan Yao,*** *Tianjin University*
12.00 – 13.00	***S2. S.N. Bagayev,*** *Institute of Laser Physics, SB RAS, Novosibirsk*
13.15 – 14.30	**LUNCH**
Chairmen: S.N. Bagayev / Lianhui Wang	
14.30 – 15.30	***S5. V.Ya.Panchenko,*** *Institute on Laser and Information Technologies, RAS, Shatura, Moscow Region*
15.30 – 16.30	***S5. Feng Song,*** *Nankai University, Tianjin*
16.30 – 17.00	**COFFEE BREAK**
Chairmen: V.Ya. Panchenko / Jianquan Yao	
17.00 – 18.00	***S2. V.A. Makarov,*** *International Laser Center, M.V.Lomonosov Moscow State University*
18.30 – 21.00	**WELCOME PARTY**

September 24, Saturday
(Suzdal Tourist Center)

Chairmen: T.A. Vartanyan / Wei Huang

09.00 – 10.00	***S2. V.I. Balykin,*** *Institute of Spectroscopy, RAS, Troitsk, Moscow Region*
10.00 – 11.00	***S5. Lianhui Wang,*** *Institute of Advanced Materials, Nanjing University of Posts and Telecommunications*
11.00 – 11.30	**COFFEE BREAK**

Chairmen: V.N. Zadkov / Jiancun Gao

11.30 – 12.15	***S4. A.A. Shaykin,*** *Institute of Applied Physics, RAS, Nizhny Novgorod*
12.15 – 13.00	***A.V. Naumov,*** *Institute of Spectroscopy, RAS, Troitsk, Moscow Region*
13.15 – 14.30	**LUNCH**

Chairmen: S.M. Arakelian / Degang Xu

14.30 – 15.00	***V.N. Zadkov,*** *Department of Physics, M.V.Lomonosov Moscow State University*
15.00 – 15.30	***M.G.Gladush,*** *Institute of Spectroscopy, RAS, Troitsk, Moscow Region*
15.30 – 16.00	***V.I. Trunov,*** *Institute of Laser Physics, SB RAS, Novosibirsk*
16.00 – 16.30	***A.P. Shkurinov,*** *International Laser Center, M.V.Lomonosov Moscow State University*
16.30 – 17.00	**COFFEE BREAK**

Chairmen: M.G. Gladush / Linghai Xie

17.00 – 17.20	***Hongjun Li,*** *Shanghai Institute of Ceramics*
17.20 – 17.40	***E.V. Gorsky,*** *Institute of Spectroscopy, RAS, Troitsk, Moscow Region*
17.40 – 18.00	***Bing Gu,*** *School of Physics, Nankai University*
18.00 – 18.20	***A.A. Lotin,*** *Institute on Laser and Information Technologies, RAS, Shatura, Moscow Region*
18.30 – 20.00	**Poster (Student) Session**

September 25, Sunday
(Suzdal Tourist Center)

Chairmen: V.I. Balykin / Xinzheng Zhang

09.00 – 10.00	***S4. Wei Huang,*** *Nanjing University of Posts and Telecommunications*
10.00 – 11.00	***S1. S.G. Tikhodeev,*** *A.M. Prokhorov Institute of General Physics of RAS, Moscow*
11.00 – 11.30	**COFFEE BREAK**

Chairmen: S.G.Tikhodeev / A.V. Naumov

11.30 – 12.15	***A.P. Alodjants,*** *A.G. & N.G. Stoletovs Vladimir State University*

12.15 – 13.00	***Jiancun Gao,*** *Department of Physics, Tsinghua University*
13.15 – 14.30	**LUNCH**
Chairmen: V.I. Trunov / Kai Zhong	
14.30 – 15.00	***V.I. Denisov,*** *Institute of Laser Physics, SB RAS, Novosibirsk*
15.00 – 15.30	***Degang Xu,*** *Tianjin University*
15.30 – 16.00	***A.P. Kuzmenko,*** *South-West State University, Kursk*
16.00 – 16.30	***A.O. Kucherik,*** *A.G. & N.G. Stoletovs Vladimir State University*
16.30 – 17.00	**COFFEE BREAK**
Chairmen: E.V. Gorsky / Hongjun Li	
17.00 – 17.20	***Kai Zhong,*** *Tianjin University*
17.20 – 17.40	***I.Yu. Chestnov,*** *A.G. & N.G. Stoletovs Vladimir State University*
17.40 – 18.00	***Linghai Xie,*** *Institute of Advanced Materials, Nanjing University of Posts and Telecommunications*
18.00 – 18.20	***A.V. Maslennikova,*** *Moscow State Pedagogical University*
18.30 – 20.00	**Poster (Student) Session**

September 26, Monday
(Vladimir State University)

08.00	**Transfer from Suzdal to Vladimir**
Chairmen: V.G. Prokoshev / Qiang Wu	
09.00 – 10.00	***S1. T.A. Vartanyan,*** *National Research University of Information Technologies, Mechanics and Optics, Saint-Petersburg*
10.00 – 11.00	***S1. Xinzheng Zhang,*** *School of Physics, Nankai University*
11.00 – 11.30	**COFFEE BREAK**
Chairmen: A.P. Alodjants / Bing Gu	
11.30 – 12.15	***S.V. Garnov,*** *A.M. Prokhorov Institute of General Physics of RAS, Moscow*
12.15 – 12.45	***Qiang Wu,*** *School of Physics, Nankai University*
12.45 – 13.15	***Yu.S. Tver'yanovich,*** *Saint-Petersburg State University*
13.15 – 13.30	**Round Table and Closing Remarks**
13.30 – 15.00	**LUNCH**
15.00 – 18.00	**Visit-tour to the Laboratories of Stoletovs Vladimir State University, Vladimir**
18.00 – 19.00	**Transfer from Vladimir to Suzdal**
	FREE TIME

September 27, Tuesday
(Suzdal / Vladimir)

09.00	**Cultural Program/Excursion (Suzdal/Vladimir)**

September 28, Wednesday
(Suzdal / Moscow)

07.30 – 12.30	**Departure from Suzdal to Moscow**
12.00 – 15.00	**Lab tour at Lomonosov Moscow State University**
	Transfer for Departure from Moscow (SVO Airport) **Arrival at 17.00 SVO Airport**

- **Plenary Session Topics (60 min)**
  - **S1.** Nano- and Femtophotonics: Foundations and Applications
  - **S2.** Nonlinear and Atom Optics; High Precision Measurements and Quantum Information Science
  - **S3.** Physics of Terahertz Radiation: Generation and Future Applications
  - **S4.** Modern tendency and Advantages in Lasers; Development in New Laser Materials
  - **S5.** New Laser Technologies in Biomedicine, Ecology and Industry: Bio- imaging, Laser-plasma technologies, Laser Prototyping, etc.

- **Keynote talks (45 min)**
- **Oral talks (30 min)**
- **Oral talks – Young scientists (20 min)**
- **Poster (Student) talks**

22 Sept, Thursday Suzdal	23 Sept, Friday Suzdal	24 Sept, Saturday Suzdal	25 Sept, Sunday Suzdal	26 Sept, Monday Vladimir	27 Sept, Tuesday Suzdal/Vladimir	28 Sept, Wednesday Suzdal/Moscow
19.30 For Chinese participants Transfer from Moscow SVO Airport to Suzdal 21.30 For other participants Transfer from Vladimir railway station to Suzdal	Registration 09.00-10.30	Chairmen . T.A. Vartanyan / Wei Huang S2. *V.I. Balykin* 09.00-10.00	Chairmen V.I. Balykin / Xinzheng Zhang S4. *Wei Huang* 09.00-10.00	Transfer from Suzdal to Vladimir 8.00	Cultural Program/ Excursion (Suzdal/ Vladimir) 09.00	Departure from Suzdal to Moscow 7.30 Lab tour at Lomonosov Moscow State University 12.00-15.00 Transfer for Departure from Moscow (SVO Airport) Arrival at 17.00 SVO Airport
				Chairmen V.G. Prokoshev / Qiang Wu S1. *T.A. Vartanyan* 09.00-10.00		
	Opening Ceremony 10.30-11.00	S5. *Lianhui Wang* 10.00-11.00	S1. *S.G.Tikhodeev* 10.00-11.00	S1. *Xinzheng Zhang* 10.00-11.00		
	Chairmen I.A. Shcherbakov / Feng Song S3. *Jianquan Yao* 11.00-12.00	Coffee Break 11.00-11.30 Chairmen V.N. Zadkov / Jiancun Gao S4. *A.A. Shaykin* 11.30-12.15	Chairmen S.G.Tikhodeev / A.V. Naumov *A.P. Alodjants* 11.30-12.15	Chairmen A.P. Alodjants / Bing Gu *S.V. Garnov* 11.30-12.15		
	S2. *S.N. Bagayev* 12.00-13.00	*A.V. Naumov* 12.15-13.00	*Jiancun Gao* 12.15-13.00	*Qiang Wu* 12.15-12.45		
				Yu.S. Tveryanovich 12.45-13.15		
				Round Table and Closing Remarks 13.15-13.30		
	LUNCH 13.15-14.30			LUNCH 13.30-15.00		
	Chairmen S.N. Bagayev / Lianhui Wang S5. *V.Ya.Panchenko* 14.30-15.30	Chairmen S.M. Arakelian / Degang Xu *V.N. Zadkov* 14.30-15.00	Chairmen V.I. Trunov / Kai Zhong *V.I. Denisov* 14.30-15.00			
		M.G. Gladush 15.00-15.30	*Degang Xu* 15.00-15.30	Visit-tour to the Laboratories of Vladimir State University, Vladimir 15.00-18.00		
	S5. *Feng Song* 15.30-16.30	*V.I. Trunov* 15.30-16.00	*A.P. Kuzmenko* 15.30-16.00			
		A.P. Shkurinov 16.00-16.30	*A.O. Kucherik* 16.00-16.30			
	Coffee Break 16.30-17.00					
	Chairmen V.Ya. Panchenko / Jianquan Yao S2. *V.A. Makarov* 17.00-18.00	Chairmen M.G. Gladush / Linghai Xie *Hongjun Li* 17.00-17.20	Chairmen E.V. Gorsky / Li Hongjun *Kai Zhong* 17.00-17.20			
		E.V. Gorsky 17.20-17.40	*I.Yu.Chestnov* 17.20-17.40			
		Bing Gu 17.40-18.00	*Linghai Xie* 17.40-18.00			
	Welcome party 18.30-21.00	*A.A.Lotin* 18.00-18.20	*A.V.Maslennikova* 18.00-18.20	Transfer from Vladimir to Suzdal 18.00-19.00		
		Poster (Student) Session 18.30-20.00	Poster (Student) Session 18.30-20.00	Free time		

Abstracts

Yb DOPED LuAG LASER CERAMICS

Benxue Jiang ,Shuping Liu， Min Chen , Jiang Li, Wenbin Liu， Yubai Pan,

Shanghai Institute of Ceramics, Chinese Academy of Sciences, 1295 Ding-Xi Road, Shanghai China, Corresponding author, Tel:+86-21-52412816,E-mail: jiang-sic@foxmail.com (B. Jiang)

*Project supported by National Science Foundation for Post-doctoral Scientists of China (Grant No200801207), Natural Science Foundation of Shanghai , China (Grant No 09ZR1435600), the Major Program of the National Natural Science Foundation of China (Grant No.50990300).

LuAG belongs to the cubic space group Ia3. The measured thermal conductivity of undoped LuAG is 17 W/mK at 300 K. The laser ceramic fabrication method of solid state synthesis provides us with a new way to get the LuAG materials low temperature. This makes us easy to get laser Yb:LuAG laser transparent ceramics. Moreover,Yb:LuAG ceramics also have prominent advantages in low cost, composition control, ease of fabrication, large size, multi-functional and mass production, etc.

The procedure of Yb:LuAG transparent ceramics by solid state synthesis method is shown in Fig.1. High-purity powders of LuAG, Yb_2O_3 and CaO were used as starting materials and mixed by ball-milling in anhydrous alcohol for 10h. The mixtures were dried, sieved, dry-pressed under 100 Mpa into Ø20 mm disks and cold-isostatically pressed under 200 MPa. The Yb:LuAG disks were sintered at 1840℃ under vacuum and then annealed at 1450℃ for 20h in air. Mirror-polished samples on both surfaces were used to measure optical transmittance and absorbed spectrum. The microstructure of Yb:LuAG transparent ceramics were studied using transmission microscopy.

Fig.1 shows the mirror-polished Yb:LuAG transparent ceramics sample sintered at 1840℃ under vacuum and then annealed at 1450℃ for 20 h in air. The transmission spectral shows that there are many scattering losses in the Yb:LuAG transparent ceramics.

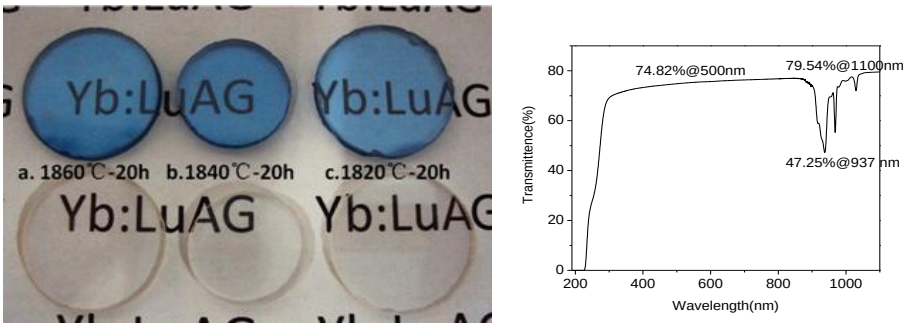

Fig.1 Yb:LuAG ceramics and transition spectra

Using Archimedes method we have measured the density of Yb:LuAG ceramics with different sintering temperatures which is shown in Table 1. From it we can see that we can get Yb:LuAG ceramics with the highest density of 6.68 g/cm^3 sintered at 1820℃.

The absorption of Yb doped LuAG transparent ceramics occur in the wavelength range 850-1050nm, as illustrated in Fig.2. We can see there are four main absorption bands in these Yb doped ceramics. The absorption centers are listed below: 917, 937, 968 and 1030nm. The biggest absorption coefficients of Yb:LuAG transparent ceramics is 3.3 cm^{-1} that is centered at 937 nm and there is a small self-absorption coefficients of 0.2 cm^{-1} centered at 1030nm. Using these absorption and fluorescence spectra we can get the level scheme of Yb^{3+} ions in LuAG ceramics. The phosphorescence spectra of 3at% Yb:LuAG transparent ceramics at room temperature are shown in Fig.2. It was acquired by a TRIAX 550 spectrophotometer with InGaAs LD as the pump source (excited at 940nm). The strongest emission peaks of Yb: LuAG transparent ceramics are located at wavelength 1030nm. The line-widths (FWHM) of fluorescence band of Yb:LuAG ceramics 1030nm are about 8nm.

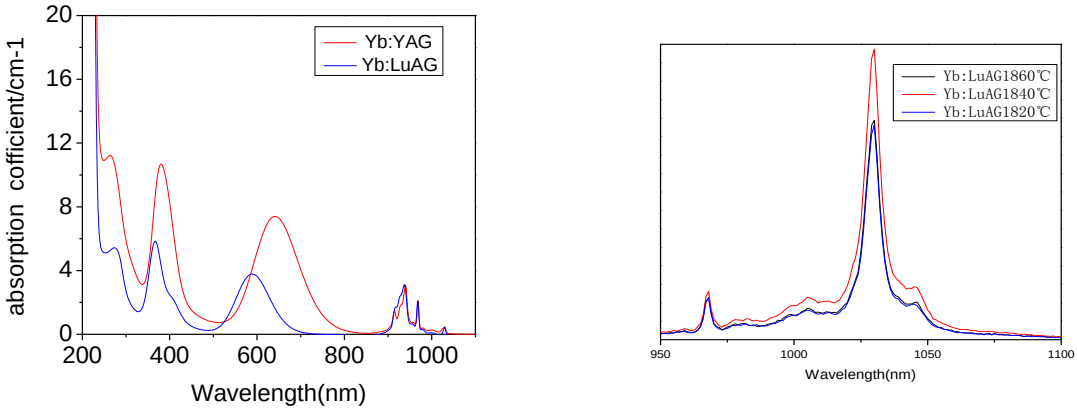

Fig.2. Absorption and fluorescence spectra of Yb:LuAG ceramics

The decay time of four Yb:LuAG transparent ceramics were measured by a computer- controlled transient digitizer. The life time of the Yb:LuAG transparent ceramics is about 1.8ms.

The calculated absorption and emission cross-section of Yb doped YAG Ceramics are shown in Fig.8 and Fig.9 using equation1 and 2. We can see that the peak absorption cross-section of Yb doped LuAG Ceramics at 937nm are 7.6×10^{-21},while the peak emission cross-section of them at 1030nm are $23\times10^{-21}cm^2$.

We have successfully synthesized Yb:LuAG transparent ceramics by solid-state reaction and vacuum sintering method. 0.75wt% CaO was added as sintering aids by a high energy ball milling. Transparent fully dense samples with grain sizes of several micrometers were obtained after 1840℃ sintered. The life time of the Yb:LuAG transparent ceramics is about 1.8ms. The full density of Yb:LuAG ceramics is about 6.68 g/cm^3. The absorption and emission cross-section of Yb:LuAG Ceramics at 937nm and 1030nm are 7.6×10^{-21} and $23\times10^{-21}cm^2$.

Reference

1. D. Pruss, G. Huber, A. Beimowski 1982 Applied Phys.B **28** 335
2. Morris J A, Pollock C R 1990 Opt. Lett.**15** 440
3. T.Y. Fan 1991 Opt. Lett. **14** 1089
4. T. Taira,W.M. Tulloch, R.L. Byer 1997 Appl. Opt. **36** 1867
5. U. Brauch, A. Giesen, M. Karszewski, Chr. Stewen, 1995 Opt. Lett. **20** 713
6. J. Saikawa, S. Kurimura, I. Shoji, T. Taira 2002 Opt. Mat. 19 169
7. E. Innerhofer, T. Südmeyer, F. Brunner 2003 Opt. Lett. 28 367.

VECTORIAL SELF-DIFFRACTION EFFECT

Gu Bing* *, *Ye Fan, Lou Kai, Chen Jin, Li Yong-Nan, and Wang Hui-Tian

School of Physics and Key Laboratory of Weak Light Nonlinear Photonics, Nankai University, Tianjin 300071, China
**E-mail: gubingnj@gmail.com*

When an intense laser interacts with a nonlinear medium, a large number of spatial self-phase modulation effects can be observed. One of the phenomena is the self-diffraction effect which has been extensively studied using a homogeneously polarized beam [1-4]. Recently, vector optical fields, which have the inhomogeneous distribution of states of polarization in the cross-section of field, have become a subject of rapidly growing interest, due to the unique features compared with homogeneously polarized fields and novel applications in various realms [5]. In the presented work, we investigate the self-diffraction effect using the cylindrical vector field and observe the vectorial self-diffraction ring, for the first time to our knowledge [6, 7].

Theoretically, we present the analytical expression of the focal fields of the cylindrical vector fields with arbitrary integer topological charges. Considering the additional nonlinear phase shift photoinduced to a cylindrical vector field by an optically thin Kerr medium, we calculate the far-field vectorial self-diffraction patterns using the Huygens-Fresnel diffraction integral method.

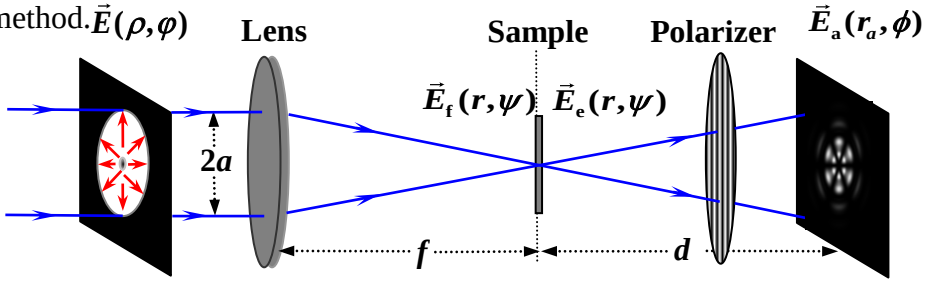

Fig. 1 Experimental arrangement for observing the vectorial self-diffraction effect of the cylindrical vector field.

To demonstrate our theory, we use the experimental arrangement as shown in Fig.1. Experimentally, we observe the vectorial self-diffraction rings of the femtosecond-pulsed vector fields with integer topological charges of $m=1$ and $m=2$ in carbon disulfide, as shown in Figs. 2 and 3, respectively. For the sake of comparison, we also simulate the far-field self-diffraction patterns with the nonlinear sample shown in Figs. 2 and 3. Clearly, the theoretical simulations are in good agreement with the experimental observations, implying that our theoretical analysis is reasonable and could gain an insight on the underlying mechanisms for

the observed vectorial self-diffraction effect. Our results could benefit the understanding of the related spatial self-phase modulation effects of the vector light fields such as spatial solitons, self-trapping, and self-guided propagation.

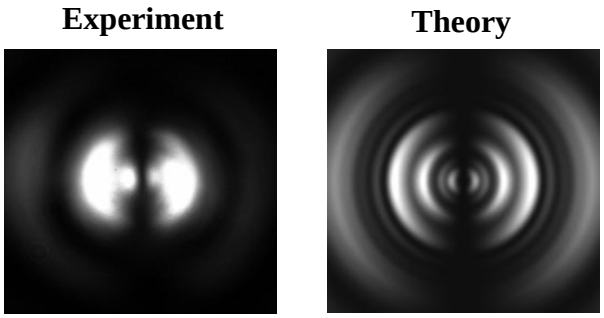

Fig. 2 The vectorial self-diffraction patterns for a cylindrical polarized field with $m=1$ induced by carbon disulfide.

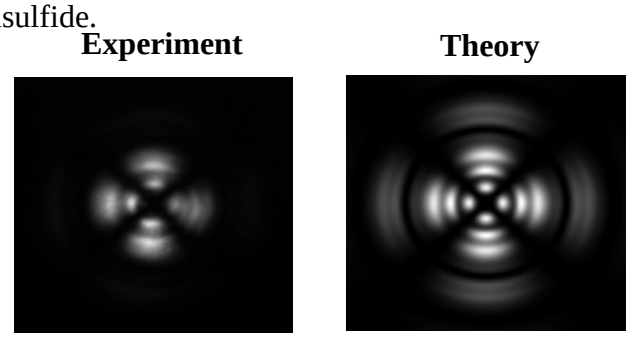

Fig. 3 The vectorial self-diffraction patterns for a cylindrical polarized field with $m=2$ induced by carbon disulfide.

References

[1] W. R. Callen, B. G. Huth, and R. H. Pantell, "Optical patterns of thermally self defocused light," Appl. Phys. Lett. **11**, 103-105 (1967).

[2] S. D. Durbin, S. M. Arakelian, Y. R. Shen, "Laser induced diffraction rings from a nematic liquid crystal film," Opt. Lett. **6**, 411-413 (1981).

[3] W. Ji, W. Z. Chen, S. H. Lim, J. Y. Lin, and Z. X. Guo, "Gravitation-dependent, thermally-induced self-diffraction in carbon nanotube solutions," Opt. Express **14**, 8958-8966 (2006).

[4] E. V. G. Ramirez, M. L. A. Carrasco, M. M. M. Otero, S. C. Cerda, and M. D. I. Castillo, "Far field intensity distributions due to spatial self phase modulation of a Gaussian beam by a thin nonlocal nonlinear media," Opt. Express **18**, 22067-22079 (2010).

[5] Q. W. Zhan, "Cylindrical vector beams: from mathematical concepts to applications," Adv. Opt. Photon. **1**, 1-57 (2009).

[6] B. Gu, K. Lou, J. Chen, Y. N. Li, and H. T. Wang, "Radially polarized field induced vectorial self-diffraction effect in Kerr media," Submitted to Opt. Lett.

[7] F. Ye, B. Gu, K. Lou, J. Chen, Y. N. Li, and H. T. Wang, "Vectorial self-diffraction effect of high-order cylindrical vector fields induced by a thin Kerr medium," Unpublished.

OPTICAL CONFIGURATIONS FOR HIGH AVERAGE POWER FREE ELECTRON LASERS WITH THEORETICAL AND NUMERICAL SIMULATION

Yang Jing[1,3], Wang Zhimin[1], Cui Da Fu[1], Peng Qinjun[1], Xu Zuyan[1],Deng Haixiao[2], Dai Zhimin[2], Zhao Zhentang[2]

1RCLPT, Key Lab of Functional Crystal and Laser Technology, Technical Institute of Physics and Chemistry, Chinese Academy of Sciences, Beijing, 100190, China
2 Shanghai Institute of Applied Physics, Chinese Academy of Sciences, Shanghai, 201800, China
3 Graduate School of the Chinese Academy of Sciences, Beijing 100190, China
Phone Number: +86 10 82543473
E-mail: yangjingeagle@163.com

Free electron laser (FEL) provides a source of powerful and tunable coherent radiation since its first demonstration in 1976[1]. With the advancement of accelerator physics and technology, now FELs have covered the electromagnetic spectrum from THz [2] to hard X-ray region [3], which are not accessible for conventional lasers. The developing trends for FELs are: (1) the radiation wavelength and pulse duration extension oriented to scientific purpose, and (2) the power scaling to High Average Power FEL (HAPFEL) [4-5] for industry, defense and other use.

In this paper, the investigation on the optical configurations of the HAPFEL is presented. Firstly, we analyzed the optical configuration of the FEL oscillator in general approach, with one-dimensional (1D) and three–dimensional (3D) simulation, respectively. Secondly, the challenges for HAPFEL in optical system are presented and some possible configurations are also given. Then a brief comparison between oscillator and amplifier configurations is followed.

The 1D evolution of FEL can be described by a group of equations. With the universal scaling of [6-7], FEL evolutions can be given by the following:

$$\frac{d\theta_j}{d\bar{z}} = p_j \qquad (1)$$

$$\frac{dp_j}{d\bar{z}} = -(A(\bar{z},\bar{z}_1)\exp(i\theta_j) + c.c) \qquad (2)$$

$$(\frac{\partial}{\partial\bar{z}} + \frac{\partial}{\partial\bar{z}_1})A(\bar{z},\bar{z}_1) = \chi(\bar{z}_1)b(\bar{z},\bar{z}_1) \qquad (3)$$

Where $j = 1,2...N$, and the N is the number of electrons in each pondermotive well. These equation are numerically solved by 1D FELO code, then we can get the FEL gain and the power evolution as well as the FEL output power versus the cavity detuning as shown in Fig.1(a). The sensitivity originates from the synchronization requirement between the electron

bunch and the FEL pulses, which are both in picosecond to femtosecond range. Therefore, the FEL cavity length control in vacumm poses a strigent requiremnet to the optical configuration of FEL. Moreover, the geometric misalignment is critical for FEL output and it is analyzed by theoretical approach in geometric optics as well as a 3D simulation with the GENESIS plus OPC code.

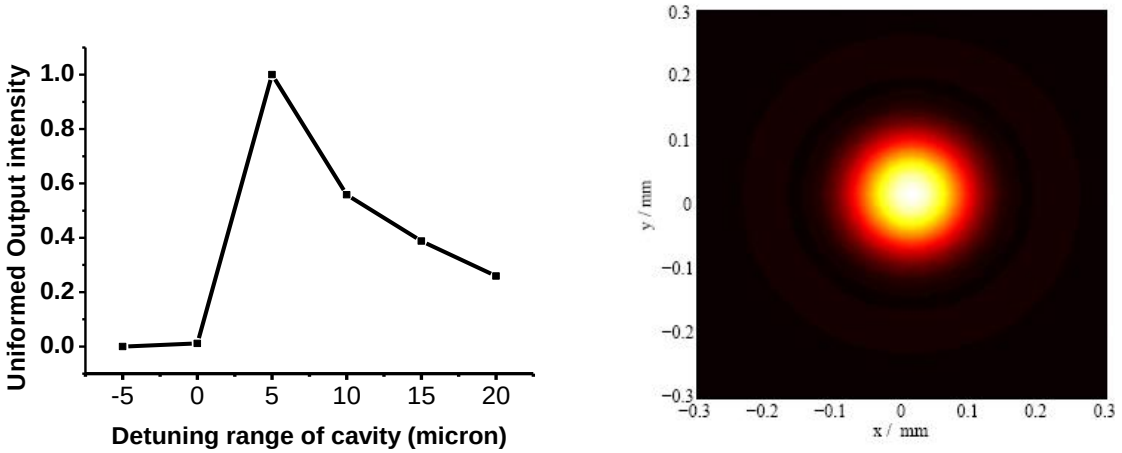

(a) (b)

Fig. 1. Simulation results (a)Sensitiveity of the cavity length from the 1D simulation and (b)output beam spot in the far field from 3D simulation

Besides the above mentioned requirement, there are additional threatens for HAPFEL's optical system due to its high average power. To run the FEL sufficiently and safely, some configurations can be adopted to lower the intracavity power on the resonator mirror, such as (1) the extended cavity with grazing incidence of laser beam on the mirror, such as the ring configuration shown in Fig.2.(a) [8] , in which the power density will decrease as the incident angle increase; (2) the long cavity with short Rayleigh length[9], in which the power density is lowered by the strong diffraction of FEL radiation; (3) the optical cavity with intracavity aperture, HR coated downstream mirror with backplane cooling, together with other output coupling methods and so on. Unfortunately, all the above mentioned configurations have pros and cons, thus in the practice of optical design, the trade-off between the optical power density and the engineering feasibility has to be considered. Meanwhile, it is necessary to control the lasing frquency, for example, when a FEL operates in NIR spectrum, UV radiation from high harmonics as well as terahertz frequencies from coherent synchrotron radiation of the elcetron beam will also be generated beside the fundamental frequency, and it will also lead to the thermal deformation or even the damage of the mirror. We analyzed the spatial distribution of the harmonics, and verified the introduction of the apeture can lower the harmonics intensity on the mirror.

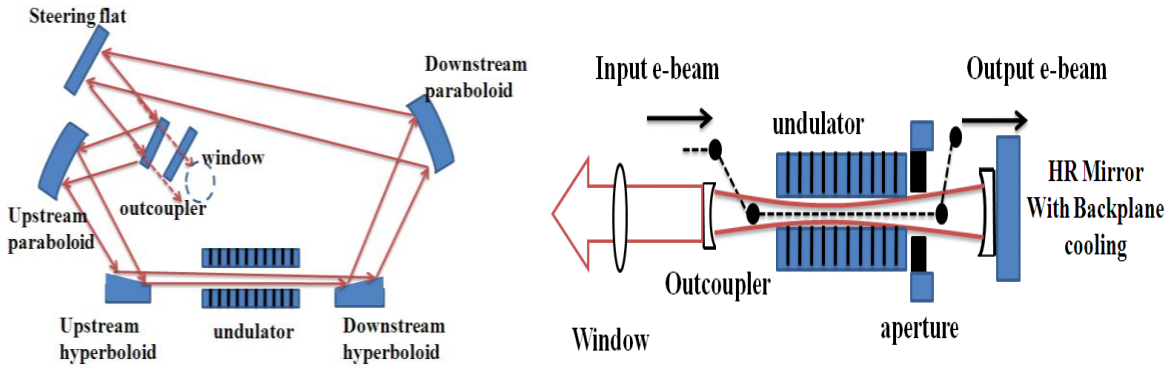

(a) (b)

Fig. 2. Examples of optical configurations which are expected to be used in HAPFEL (a) Grazing incident ring resonator (b) resonator with an intracavity aperture with backplane-cooling mirror.

Furthermore, the single pass amplifier can be used as an alternative approach for high average power FEL. With the removal of the cavity mirror, the thermal loading problem is eliminated. Admittedly, as an integrated system of electron and optical beam, the HAPFEL is also influenced by other parameters such as electron beam quality, undulator fields and so on. Accordingly, in HAPFEL generation, optical configuration should be compatible with these parameters in the process of HAPFEL design as well.

Bibliographic list

1. L.R Elias, et al. Phys. Rev. Lett. 36, 717 (1976)
2. E.A. Antokhin, et al., Nucl. Instr. and Meth. A 15, 528 (2004).
3. P. Emma et al., Nature Photonics 4, 641, (2010)
4. G. R. Neil et al. 84, 662, Phys. Rev. Lett. (2000)
5. N. Nishimori et al., Proc. FEL-2006, p.265 (2006).
6. R. Bonifacio, C. Pelligrini and L.M. Narducci, Opt. Commun.50, 373 (1984)
7. B.W.J. McNeil, Proc. FEL-2006, p.59, (2006)
8. D.H. Dowell et al., Nucl. Instr. and Meth. A 318 74--80 (1992)
9. W.B. Colson et al., Nucl. Instr. and Meth. A 505 48--51(2003)

OPTICAL TOMOGRAPHIC DEMONSTRATION WITH PRE-AMPLIFICATION OF WEAK IMAGES USING A GATED OPTICAL PARAMETRIC AMPLIFIER

Yang Jing,[1,3] Zhang Jingyuan[2], Du Shifeng [1], Cao Dong[1,3],Cui Dafu[1], Peng Qingjun [1], and Xu Zuyan [1]

1RCLPT, Key Lab of Functional Crystal and Laser Technology, Technical Institute of Physics and Chemistry, Chinese Academy of Sciences, Beijing, 100190, China

2Department of Physics, Georgia Southern University, Statesboro, GA 30460, USA

3Graduate School of the Chinese Academy of Sciences, Beijing 100190

Phone Number: +86 10 82543473

E-mail: yangjingeagle@163.com

Images play an important part for the biological, medical or even remote sensing applications. Due to the weakness of the intensity of direct imaging, it is usually too weak to be resolved. Accordingly, finding a way to record the weak images effectively or to enhance the weak images with controllable noise plays a key role in these applications. Compared with other candidates of optical image amplifier, such as Raman amplifier[1], photorefractive[2], and stimulated Brillouin scattering[3], the optical parametric amplifier(OPA) is quite competitive for its combination of compact setup, high gain[4-5], wide tunable range, and low noise figure [6].

In this paper, we demonstrate a prototype for image enhancement and tomographic analysis using a picosecond OPA as a range-gated pre-amplifier. More than 40dB image amplification has been achieved. By incorporating the gated nature of the OPA and by amplifying the back-scattered photons from the target, the images of various longitudinal positions of the target can be extracted and a 3-D profile of the target can be reconstructed. This approach allows amplification of very weak image and reconstruction of 3-D image from a target at certain distance without signal-noise-ratio (SNR) deterioration.

Firstly, a 2-D target is used to quantify the high gain of weak images, and the image's intensity is measured in terms of CCD's output gray-scale value. has been strengthened by more than four orders magnitude without Signal Noise Ratio (SNR) deterioration. The signal and pump beam is chosen as the second and third harmonics of Nd: YAG laser. The experiment scheme is shown in Fig.1.

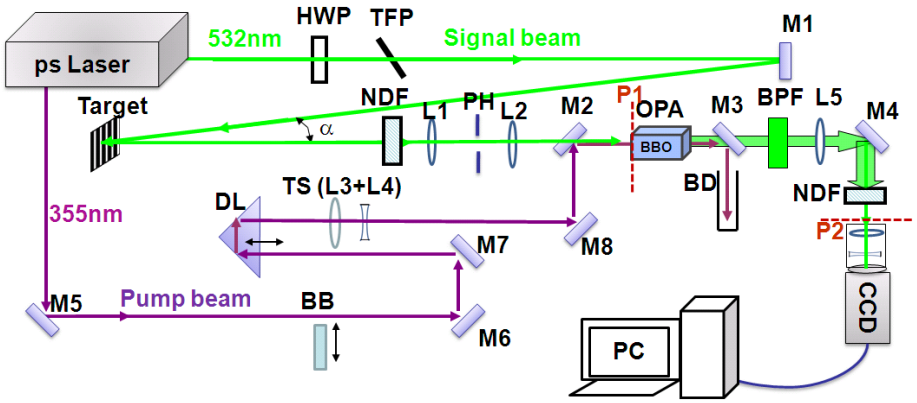

Fig. 1. Experimental setup for amplification and reconstruction of weak images using OPA as a pre-amplifier. PH : pin hole. HWP: half wave plate. TFP: thin film polarizer. BB: beam block. BPF: band pass filter. NDF: neutral density filter. M1 and M4 are highly reflected (HR)-coated at 532nm; M2 and M3 are HR-coated at 355nm and anti-reflected (AR)-coated at 532nm; M5-M8 are HR-coated at 355nm. DL: delay line. BD: beam dump. CCD: charge coupled devices. PC: personal computer. P1 and P2 are first and second image plane.

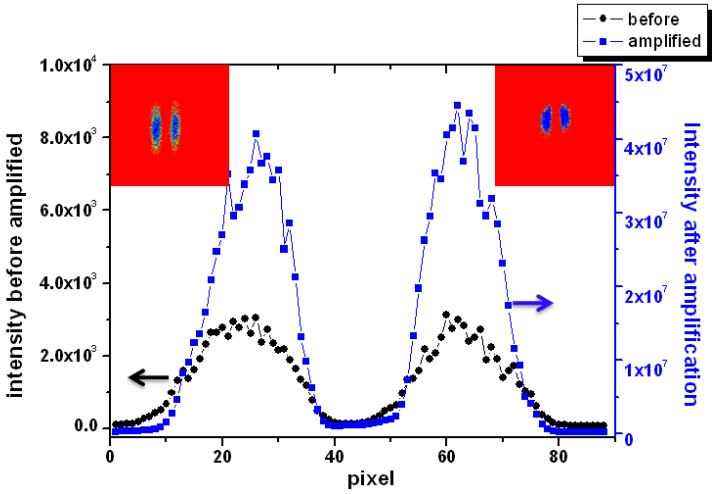

Fig. 2 Images of the plan target without OPA (upper left) and with OPA amplified after an OD=3.8 attenuation (upper right) inside the FOV and the plots of the intensity sampling along the scan line in the two images.

Based on the imaging of the plane target, we further extend the capacity of the system for amplification of the image of a 3-D target by using the gated nature of the picosecond OPA. The ballistic part of the back-scattered photons at a specific time slice, which provides the information of the target at the corresponding section, can be amplified for tomographic analysis by selecting the gate window of the OPA. Experimentally, the profiles of the target at various longitudinal locations can be chosen by adjusting the temporal delay between the pump beam and the signal. The optical configuration for 3-D imaging of the OPA is largely the same as Fig.1. The only difference is that the plane target is replaced with a cone Teflon target as shown in the left of Fig.3 (a).

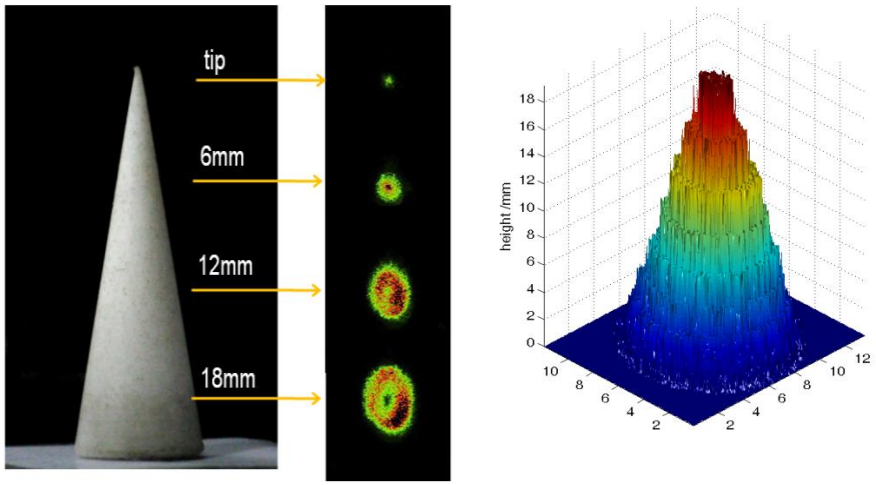

Fig. 3 (a) Tomographic analysis of target and (b) reconstruction from different slices

By extracting images from the different time slices using the gated OPA, a 3-D profile of the target can be reconstructed. We expect this technique developed in this letter could provide an option for the imaging of the weak target with range-gated capability, for instance, the range-gated remote-sensing as well as 3-D profile imaging in the turbid media.

Bibliographic list

1. N. A. Vainos, et al., Opt. Lett. 16(6) 363 (1991)
2. J. A. Moon, et al, Opt. Lett. 19(16) 1234 (1994)
3. S. Sternklar, et al., Opt. Lett. 15(11) 616 (1990)
4. S. F. Du, et al., Opt. Comm. 281, 2638(2008)
5. X. F. Han, et al., J. Opt. Soc. Am. B 24, 1633 (2007)
6. S. K. Choi, et al., Phys. Rev. Lett. 83, 1938 (1999)

DIRECT ADDITIVE MANUFACTURING OF INDIVIDUAL AND CUSTOMIZED METAL PARTS BY SELECTIVE LASER MELTING

Yongqiang Yang, Fuhai Li

Guangzhou Research Institute of Non-Ferrous Metals, China;

Correspondent: Prof. Dr. Yongqiang Yang

Director, Institute of Welding Technology, Guangzhou Research Institute of Non-Ferrous Metals, China;

Director, E.O. Paton Chinese-Ukrainian Institute of Welding, Guangdong General Research Institute of Industrial Technology

Professor, School of Mechanical and Automotive Engineering, South China University of Technology

Selective Laser Melting (SLM) is a new technology of Rapid Prototyping (RP) and can make high density metal parts with metallurgical bonding and good mechanical properties from CAD model layer-by-layer by using a focused laser beam with high energy density. This paper reports the research progress and some new applications of SLM based on design with free structure for individual and customized medical devices, new gear wheel with screw gears, coaxial nozzle with holes and water cooling channels, non-assembly mechanism with kinetic joint and complex parts with hollow or inner structure. The SLM technique implies a new methodology that allows more design freedom and faster fabrication of function parts, which changes the conventional design concept of function parts. We can expect that more function parts with structure for better performance will be developed and be used in some practical applications after the improvement of the process strategy of SLM.

Keywords: direct manufacturing; design with free structure; individual and customized metal parts, Selective Laser Melting (SLM)

His main research interests include Laser Processing and Rapid prototyping of selective laser melting. He had been completed more than 20 projects including the projects from Fund of state and Guangdong province, industry and Eureka international cooperation. Main academic achievements include over 130 journal papers and 48 patents (24authorized) in the field of selective laser melting rapid prototyping for direct manufacturing of metal parts, laser material processing and laser welding.

ANALYSIS ON POLARIZATION CHARACTERISTIC OF CHERENKOV RADIATION BY OPTICAL RECTIFICATION IN $LINBO_3$

Pengxiang Liu

The Institute of Laser & Opto-electronics, College of Precision Instruments and Opto-electronics Engineering, Tianjin University, Tianjin 300072, P. R. China
Key Laboratory of Opto-electronics Information Technology (Tianjin University), Ministry of Education, Tianjin 300072, China
phone number: +86-22-27407676; e-mail: sxtb631@126.com

In this paper, we investigated two dimensional Cherenkov THz radiation via optical rectification of ultra-short laser pulse focused into a line in LiNbO3 crystal. Based on the 2D model developed by Bakunov *et al.*, we did further calculation on p-polarized THz wave generation and got the expression of p-polarized THz electric field. Geometries of p- and s-polarized THz generation were presented in figure 1.

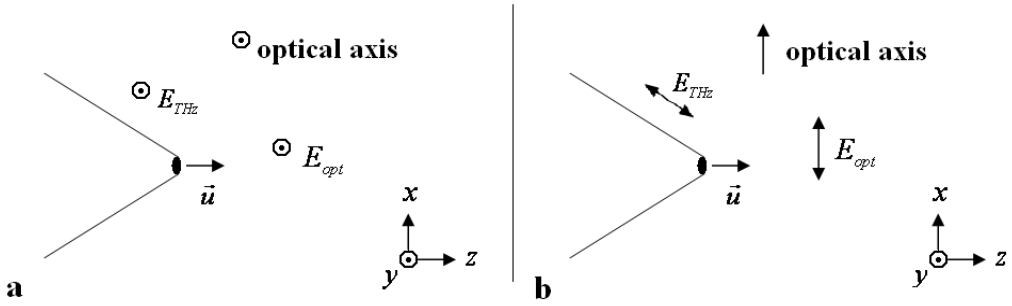

Fig. 1 geometry of s-polarized (a) and p-polarized (b) Cherenkov radiation

We designed Brewster-cut geometry, shown in figure 2. In this geometry, the transmitting coefficient of p-polarized THz wave at exit boundary is 100%. It can provide these advantages. First, two parts of Cherenkov wedge are both utilized. Second, output THz beam is compressed and intensity is increased. Third, the absorption is less than that in Cherenkov-cut geometry. In a word, the coupling efficiency could be higher.

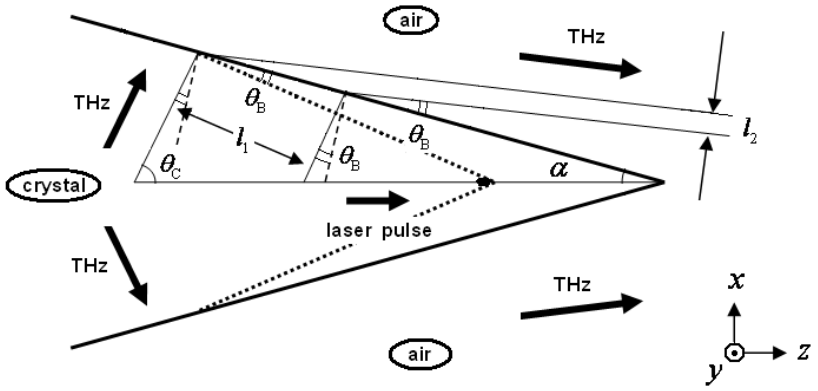

Fig. 2 Brewster cut geometry

The energy of p-polarized THz radiation and conversion efficiency was roughly estimated. Comparison between p- and s-polarized radiations was shown in table 1. Here, peak pump intensity I_0 was chosen as 10GW/cm^2 (corresponding pulse energy is 1.02μJ). It was indicated that p-polarized THz radiation has lower energy and conversion efficiency, but higher intensity and better beam quality.

Table 1 Comparison between P- & S-polarization

	p-polarized Brewster cut	s-polarized Cherenkov cut
amplitude	0.27kV/cm (low)	0.6kV/cm
energy	6.36pJ	7.1pJ (T =0.54)
efficiency	6.2×10^{-6}	6.96×10^{-6}
intensity	83.94W/cm^2 (high)	51.9W/cm^2

In the last section, we considered the effect of angular dispersion of this ultra-short THz pulse after refraction at the Brewster surface, which would cause the divergence of output THz beam in free space. We did calculation on this effect and plotted the angular spectrum (solid curve in figure 3). It can be seen that higher frequency corresponds to a larger radiation angle δθ, which varies from -1.5° to 12°. However, most of the radiated energy (99.3%) is within a range of -1.5°~4°.

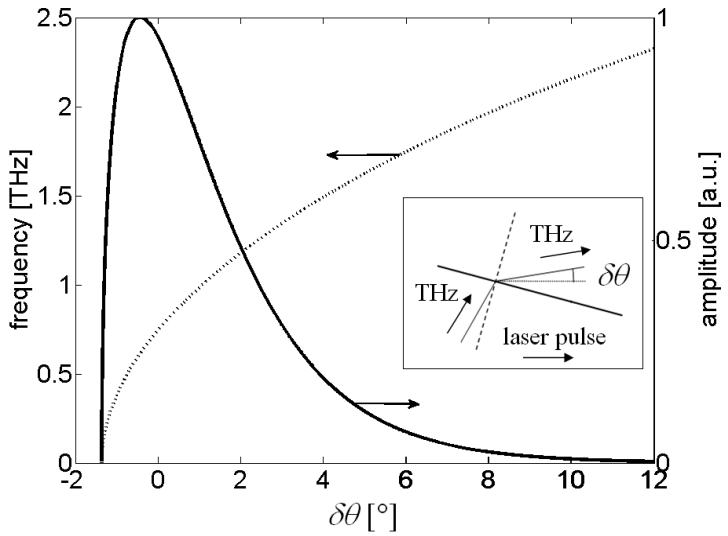

Fig. 3 angular spectrum of THz radiation after refracted by interface

Reference

[1] M.I. Bakunov, S.B. Bodrov, A.V. Maslov and M. Hangyo “Theory of terahertz generation in a slab of electro-optic material using an ultrashort laser pulse focused to a line”, Phys. Rev. B 76 (2007) 085346

[2] P.X. Liu, D.G. Xu, C.M. Liu, D. Lv, Y.J. Lv, P. Wang and J.Q. Yao “p-polarized Cherenkov THz wave radiation generated by optical rectification for a Brewster-cut LiNbO3 crystal”, J. Opt. 13 (2011) 085202

Pengxiang Liu received the Bachelor degree in opto-electronic science and technology in 2009 from Tianjin University, China. He is currently working toward the Ph.D. degree in opto-electronic technology at Tianjin University, China. His current research focuses on terahertz generation.

SYNTHESIS OF CARBON NANOFIBERS AND NANOCLUSTERS BY LASER RADIATION OF A CARBON TARGETS PLACED IN THE EXTERNAL FIELDS

A. A. Antipov, S. M. Arakelyan, S. V. Kutrovskaya, A. O. Kuchrik, A. V. Osipov, V. G.Prokoshev, and A. A. Schekin

Vladimir State University, ul. Gor'kogo 87, Vladimir, 600000 Russia
ZAO NT-MTD, Zelenograd, korpus 100, Moscow, 124482 Russia
e-mail: laser@vlsu.ru; kucherik@vlsu.ru

Results of the laser synthesis of carbon nanomaterials during the deposition of carbon vapors have been presented. One feature of this method is the action on the carbon samples in atmospheric air and external fields. Experiments on the laser action on the carbon targets in the presence of constant electric and inhomogeneous magnetic fields have been performed. The possibility of obtaining carbon micro- and nanofibers upon the deposition of particles in the electric field and carbon micro- and nanoclusters upon the deposition of particles in the magnetic field has been demonstrated. It has been shown that a change in the target material and action modes allows one to change the structure of the deposited layer.

At the same time, the effect that the laser has on carbon materials in atmospheric air and/or oxygen has been studied in a series of works, and the possibilities of a directed change in the morphological properties of the obtained nanostructures have been discussed

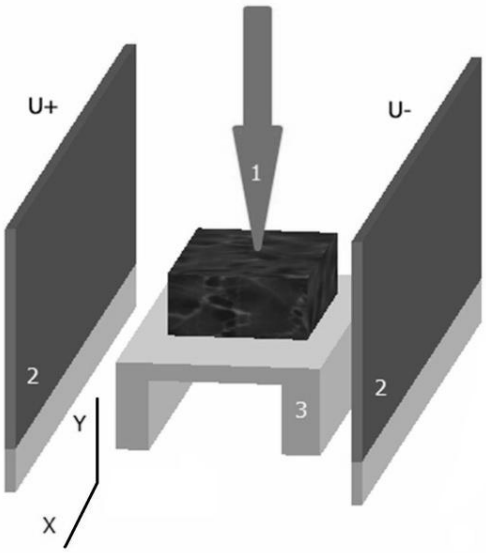

Fig. 1. Experimental scheme on the laser synthesis of carbon nanostructures upon action on the graphite sample placed in a constant homogeneous electric field: (1) direction of the action of the laser radiation, (2) metal plates under constant electric voltage, and (3) coordinate table with a graphite sample on it. Carbon nanostructures are formed on the metal plate with the negative potential by the deposition of the graphite particles on it upon laser ablation.

Such control over the properties of the deposited materials when obtaining nanostructures is particularly promising in the additional quasistatic external fields. For example, in it was shown that the macropattern of the formed nanostructures dramatically changes in the external electric field during their synthesis: the finest grid carbon structure, a web consising of single wall nanotubes, is formed instead of typical carbon nanostructures.

This work presents the results of obtaining carbon nanofibers and nanoclusters under the action of a laser on graphite samples placed in a constant electric and/or magnetic field. The experimental scheme was chosen analogous to, where the principle possibility of the formation of nanostructured amorphous and diamondlike carbon films during the laser's action in the air medium was shown.

A sample of spectrally pure graphite was placed between textolite plates covered with a copper foil, to which a constant voltage of up to 1000 V was applied; the distance between the plates was 1 cm. With a laser radiation power of 30 W and a laserbeam diameter of 30 μm affecting the graphite sample, an intensive plasma strip was formed, one end of which was located on the sample and the other end on the plate with a negative potential at the height of 2–3 mm from the sample surface. This plasma strip determined the process of the laser synthesis of carbon nanostructures. The deposition of the carbon compound on

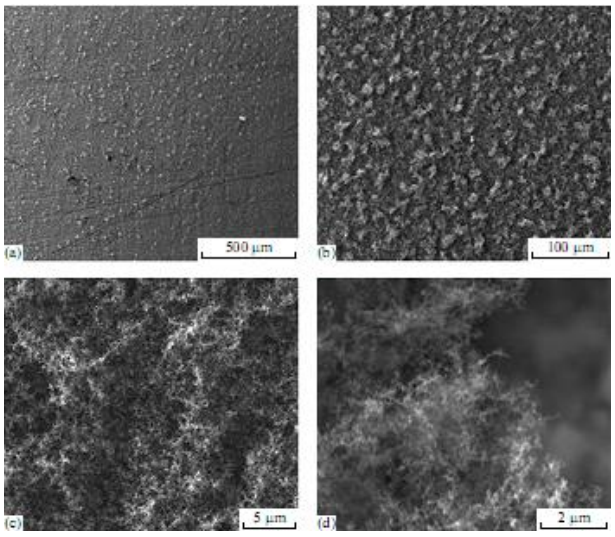

Fig. 2. REM image of the region of the deposition of carbon particles on the metal plate with the negative potential at different magnifications (the voltage between the plates is 1000 B): (a) 150×, (b) 600×, (c) 8000×, and (d) 26267×.

the surface of the metal plate with a negative potential via the laser ablation mechanisms were visually recorded as the formation of dark spot dimensions on the order of 1 cm on the X axis and 1.5 cm on the Y axis. A study of this deposited layer on a raster electron mi-

croscope (REM) made it possible to detect the formation of carbon fibers over the total deposition area (Fig. 2).

Thus, this experiment vividly demonstrated that it is possible for carbon nanofibers to form on the surface of the metal plate serving as a negative electrode for the applied external electric field upon the action of the laser on a graphite sample placed in this electric field in atmospheric air. Carbon nanostructures obtained as a result of such laser ablation are close in type to the nanofibers synthesized. However, in our case no

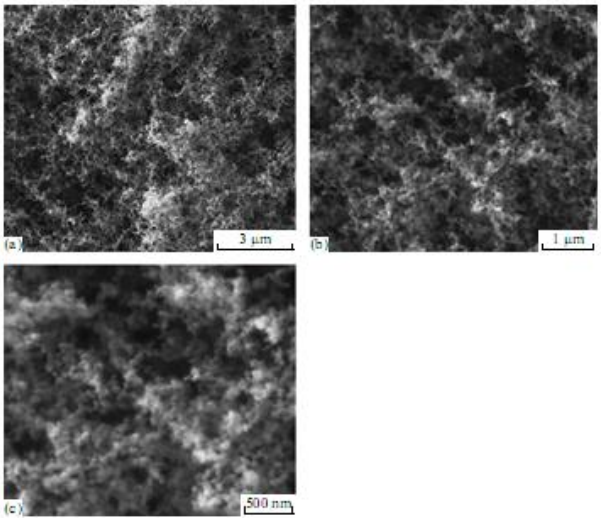

Fig. 3. Carbon nanofibers formed in the metal plate with a negative potential under the action of the laser on a sample of spectrally pure graphite under a voltage of 800 V between the metal plates: (a) image of the region with the carbon nanofibers (20000×); successive magnification of this image (b) 40000× and (c) 80000×.

The other possibility of controlling the properties of the deposited layer upon the laser radiation of carbon samples is implemented when they are located in the inhomogeneous magnetic field. In this case the deposition of carbon nanolayers occurs in a unique element on a glass substrate spatially separated from the graphite target by a layer (ceramic washer) (Fig. 4).

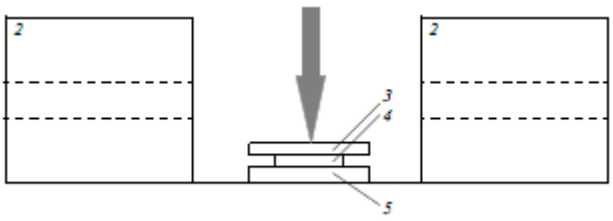

Fig. 4. Scheme of the laser experiment in the presence of the inhomogeneous magnetic field : (1) direction of the action of the laser radiation, (2) cylindrical magnets, (3) cold substrate (glass) on which the carbon nanolayer is synthesized, (4) layer, and (5)graphite target. Nanostructures on the substrate surface are formed due to laser ablation from the surface of the graphite target.

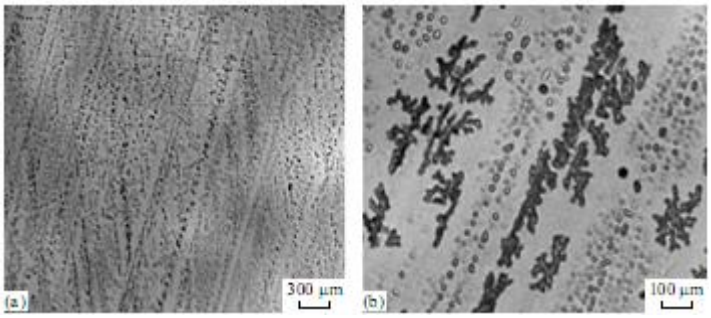

Fig. 5. Optical images of the ordered structures formed on the substrate surface in the form of the isoslope bands of graphite particles with different diameters (à) and carbon clusters (b).

After the laser radiation of the target, the substrate on which the nanostructured carbon layer was deposited was studied on a highresolution optical microscope and an Integra Aura probe nanolaboratory (atomic force microscope (AFM)). The images for these two diagnostic methods are shown in Figs. 5 and 6, respectively.

The formation of clusters of nanoparticles makes it possible to suppose that the process of the formation of the carbon layer at the laser deposition is similar to the growth of dendrites: depending on the experimental parameters (the distance to the center of the laser beam, the concentration of the paticles in the flow in the gap between the target and the substrate and on the substrate surface, their energy etc.), the “centers of nucleation” of nanostructures are formed.

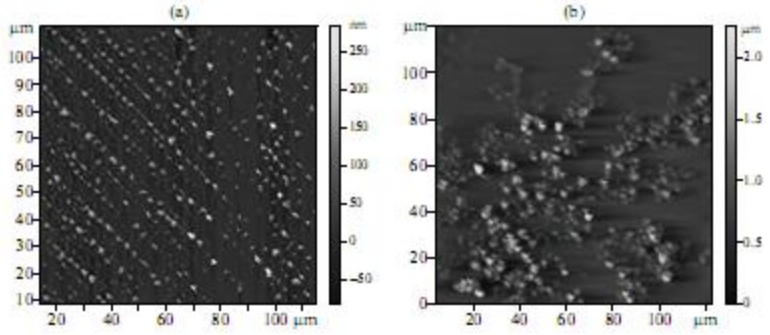

Fig. 6. AFM image of the structure of the carbon nanolayer deposited on the substrate: (a) ordered deposition and (b) clusterstructure.

Further, this leads to the growth of clusters due to the thermal–fluctuation motion of nanoparticles. Figure 6 corresponds to the nanostructure formed on the substrate 6 mm from the center of the laser irradiation of the graphite target. Preferably ordered groups of nanostructures were formed at lower distances from the center of the laser beam, which were distributed as parallel bands over the substrate surface at a distance of 1–5 mm from the center of the laser beam. No formation of nanoclusters was observed upon the decrease in the time of the action.

CONCLUSIONS

This work presents the first results on obtaining carbon nanostructures in a controlled manner under the action of laser radiation on the carbon target in atmospheric air in the presence of the external electric and/or magnetic fields. A change in the morphology of the structure of the layer deposited on the substrate was observed, and it can be controlled by varying the parameters of the experiment. The principle result is the formation of carbon nanofibers and nanoclusters upon the laser deposition of carbon nanoparticles on the substrate from the laser-induced torch arising directed above the irradiated target without the application of additional catalysts.

The effect that the external static electric field has on such carbon-nanofiber formation can be related to the fact that it orients the flow of the particles propagating in the plasma along its force lines so that it is possible to form fibers along the physically chosen direction. In the presence of a magnetic field, the mechanism of the formation of carbon nanofibers is analogous to the previous case, but, due to the magnetic field inhomogeneity, the structure of the deposited layer changes as well.

REFERENCES

1. A. I. Gusev, Nanomaterials, Nanostructures,and Nanotechnologies (FIZMATLIT, Moscow, 2005) [in Russian].

2. P. N. D'yachkov, Carbon Nanotubes: Structure, Properties,and Applications (BINOM, Moscow, 2006) [in Russian].

3. A. V. Eletskii, "Carbon Nanotubes," Usp. Fiz. Nauk 167 (9), 945 (1997) [Phys.—Usp. 40 (9), 899 (1997)].

4. P. M. Ajayan, "Carbon Nanotubes," in Handbook of Nanostructured Materials and Nanotechnology, Ed. By H. S. Nalwa (Academic, San Diego, California, United States, 2000), Vol. 5, Chap. 6, p. 375.

5. S. Eliezer, N. Eliaz, and E. Grossman, D. Fisher, I.Gouzman, Z. Henis, S. Pecker, Y. Horovitz, M. Fraenkel, S. Maman, V. Ezersky, and D. Eliezer, "Nanoparticles and Nanotubes Induced by Femtosecond Laser," Laser Part. Beams 23 (1), 15 (2005).

6. A. Ya. Vul' and A. S. Udovichenko, "Development of the Technology for Preparation of Multifunctional Materials Based on Nanocarbon," Ross. Nanotekhnol. 2 (7–8), 63–64 (2007).

THEORETICAL INVESTIGATION ON THE ATMOSPHERIC PROPAGATION OF THZ RADIATION

Ran Wang*[a,b] , Jianquan Yao[a,b], Haixia Cui[a,b], and Kai Zhong[a,b]

[a]College of Precision Instrument and Opto-electronics Engineering, Institute of Laser and Opto-electronics, Tianjin University, Tianjin 300072, China
[b]Key Laboratory of Opto-electronics Information Science and Technology, Ministry of Education, Tianjin University, Tianjin 300072, China
**Phone:+86-022-27407676; Email:wangran19861014@163.com*

Terahertz (THz) radiation is the electromagnetic spectrum with the frequency defined from 0.1 to 10 THz (1THz=10^{12}Hz). Recent advances provide new opportunities and widespread potential applications of THz in material identification, imaging, communication, non-destructive examination, and global environmental monitoring. The rapid development can be attributed to the nature of terahertz radiation, which offers advantages of both microwave and light wave.

The characteristics of THz atmospheric propagation now rank among the most critical issues in the principal application of space communication and atmospheric remote sensing. THz communication will benefit from the high-bit-rate wireless technology which takes advantage of higher frequency and broader information bandwidth than microwave. Many biological and chemical compounds exhibit distinct signature responding to THz radiation, which presents tremendous potential of THz atmospheric remote sensing.

To provide theoretic instructions for the applications above, an accurate research is carried out on the propagation characteristic of THz radiation in different atmospheric conditions. This paper presents the fundamental physical concepts and processes systematically, including the effect of extinction and emission. A special focus is put on the attenuation effect (especially the absorption of water vapor) and the Mie scattering of aerosol particles.

THz radiation is attenuated by atmospheric absorption as well as scattering out of their straight path. Extinction coefficient is defined mathematically as the sum of absorption and scattering coefficient, and the atmospheric attenuation is illustrated by Lamber-beer law:

$$dI(\nu) = -\alpha_\nu(z)I(\nu)dz \qquad I_{r_1}(\nu) = I_{r_0}(\nu)e^{-\int_{r_0}^{r_1}\alpha_\nu(z)dz}$$

The scattering effect comprises the molecular Rayleigh scattering and the Mie scattering by aerosols and water vapor coagulum. Only Mie scattering should be taken into consideration with the wavelength of THz radiation being in the order of aerosols.

THz radiation propagating in the atmosphere also experiences the process of enhancement. The atmospheric THz emission is defined as a source term J, comprising the

thermal emission J_B and the scattering source term, which includes the source sole scattering on direct radiation condition J_{SS} and the multiple scattering source J_{MS}. The expression of source term is

$$J = J_B + J_{SS} + J_{MS}$$

The radiative transfer equation is determined by the three concepts, attenuation, enhancement, and background radiation occurring along the line-of-sight, the integral form of which is as follow:

$$I_\nu(r_1) = I_\nu(r_0)e^{-\int_{r_0}^{r_1}\alpha_\nu(r)dr} + \int_{r_0}^{r_1} e^{-\int_{r}^{r_1}\alpha_\nu(r')dr'} S_\nu(r)\alpha_\nu(r)dr$$

It is the foundation of atmospheric propagation model, and the derivation in detail will be described in this paper. The physical significance of radiative equation lies in the processes of attenuation and emission of atmosphere along a given optical path. Resulting from energy conservation law, the radiative transfer equation is applicable to the whole electromagnetic spectrum, from radio wave to visible light.

The last part comprises the demonstration and comparison of THz atmosphere propagation models like Moliere(V5), SARTre and AMATERASU. The last one has a strong heritage from the former two, respectively in the non-scattering case and scattering version. To verify these models above, they should be compared with each other and validated against real laboratory measurements in order to check the correctness of the data accuracy and the algorithm hypothesis.

The critical issues of THz atmospheric propagation lie in the construction of radiative transfer algorithm, the collection of accurate spectral parameters, such as linear and continuum absorption and complex refractive index in THz region, and the standardization of measurement procedures. The final objective is to construct the atmospheric propagation model under different kinds of climatic conditions.

QUANTITATIVE IMAGING OF TERAHERTZ PHONON POLARITON AND ITS APPLICATIONS

Qiang Wu*, Chengliang Yang, Bin Zhang, and Jingjun Xu

The MOE Key Laboratory of Weak Light Nonlinear Photonics, TEDA Applied Physics School and School of Physics, Nankai University, Tianjin 300457, P. R. China

Christopher A. Werley and Keith A. Nelson

Department of Chemistry, Massachusetts Institute of Technology, Cambridge, Massachusetts 02139, USA
*email: wuqiang@nankai.edu.cn

Terahertz frequency phonon polariton generation, control and detection have received extensive attention in recent years due to their outstanding capabilities in terahertz (THz) spectroscopy, imaging and advanced signal processing. They also have huge potential ability to be used in ultrafast optics and photonics. THz phonon polariton waves result from the coupling of lattice vibrational waves and electromagnetic waves, and can be generated in ferroelectric crystals such as $LiNbO_3$ (LN) via impulsive stimulated Raman scattering (ISRS) using femtosecond optical pulses. They do not propagate collinearly with the pump beam in the sample due to the large index-mismatch between optical and THz frequencies. Instead they generate a Cherenkov radiation pattern and propagate primarily in the lateral direction, nearly perpendicular to the optical beam that generates them. As the THz waves propagate through the crystal, their electric fields change the refractive index of the sample through the electro-optic effect. The time-resolved optical probe pulses travel nearly collinear with the pump, experiencing a spatially dependent phase shift proportional to the refractive index change and yield a "side view" of the THz pulse which shows spatiotemporal field oscillations. Because both spatial and temporal information are important, time-resolved imaging becomes a powerful tool for studying THz phonon polariton. Previously the phase images have usually been visualized using the Talbot effect by translating the camera out of the image plane of the sample. Thus some phase information will be converted to amplitude information, but only certain wave vector components of the phase image will be efficiently detected, which makes quantitative E-field measurement impossible. Another drawback of the Talbot method is that static structures in the sample will be blurred because the CCD camera is not in the image plane. Thus previous phonon-polariton imaging has not yielded quantitative characterization of broadband field profiles or sharp, in-focus view of polaritons and the structures in which they propagate.

In this presentation, we demonstrate quantitative measurement of THz phonon polariton and in-focus imaging of static structures with time-resolved phase contrast imaging and self-compensating polarization gating, which address the deficiencies of Talbot imaging. We also compare four phase-sensitive imaging techniques which can be used to detect THz waves: Talbot imaging, Sagnac interferometry, phase contrast imaging, and polarization gating. The results show that polarization gating offers the best sensitivity and most reliable field quantification, while phase contrast imaging is best in situations requiring high spatial resolution. We also detect the THz phonon polariton waves in a 50 micrometer lithium niobate slab, which acts as a subwavelength, anisotropic planar waveguide. The spatial and temporal electric field profiles of the THz waves were recorded for different propagation directions using a polarization gating imaging system, and experimental dispersion curves were determined via a two-dimensional Fourier transform. Dispersion relations for an anisotropic slab waveguide were derived via analytical analysis and found to be in excellent agreement with all observed experimental modes. From the dispersion relations, we analyze the propagation-direction-dependent behavior, effective refractive index values, and generation efficiencies for THz-frequency modes in the subwavelength, anisotropic slab waveguide. In the end of the presentation, we will discuss how to use these techniques in the research of ultrafast optics, nonlinear phonon polariton, and the interaction of THz phonon polartion with material deposited on the crystal surface.

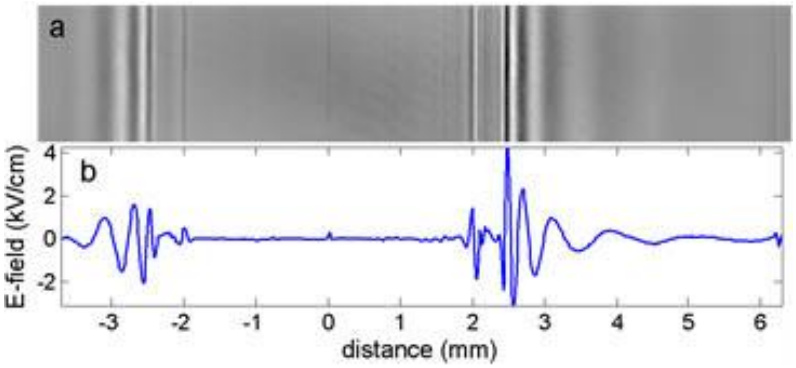

Fig. 1. (a) Image of a THz field in a 53-μm LN crystal slab 42 ps after excitation by a cylindrically focused pump pulse. The chirping of the pulse because of waveguide dispersion and the first three waveguide modes are apparent. (b) The field profile from (a), averaged over the vertical dimension. Initial field strengths are higher but dispersion quickly broadens the pulse and lowers peak field amplitudes.

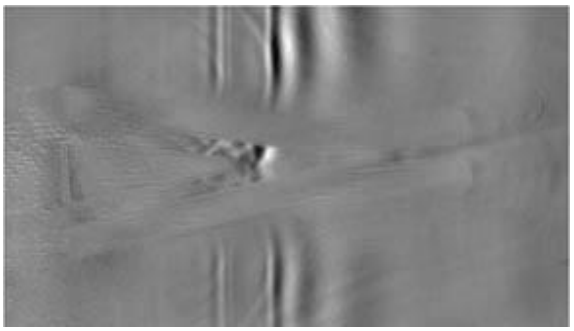

Fig. 2. The z-component of the THz E-field in a structured, 53 μm LN substrate.

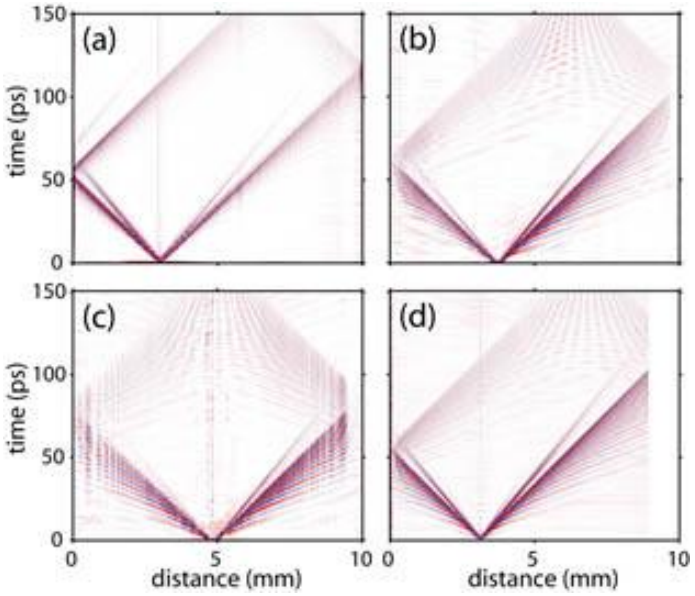

Fig. 3. Space-time plots from each imaging method showing a broadband THz wave propagating in a 50 um thick, 1 cm wide, unstructured LN slab. The color scale indicates the relative value of the electric field. (a) Talbot imaging. (b) Phase contrast imaging. (c) Sagnac imaging. (d) Self-compensating polarization gating imaging.

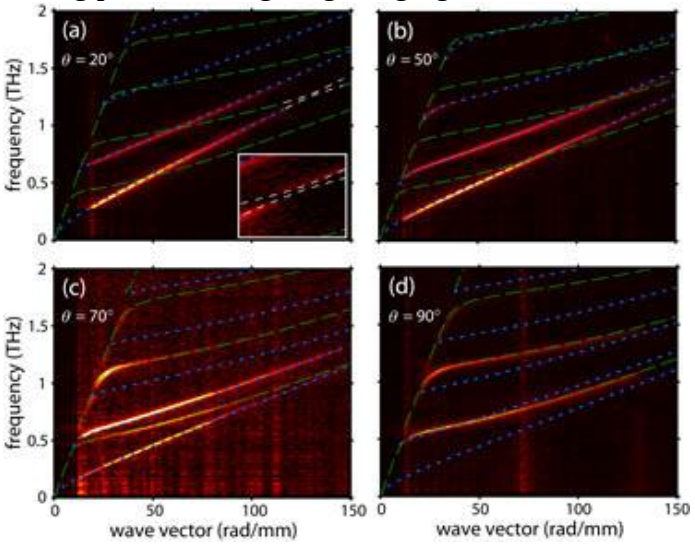

Fig. 4. (a) Dispersion curves for $\theta = 20°$. Blue dotted lines are calculated TE-like mode dispersion curves and green dashed lines are TM-like modes. Experimentally we see three TE-like modes and no TM-like modes. The white box in the lower right shows a blow-up of the region around an avoided crossing between the two lowest symmetrical modes. (b)

Dispersion curves for θ = 50°. In this case, TE-like modes still predominate and TM-like modes are too weak to be observed. (c) Dispersion curves for θ = 70°. We can see both TE- and TM-like modes, and all of the first 7 modes are observed experimentally. (d) Dispersion curves for θ = 90°, in which only the TM modes are excited. All the experimental data agree well with the calculated curves.

Bibliographic:

1. Q. Wu, C. A. Werley, K. H. Lin, A. Dorn, M. G. Bawendi, and K. A. Nelson, "Quantitative phase contrast imaging of THz electric fields in a dielectric waveguide", Optics Express, **l**, 9219 (2009).

2. C. A. Werley, Q. Wu, K. H. Lin, C. R. Tait, A. Dorn, and K. A. Nelson, "A comparison of phase sensitive imaging techniques for studying THz waves in structured $LiNbO_3$", JOSA B, **27**, 2350 (2010).

3. Y. Yang, Q. Wu, J. Xu, K. A. Nelson, and C. A. Werley, "Experimental and theoretical analysis of THz-frequency, direction-dependent, phonon polariton modes in a subwavelength, anisotropic slab waveguide", Optics Express, **18**, 26351 (2010).

NANO- AND MICROSCALE STRUCTURES SYNTESIS BY CONTROLLED LASER ACTION

S.M. Arakelian, S.V. Kutrovskaya, A.O. Kucherik, V.G. Prokoshev

Department of Physics and Applied Mathematics, Vladimir State University,
Gorky st. 87, Vladimir, 600000 Russia
Phone: +7(4922) 479621
Fax: +7(4922) 333369
E-mail: kucherik@vlsu.ru

Opportunity of formation of nanostructures on is one of most actively developing directions of laser physics. Development of the given direction is connected by dependence of properties formed nanostructures from parameters of laser radiation (length of a wave, duration of a pulse, the form of a beam). The modern laser systems allow to control of the laser radiation parameters and to generate nanostructures with the set properties.

In the given work the objects of research are the samples from glass carbon (GC), pirolitic graphite, spectral clean graphite, natural graphite. In the carried out experiments the dependences of morphological properties generated nanostructures from distance to the center of area of action are found out. It is shown, that mechanisms of their formation have the various character. Conditions of formation of melted carbon in the center of a laser cavity and precipitated from a gas phase layer behind its borders of area are fixed. Deposition's investigation of evaporated carbon on a surface of a cold substrate are presented. The investigation has been carried out at action to target by radiation of the continuous, nanosecond and femtosecond laser in various environments: atmospheric air, vacuum.

PHYSICAL AND MATHEMATICAL MODELLING OF CONTROLLED DEPOSITION OF PARTICLES FROM LASER-INDUCED PLASMA IN THE GASDYNAMICAL CHANNEL WITH THE SET GEOMETRY

A.A. Antipov, S.M. Arakelian, D.N. Buharov, N.N. Buharov, S.V. Kutrovskaya, A.O. Kucherik, V.G. Prokoshev

Department of Physics and Applied Mathematics, Vladimir State University,
Gorky st. 87, Vladimir, 600000 Russia
Phone: +7(4922) 479621
Fax: +7(4922) 333369
E-mail: kucherik@vlsu.ru

Introduction

Problems of controlled formation of extended files of nanostructures is actual [1-4]. On a background of many used methods, laser-plasma deposition have a some advantages: high selection of the size of particles, easy change of principal geometry, control of plasma propagation in external fields, etc.

In the given work the opportunity of control by process of deposition the particles ablated by laser radiation from surfaces of various targets (carbon of various density and a order degree, silver, the titan, nickel, aluminium, etc.) was investigated. The plasma propagation in dynamical channel with set geometry is organized. In this work is organized only hydrodynamic control, without particles interaction. The carried out experiments have shown an opportunity of selection of particles in the sizes and weights and obtaining of extended files of nanostructures with the set geometrical distribution.

Experiments of controlled plasma deposition

For creation micro- nanorelief with controlled topology the following experimental schema (see fig.1) was used. The plasma torch generated by continuous fiber laser λ=1.06 μm, power of radiation consist 10-30W, laser spot on the surface of target is 30 μm, thus intensity of laser radiation is 10^5 W/sm^2.

At distribution of particles to such geometry of the channel we expect, that easy and heavy particles will be separated in space. Easy particles will be distributed more distance, than heavy which will deposit closer to the center of substrate. Easy particles will be propagate on the channel formed a substrate and metal layer.

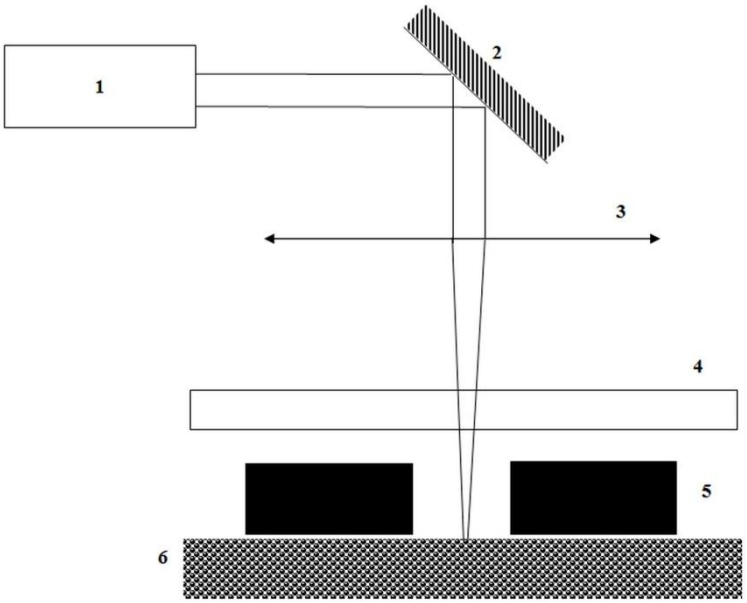

Fig. 1. . The scheme of control vapour deposition in layered structure. 1 – laser; 2 - a rotary mirror; 3 - objective; 4 - cold substrate; 5 – metal layer; 6 - target.

In series of experiments was made deposition of carbon particles from a plasma erosive torch on a surface of a cold substrate in air. The stream of particles was separated at approach a substrate by a metal layer which settled down closely between a sample and a substrate [5]. For separate particles an metal disk with various thicknesses was used. The results of deposited of particles with lost speed are shown on fig. 2. Time of deposition is 20s, thickness of a metal layer – 5mm. In zone of metal layer elements of image form are original "labyrinth" are observed (see fig. 2a). It is necessary to notice, that the height of the branching tubes is about 20nm, and thickness of separately worth structures changes from 100 to 300nm. Outside a metal layer distribution of deposited layer is stratified by domain structure (see fig. 2b.).

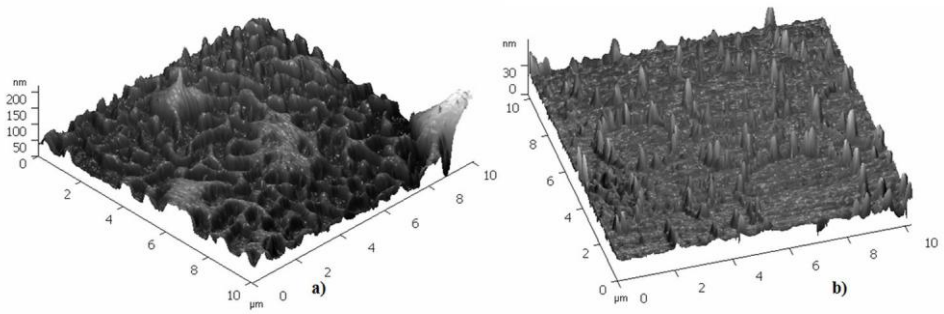

Fig. 2. The AFM image of a surface of deposited layer: a) in zone of metal layer; b) outside a metal layer

The mathematical models

Possibilities of mathematical modelling - modelling of movement of ablated products and process of their deposition on a substrate have been used for this purpose. The most simple and convenient way of modelling of movement of products laser ablation is using hydrodynamic model [6, 9]. The model based on principles of molecular dynamics has been used as a first approximation developed. For the description of process of deposition and allowing to define point co-ordinate in which particle sticking to a substrate is possible. By means of this model it is possible to receive estimations of the basic characteristics of a formed film.

In the frame of this work the calculations in the channels where in settlement area there is one entrance section and exits(fig. 3) have been carried out.

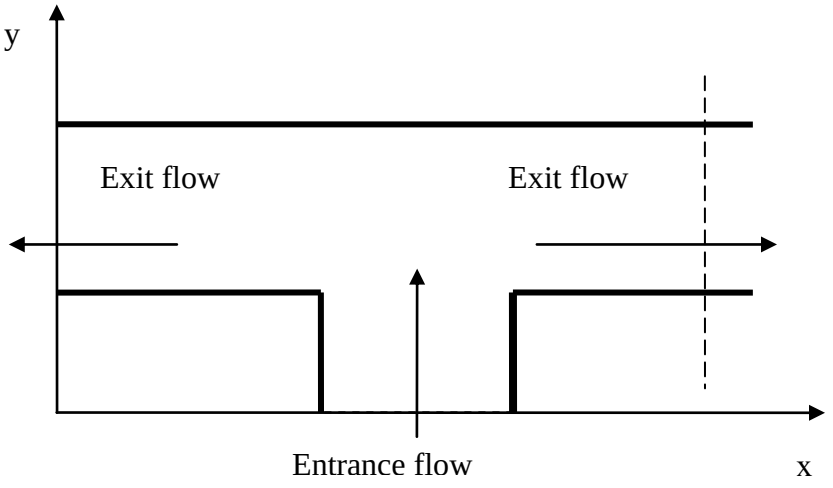

Fig. 3. Geometry of settlement area

The hydrodynamic model of distribution of products of laser ablation is described by stationary equations Navier-Stokes for a problem with flat geometry. [3] Mathematical model represents as system of the dimensionless equations for flow function and a circle.

$$\frac{\partial \Psi}{\partial y}\frac{\partial \omega}{\partial x}-\frac{\partial \Psi}{\partial x}\frac{\partial \omega}{\partial y}=\frac{1}{Re}\left(\frac{\partial^2 \omega}{\partial x^2}+\frac{\partial^2 \omega}{\partial y^2}\right)$$

$$\frac{\partial^2 \Psi}{\partial y^2}+\frac{\partial^2 \Psi}{\partial x^2}=-\omega$$

$$\frac{\partial \Psi}{\partial y}=\upsilon_x, \quad -\frac{\partial \Psi}{\partial x}=\upsilon_y$$

At construction of numerical model the uniform grid was used. The finite-differ equations for decision definition in grid knots are received on a five-dot template. The differ

scheme approximates an initial problem with the second order concerning grid steps. The equations for a whirlwind are received on the basis of an integrated method so the differ scheme is conservative.

The important feature of the scheme is monotony that provides its stability without special restrictions on size of steps of a grid. The system of the equations concerning values of the decision in grid knots dares a relaxation method.

The Boundary conditions on entrance and target border represent exact values, proceeding from corresponding values for Poisele flow. On walls of the channel of value of function of a flow are set precisely Ψ =0 for the bottom wall and Ψ =1 - for top, that will be coordinated with the task of boundary conditions for entrance and target border of a stream. As each firm wall is a flow line for the correct task of boundary conditions it is necessary to make additional assumptions of flow parametres. Such assumption can be formulated proceeding from the law of preservation of weight which in this case is reduced to the statement: the sum of expenses through target sections is equal to the expense through entrance section, $q_{ent} = q_{ext1} + q_{ext2}$.

The molecular-dynamic model of process of deposition is system of the dimensionless equations of Newton, and for the account of interactions between besieged atoms and atoms of a substrate Lennard-Jhones potential [7] is used.

Dynamics of particles is described by the dimensionless Newton movement equations.

$$\frac{du}{dt} = \sum\left(\frac{1}{r_i}\right)^7\left(2\left(\frac{1}{r_i}\right)^6 - 1\right)\frac{(x - x_i)}{r_i}$$

$$\frac{d\upsilon}{dt} = \sum\left(\frac{1}{r_i}\right)^7\left(2\left(\frac{1}{r_i}\right)^6 - 1\right)\frac{y}{r_i}$$

$$\frac{dx}{dt} = u, \quad \frac{dy}{dt} = \upsilon,$$

$$x(0) = x_0, \quad y(0) = y_0, \quad u(0) = u_0, \quad \upsilon(0) = \upsilon_0.$$

Where x, y - coordinates of moving atom, u, υ - projections of speed of atom to axes 0x and 0y respectively, $r = \sqrt{(x - x_i)^2 + y^2}$ Distance between atom from a stream of besieged substance and i atom of a substrate.

The mathematical model of process of deposition represents Koshi problem for system of the ordinary differential equations, describing movement of besieged atom. In considered model the “leap-frog” method[10] is used.

The considered scheme is implicit, therefore the step on time is necessary for choosing taking into account a stability condition - Thus on a grid step restriction in a kind $\tau\omega_{max} \leq 2$, where ω_{max} - the maximum frequency of modelled system is imposed.

For considered above channel geometry there are reliable enough experimental data on deposition of molecular carbon C_2 on a glass substrate. In figure 4 the channel geometry is shown, and the characteristic sizes in relative units have following values: $d_1=1$, $d_2=0,1$, $l=0,5$. The film is formed in the form of a ring with internal radius $r_1=0,1$ and $r_2=0,5$.

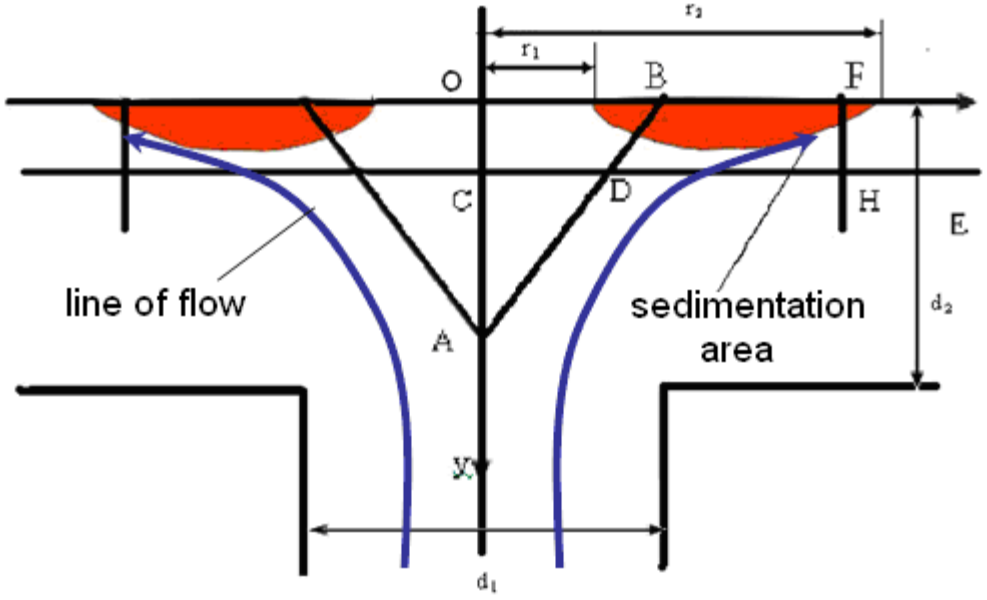

Fig. 4. Experiment geometry

Non-uniform deposition of ablated products , apparently, speaks a substrate non-uniform distribution of concentration of molecular carbon in a zone from which deposition is possible. For construction of this zone a series of calculations of a flow for various values of number of Reynolds is spent. Thus Re varied in a range 10÷1000, that approximately corresponds to experiment conditions (fig. 5).

The analysis of results of calculation of hydrodynamic model shows, in the central area of the channel there is an area in which speed of a flow on one, two order is less than speed of an entrance stream.

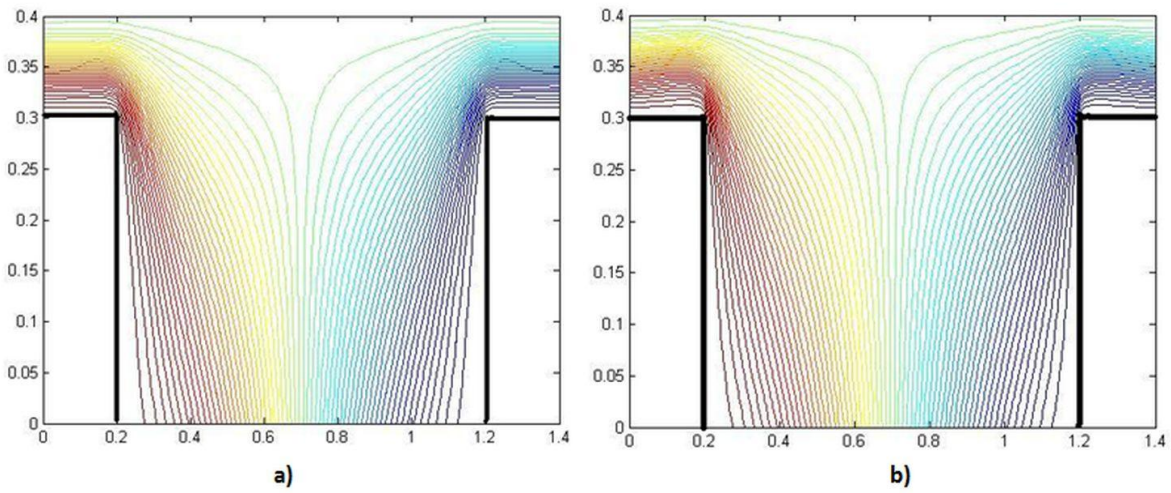

Fig. 5. The example of calculation of stream: a) h_{entr}=1, h_{entr1} = $h_{вых2}$=0,1 q_{ext1}=q_{ext2}=0,5, Re=10; b) h_{entr}=1, h_{ext2} = h_{ext2}=0,1 q_{ext1}=q_{ext2}=0,5, Re=100

As in this area movement practically is absent, it turns out, that concentration of products of deposition here is insufficient that there was an appreciable deposition (fig. 5).

As a first approximation it is possible to consider, that the border of this area passes through points, in which speed 10 times less speeds of an entrance stream. In figure 4 this border passes on straight line AB. In process of removal from this border in a direction to target section speed of a flow increases, so the maximum speed of target section in 5 times surpasses the maximum speed of entrance section. As a first approximation it is possible to consider, that concentration of products абляции as decreases in this direction and, therefore, as the second border of area of deposition it is possible to accept a line, on which speed of a flow 10 times less speeds of a flow in target section. As the nobility suffices for calculation of process of deposition this border in the field of a substrate for its construction it is possible to use the information in several knots of settlement area. In figure 2 this border corresponds to straight line FH.

Results of calculations of a zone of deposition for various values of number of Reynolds (Re) are resulted in table 1.

Table 1.

Deposition zone at Reynolds's various numbers

Re	AO	OB	OF	BF
1	0,10	0,22	0,40	0,18
10	0,08	0,21	0,40	0,19
50	0,07	0,15	0,37	0,22
100	0,06	0,12	0,36	0,23
500	0,05	0,07	0,27	0,20
1000	0,05	0,06	0,25	0,19

From the table it is visible, that with increase in number of Reynolds the deposition zone moves to the substrate centre that should lead to reduction of internal radius of a film. Thus the width of a zone changes a little, however concentration of ablation products with increase in the module of speed of a flow should decrease, that should lead to reduction of a thickness of a film.

Deposition of molecular carbon in the given point of a substrate grows out of interaction of atoms of a substrate with a molecule. At the big distances of force of interaction are insignificant, therefore in deposition models it is accepted to limit a zone of deposition in distances in some tens internuclear distances, characteristic for interaction potential. In figure 2 corresponding border of a zone of deposition is presented straight line CE. In calculations zone height from which probably deposition changed from 2 to 50 internuclear distances. Film formation occurs far from substrate border, therefore, considering rather small radius of action of forces, it is possible to assert, that influence is symmetric concerning the located particles of a substrate should be identical. It is possible to assert, that at the big distances from a substrate the longitudinal component of speed of a molecule practically does not change, and consequently the moving projection on 0x basically is defined by time of approach of a molecule to a substrate.

For definition of the basic characteristic of model of deposition - time of deposition of a molecule for a substrate, a series of calculations has been spent. Thus for potential interaction were used given corresponding to carbon [7]. On the basis of these data scale or basic sizes have following values: $l_b=3\cdot10^{-10}$ m, $t_b=10^{-12}$ with, $\upsilon_б=500$ km/s. Distance between atoms of a substrate are accepted equal to equilibrium value, i.e. lat=r_0. Results of calculations are tabulated.

Table 2. Results of calculations of deposition

	$u_0=0$, $\upsilon_0=0$	$u_0=1$, $\upsilon_0=0$	
y	t_0	Δx	t_1
2	9,10	9,10	9,10
3	$3,91\cdot10^{1}$	$3,91\cdot10^{1}$	$3,92\cdot10^{1}$
4	$1,08\cdot10^{2}$	$1,08\cdot10^{2}$	$1,08\cdot10^{2}$
5	$2,36\cdot10^{2}$	$2,36\cdot10^{2}$	$2,36\cdot10^{2}$
10	$2,70\cdot10^{3}$	$2,70\cdot10^{3}$	$2,70\cdot10^{3}$
15	$1,15\cdot10^{4}$	$1,14\cdot10^{4}$	$1,14\cdot10^{4}$
20	$3,32\cdot10^{4}$	$3,33\cdot10^{4}$	$3,33\cdot10^{4}$
25	$7,65\cdot10^{4}$	$7,65\cdot10^{4}$	$7,65\cdot10^{4}$
30	$1,53\cdot10^{5}$	$1,51\cdot10^{5}$	$1,51\cdot10^{5}$
40	$4,56\cdot10^{5}$	$4,56\cdot10^{5}$	$4,56\cdot10^{5}$
50	$1,11\cdot10^{6}$	$1,09\cdot10^{6}$	$1,09\cdot10^{6}$

The first column of table 2 sets relative initial distance from a moving molecule to a substrate (y), the second - relative time of deposition at zero initial speed (t_0), the third - a projection of moving of a molecule to an axis x at $u_0=0$, $\upsilon_0=0$, the fourth - deposition time at $u_0=1$, $\upsilon_0=0$. The analysis of data from the table shows, that at y> 2 and υ =0 moving of a moving molecule along a substrate can be defined under the simple formula $\Delta x=u\cdot t_0$.

At carrying out of calculations the size of the maximum value of vertical making speed of a molecule also was supervised. y=1,5 $\upsilon_{max}=0,28$, at y=2 it is had $\upsilon_{max}=0,34$, at y=4 $\upsilon_{max}=0,35$. For values y from 4 to 50 size υ_{max} differs from 3,5 less than on 1 %. From here follows, that «effective dispersal» molecules under the influence of considered forces really occurs on distances from a substrate in some internuclear distances. Nevertheless, the model works and for the big distances as calculations show, that small accelerations as a result lead to deposition that speaks about steady work of the program. Therefore it is possible to assert, that computing errors which can collect and influence, generally speaking, result of calculations at a considerable quantity of steps of algorithm, in our case do not lead to essential distortions of results of calculation.

For definition of width of a film it is necessary to have the information on height of a zone of deposition (y_{max}) and distribution of speeds of molecules. Then on the basis of calculations under the deposition program it is possible to receive sample of values Δx, average value on which will allow to define change of width of the film, caused by movement of molecules at deposition.

As the information on distribution of speeds is absent now, it is possible to receive only rough estimates of width of a film, proceeding from simple estimations of moving $\Delta x=u\cdot t_0$. If y_{max} lays in a range 30÷40 for u=1 molecule moving belongs to a range 40÷110 (micron). Taking into account a zone of deposition for Re=50 at $y_{max}=30$ following values of parametres of width of a film r_1=150-40=110 (micron), r_2=370+40=410 (micron) turn out. For $y_{max}=40$ following values r_1=10 (micron), r_2=510 (micron) similarly turn out. These two variants in our opinion is better correspond to experimental data, for which $r_1\approx100$ (micron), $r_2\approx500$ (micron). Thus, it is possible to tell, that the developed model with sufficient reliability models real systems and can be used for an estimation of character of position of a film as a first approximation.

Conclusion

In given article the first results on creation carbon micro and nanostructures with controlled topology are presented. The control of process of deposition is organized at change of geometry of the channel in which plasma is propagated. For modeling process of plasma

distribution the mathematical model stationary flow of a viscous incompressible liquid in the infinite channel formed by horizontal surfaces is considered. Flow are described by stationary equations Navier-Stokes for a task with planar geometry. The mathematical model represents system of the dimensionless equations for function of a flow and a vortex. At construction of numerical model the uniform grid was used. The dependence of flow condition from geometry and velocity are presented. We modeling the interaction between the particles in plasma and between the plasma particles and atoms of substrate. The principal experiments of formation micro- nanostructures have been carried out.

References

1. Andrievskii R.A., Ragulya A.V. Nanostrukturnye materially: Nanostructural Materials. A Textbook for Students, Moscow: Izd. Tsentr`Akademiya', 2005.
2. Lozovik Yu.V., Popov A.M. Usp. Fiz. Nauk, 167, 151 (1997).
3. Suzdalev I.P. Nanotekhnologiya: Fiziko-khimiya nanoklasterov, Nanotechnology: Physics and Chemistry of Nanoclusters, Nanostructures and Nanomaterials,, Moscow: KomKniga, (2006).
4. Gusev A.I. Nanomaterials, Nanostructures and Nanotechnologies, Moscow: Fizmatlit (2005).
5. S.M. Arakelian, M.N. Gerke, S.V. Kutrovskaya, A.O. Kucherik, V.G. Prokoshev Quantum Electronics 38 (1) 73 -76 (2008)
6. Bordovsky A, etc. Physical bases of mathematical modeling/A.Bordovsky, A.S.Kondratyev, A.D.R. Choudery. - Moskow: publishing centre "Academy", 2005. - 320 p.
7. Zaliznjak V. E. Bases of computing physics. A part 2. Introduction in methods of particles. - Moscow - Izhevsk: Regular and chaotic dynamics: Institute of computer researches, 2006. - 156 p.
8. Lojtsjansky L.G. Mechanics of a liquid and gas. - Moskow: Drofa, 2003. - 840 p.
9. Morozov A.I.introduction in plasmadynamics. - Moskow: Fizmatlit, 2008. – 616 p.
10. Zvetkov I.V. Application of numerical methods for modelling of processes in plasma: the manual. Moskow: MEPhI, 2007. - 84 p.

ALL-FIBER OPTICAL MODULATOR FOR CONTROL THE OPTICAL PHASE OF LASER RADIATION

Koliada N.A., Nyushkov B.N.

Institute of Laser Physics, the Siberian Branch of the Russian Academy of Sciences
Novosibirsk, Russia
Ph: +7 (383) 333-21-27, e-mail: n.koliada@mail.ru

The aim of the work was the development of the device to ensure the effective phase modulation in optical fiber systems. The phase modulator should work in a wide wavelength range, make a negligible optical loss and be insensitive to the state of the input polarization. Modulator should have a simple and reliable design. Such modulator can be used as a part of optical phase locking loops in fiber laser frequency synthesizer, and as an active mode-locker in long-cavity fiber lasers. Creation a compact optical frequency synthesizer based on the fiber laser offers great opportunities for metrology [1], satellite navigation, communication, etc.

We propose a novel all-fiber optical phase modulator based on the electristrictive effect. The modulator employs a standard telecom fiber tightly clamped with specially designed electrodes. Its working principle is based on the optical-path-length change induced for light guided in the fiber subjected to electrostriction. The modulator is driven by a high-voltage electric signal. The half-wavelength voltage is about 80 V. The experimentally proved modulation frequency bandwidth is nearly 60 kHz.

Though some experimental studies of electrostriction effect in optical glasses and fibers have been already done in works [2, 3], there are no reports on the practical design application of all-fiber optical modulators. Our all-fiber phase modulator includes: cylindrical dielectric substrate; first conductive plate (a foil, a thin strip or a film of a material with high electrical conductivity) that is fixed on lateral surface of the dielectric substrate; the optical fiber that wound tightly over the foil; and the second conductive plate tightly fixed over the fibers. Modulated optical signal propagates in coiled fiber and the control voltage is applied to the plates.

Thus, modulation of the optical path is carried out in a long segment of single-mode optical fiber, placed between two external electrodes (plates), and applying a voltage to that a strong electric field is created inside the fiber. Due to the phenomenon of electrostriction, the size and density of the optical fiber material slightly modify in the segment located between the metal plates of an electric field. As a result, the laser radiation becomes phase modulated at the modulator output. At a sufficiently large fiber length (from several meters to several tens of meters) enough depth of modulation can be achieved for practical use.

It is also possible the implementation of this modulator in different configurations, for example with an electrically conductive cylindrical substrate. In this case, no need to use a first conductive plate, the substrate plays its role. The geometry of the substrate may also be varied; it may not only be solid or hollow cylinder but the ring, ellipse, etc. The material, geometrical shape and size of the substrate, the area of the plates, the amplitude of the applied voltage, the length and the type of fiber between the plates determine the sensitivity, the maximum depth and frequency modulation.

Cylindrical glass-cloth laminate and stainless steel substrate with different diameters (32 to 100 mm) were used in experiments. Standard telecommunication single-mode fiber SMF-28e with lengths ranging from 2.8 to 15.7 m was studied. Copper and aluminum foil was exploited as the metal plates.

To test the all-fiber phase modulator the fiber Mach-Zehnder interferometer was designed. Figure 1 shows the spectrum of the signal with an interferometer for one of the configurations of the modulators (the substrate is glass-cloth laminate, the SMF-28e fiber length is 2.8 m, the variable voltage frequency is 10.6 kHz, it's amplitude is 184 V). Single-frequency diode laser radiation with a wavelength of 1.52 micrometers was modulated.

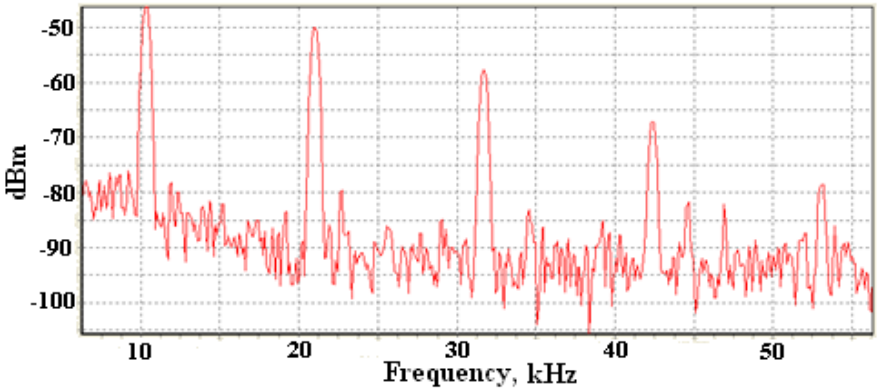

Fig.1. Spectrum of the signal with a fiber Mach-Zehnder interferometer for one of the configurations of the all-fiber modulators (the substrate is glass-cloth laminate, the SMF-28e fiber length is 2.8 m, the variable voltage frequency is 10.6 kHz and it's amplitude is 184 V)

All-fiber modulators have been introduced into the cavity of a mode-locked fiber laser also (Er fiber laser with linear resonator with a pulse repetition rate of 14,3 MHz at 1,55 μm). Applying an alternating voltage to the plate of the modulator the sideband amplitude was studied. Figure 2 shows one of the radio frequency intermode beat spectrums (second harmonic) for the modulator with the characteristics mentioned above. The narrow sidebands are

clearly visible. Figure 2 was obtained at a modulation frequency is about 200 Hz, the amplitude of the control voltage applied to the plates is 70 V.

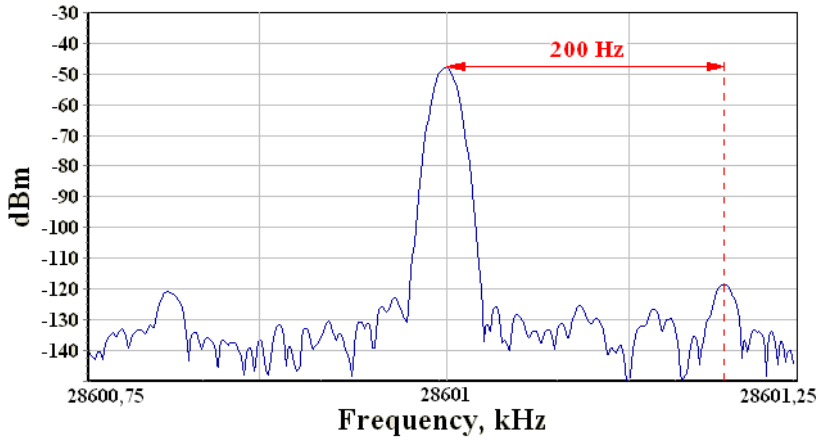

Fig.2. Radio frequency intermode beat spectrum of the mode-locked Er fiber laser. Modulation frequency is about 200 Hz, the amplitude of the control voltage applied to the plates is 70 V.

Thus, all-fiber optical modulator having a very simple design was developed. It is possible to use most every type of optical fibers (including conventional telecommunication fibers). The modulator can effectively perform continuous dynamic control (modulation) of phase of the laser radiation, regardless of the state of polarization, while making a negligible optical loss. It is also possible to increase the depth of phase modulation by increasing the fiber length.

Bibliographic

F. Adler, K. Moutzouris, A. Leitenstorfer, H. Schnatz, B. Lipphardt, G. Grosche, and F. Tauser, “Phase-locked two-branch erbium-doped fiber laser system for long-term precision measurements of optical frequencies”, Opt. Express, Vol. 12, N 24, pp. 5872-5880 (2004)

E. L. Buckland and R. W. Boyd, ‘‘Measurement of the frequency response of the electrostrictive nonlinearity in optical fibers,’’ Opt. Lett. 22, 676–678 (1997)

A. Fellegara, A. Melloni, and M. Martinelli, ‘‘ Measurement of the frequency response induced by electrostriction in optical fibers,’’ Opt. Lett. 22, 1615–1617 (1997)

FROM NANO- TO TERA-: APPLICATIONS OF THE TERAHERTZ RADIATION FOR STUDIES OF ARTIFRITIAL MATERIAL NANOSIZE STRUCTURES

Alexander Shkurinov, Maxim Nazarov

Department of Physics and International Laser Center,
M.V.Lomonosov Moscow State University**.**

Anatoly Khodan, A.N.Frumkin

Institute of Physical Chemistry and Electrochemistry RAS

We present and we study in terahertz range a new porous materials made from nanostructured alumina oxyhydroxides (NAO). Analysis of the experimental results obtained with the raw, annealed, and chemically modified NOA samples show potential application of such materials for development light driving terahertz devices in the form of photonic band gap (PBG) and low loss holey waveguides. We report the studies of dielectric properties in the terahertz frequency range of different types of water molecules existing in the bulk, structural or interfacing forms in the nanostructured alumina oxyhydroxide (NAO).

Metamaterials can be used for obtaining the optical properties "on-demand". This study was focused on NOA based materials possessing very low density ~ 0.04 g/cm^3), high specific surface area (300 – 800 m^2/g) and fine fibrous structure [1]. The particular interest of this work was terahertz properties of porous NOA samples after physical and chemical treatment . The chemical modification by using gaseous or liquid absorption at the NAO surface allows predictable changes in the optical properties. The preliminary results of the studies of the native, thermally treated and chemically modified NAO in the terahertz frequency range are presented. The first application of NAO based materials for photonic band gap (PBG) and a waveguide application was demonstrated. We also report an attempt to use NOA based composites with TiO_2 and ZrO_2 nanocrystals for making light driving terahertz devices.

The synthesis of NAO is based on selective oxidation of the surface of liquid alloys in a humid atmosphere at temperature range from 20 up to 70 ºC [1]. Two synthesis methods using the Hg alloys and the Ga alloys are used. The structure of NAO consists of the three-dimensional network of amorphous nanofibrils with diameter ~ 5 nm, having the composition $Al_2O_3 \cdot nH_2O$, n = 1 – 4. The NAO annealing in the temperature range 900 – 1700 °C does not destroy the solidity and the porous structure of the samples, but the linear sizes of the samples isotropically decrease; the density increases from 0,02 up to 3 g/cm^3; the porosity and the specific surface area decreases from 99,3 to 25 % and from 800 to 1 m^2/g respectively.

The THz absorption spectra of native NOA material exhibit low absorption with the nearly n=1 refraction index value. The two dimensional PBG structure of NAO sample is shown on the insert to the figure. Depending on the angle of incidence the terahertz transmission spectra of the NAO based PBG sample may demonstrate a clear dip which corresponds to the forbidden regime of the THz wave propagation (solid line) or the good waveguiding properties (dashed line). The depth, width and the quality of the frequency “forbidden” and “propagation” zones can be varied by the modification of the sample such as thermal treatment and chemical modification. By using numerical simulation [3], the THz waveguide and transmission properties of NAO are studied. The structure of NAO is simulated by set of alternate layers. One of them is homogeneous, and another one corresponds the 1D grating

The essential part of the work is concerned with the detection of OH^- and H_2O molecules absorbed on the NAO surface and bonded inside phase structure. At room temperature the NAO structure consists of amorphous nanofibrils of aluminum oxihydroxide with composition $Al_2O_3 \cdot 3.6H_2O$. In the work the possibility of the detection and separation of the different state of OH^- and H_2O molecules are discussed. We show for the first time the THz detection of molecular monolayers at the NAO surface and also the properties of NAO composites with TiO_2 and ZrO_2 nanocrystals and we observed the real-time condensation and desorption of the atmospheric water on and out of the NAO surface.

REFERENCES

[1] T. di Costanzo, A. A. Fomkin, C. Frappart, A. N. Khodan, et al, Mater. Sci. Forum **453-454**, 315 (2004).
[2] N. N. Brandt, A. Yu. Chikishev, A. V. Kargovsky, et al, N. V. Sumbatyan, Vibrational Spectroscopy, **47**,53 (2008).
[3] Andreev A.V., Korneev A.A., Mukina L.S. et.al //Phys.Rev. B. 2006 V.74 P.235421

CONJUGATED POLYMER COLLOID-BASED SOFT SEMICONDUCTORS TOWARD NEXT-GENERATION ORGANIC OPTOELECTRONIC MATERIALS

Ling-Hai Xie*, Wei Huang

Key Laboratory for Organic Electronics & Information Displays (KLOEID), Institute of Advanced Materials (IAM), Nanjing University of Posts and Telecommunications, 9 Wenyuan Road, Nanjing 210046, China
Email: iamlhxie@njupt.edu.cn; wei-huang@njupt.edu.cn;

Abstract: Combination of organic synthesis with supramolecular assembly technique afford powerful platform to explore advanced optoelectronic materials. The principle of supramolecule-functionalized π-conjugated polymers (SFCPs) has been proposed to design versatile π-conjugated precursors for self-assembly without surfactants. The modeling precursor of polyfluorene-based tertiary alcohol (PPFOH) via the Yamamoto polycondensations exhibited excellently hierarchical self-assembly behaviors to achieve a series of robust and high-quality supramolecular nanoparticles and colloidal microgels over a broad size range through the solvent evaporation or reprecipitation according to the characterization of SEM and TEM. PPFOH exhibit abundant colors and various wavelengths of light dependent on the size of colloids. Preliminary polymer nanostructure-based light-emitting devices (PNLEDs) with the configuration of Au/*p*-type SiC/ nanosphere films/ ITO have been fabricated to give a white emitting color with a turn-on voltage of 25 V. Conjugated polymer-based supramolecular nanoparticles (CPSNs) will have potential polymer soft semiconductors (PSS) in the areas of printed electronics, organic optoelectronics, photonic crystals, mechanoelectronics as well as spinelectronics.

POLARIZATION DEPENDENCE OF NONLINEAR OPTICS IN ISOTROPIC MEDIUM

Xiao-Qing Yan, Zhi-Bo Liu, Jian-Guo Tian

The Key Laboratory of Weak Light Nonlinear Photonics, Ministry of Education, Teda Applied Physics School, Nankai University, Tianjin 300457, China
Tel: +86-022-66229449; Email: yanxiaoqing@mail.nankai.edu.cn

The polarization dependence of nonlinear optics (nonlinear refraction, nonlinear scattering and nonlinear absorption) in isotropic medium is present [1-2]. The physical mechanisms for polarization dependence are systemically analyzed. Throughout this talk, we will focus on polarization state (linearly, elliptically and circularly polarized) and nonlinearity [3-4]. The details are described as follows:

The dependence of nonlinear refraction on polarization state of incident beam in four solvents (CS_2 (Fig.1), toluene, N,N-dimethylmethanamide (DMF) and o-dichlorobenzene (ODCB)) is studied at 800 nm by using femtosecond (fs) pulses polarized lights Z-scan method [5]. The nonlinear refractive index decreases with the ellipticity of polarization ellipse. Because the polarization state could control the contribution of $\mathrm{Re}(\chi^{(3)}_{xyyx})$ to nonlinear refractive index n_2. Then, we calculate the values of susceptibility components for the four solvents. From the ratio of $\mathrm{Re}(\chi^{(3)}_{xyyx})$ to $\mathrm{Re}(\chi^{(3)}_{xyxy})$, we can conclude that both nonresonant electron and fast non-instantaneous nuclear contribute to the third-order nonlinear susceptibility.

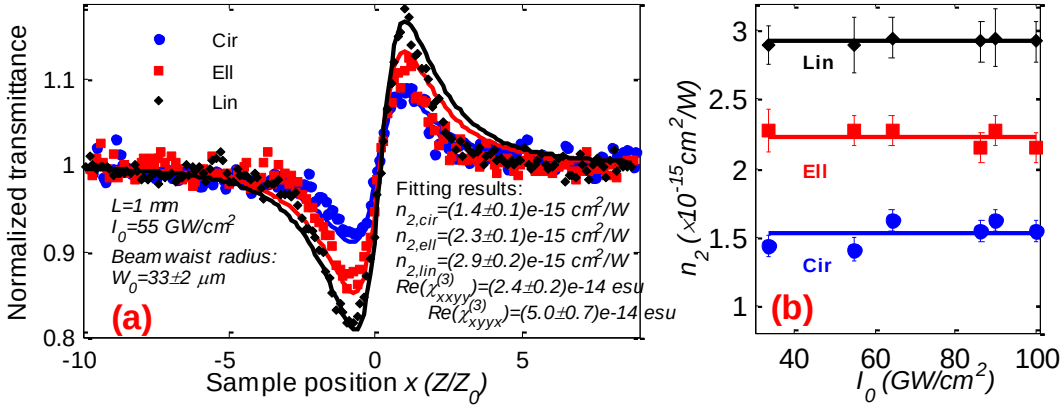

Fig. 1. (a) CA Z-scan traces of different polarized lights and theoretical fitting curves at 55 GW/cm^2. (b) The dependence of n_2 on I_0 and polarization state.

By using polarized light open-aperture (OA) Z-scan method at 800 nm, the dependence of nonlinear scattering on polarization state and sample length in above four solvents is studied. At the same pulse energy, the intensity of nonlinear scattering decreases with the ellipticity of polarization ellipse, or increases with sample length. The energy threshold of nonlinear scattering also depends on polarization state and sample length. The dependence is re-

lated to self-focusing effect. As we know, the nonlinear refractive index decreases with ellipticity, so the self-focusing effect (also, peak light intensity) decreases with ellpticity. If the intensity threshold for nonlinear scattering is the same, we could understand the dependence of nonlinear scattering on polarization state and sample length. When the nonlinear scattering is studied using OA Z-scan method, the shape of Z-scan traces is different for the four solvents, and it may be determined by the viscosity.

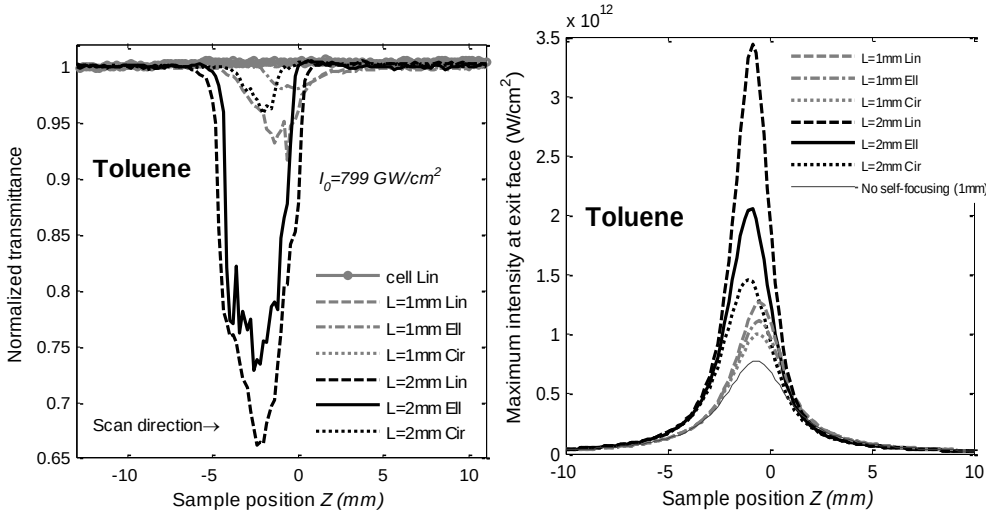

Fig. 2. (Left) The nonlinear scattering signal against sample position for different polarization and sample length; (Right) the peak intensity of exit beam at the surface of sample against sample position for different polarization and sample length from simulation.

The nonlinear absorption of DMF and toluene at 400 nm are studied by fs polarized lights Z-scan method (Fig. 3). The intensity of nonlinear absorption decreases with the ellipticity of polarization ellipse. The OA Z-scan traces of the two solvents could be fit by two-photon absorption (2PA) model at low intensity, however, the traces could not be well dealt with two-photon absorption model at high intensity. And nonlinear absorption coefficient from 2PA model fitting increases with intensity for all polarized lights. The time-resolved degenerate pump-probe experiment shows that the nonlinear absorption is instantaneous. The polarization characteristic of nonlinear absorption might origin from the dependence of self-focusing effect (which could increase the nonlinear absorption) on polarization state, as the dependence of nonlinear scattering on polarization state.

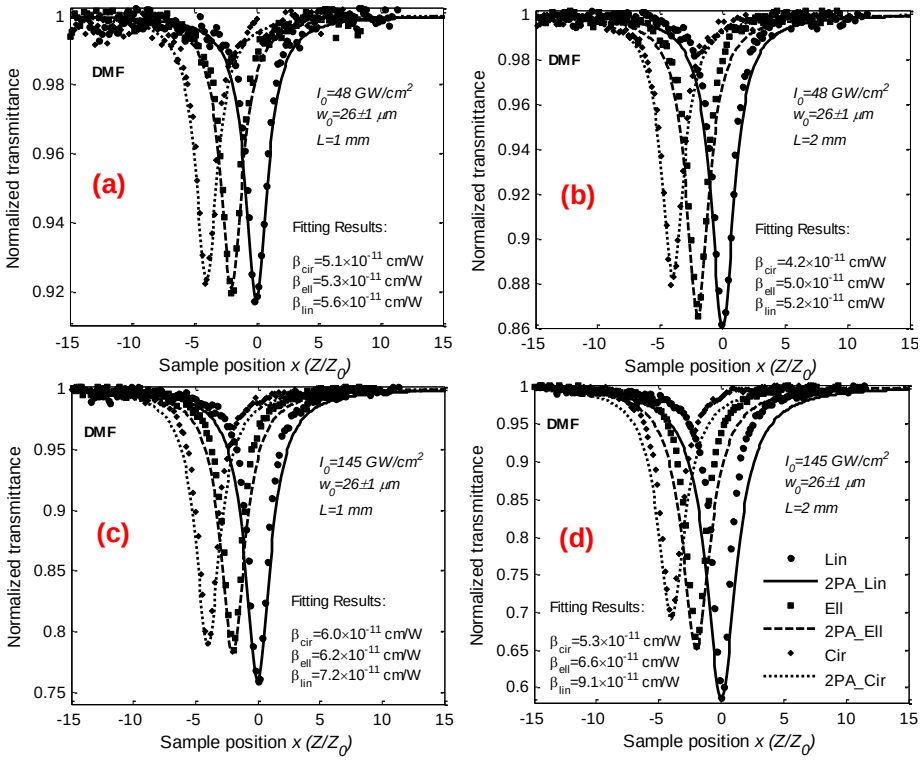

Fig. 3. The dependence of open-aperture Z-scan trace on polarization for different intensity and sample length.

From the study, we find that the nonlinearity of isotropic medium is a function of polarization state. So, it could be a simple way to control continuously the nonlinearity of isotropic medium by modifying the polarization state of incident beam.

References

1. M. Lefkir, X. Nguyen Phu, G. Rivoire, "Existence of a bistable polarization state in a Kerr medium in the presence of two-photon absorption," Quantum Semiclass. Opt. **10**, 283-292 (1998).

2. S. Polyakov, F. Yoshino, and G. Stegeman, "Interplay between self-focusing and high-order multiphoton absorption," J. Opt. Soc. Am B 18, 1891 (2001).

3. R. L. Sutherland, *Handbook of Nonlinear Optics* (Marcel Dekker Inc, New York, 1996).

4. R. W. Boyd, *Nonlinear Optics*, 2nd ed. (Academic Press, San Diego, 2003).

5. X.-Q. Yan, X.-L. Zhang, S. Shi, Z.-B. Liu, and J.-G. Tian, "Third-order nonlinear susceptibility tensor elements of CS_2 at femtosecond time scale," Opt. Express 19, 5559-5564 (2011).

AN EFFICIENT DUAL-WAVELENGTH ND,GD:YSGG LASER

Kai Zhong[1,2*], Jianquan Yao[1,2] , Chongling Sun[1,2] , Degang Xu[1,2], Qingli Zhang[3] , Dunlu Sun[3], Shaotang Yin[3]

[1]College of Precision Instrument and Opto-electronics Engineering, Tianjin University, Tianjin 300072, P. R. China,

[2]Key Laboratory of Opto-electronics Information Technology (Tianjin University), Ministry of Education, Tianjin 300072, China

[3]Anhui Provincial Key Laboratory of Photonic Devices and Materials, Anhui Institute of Optics and Fine Mechanics, Chinese Academy of Sciences, Hefei 230031, China

**Corresponding author. Tel: 0086-22-27406436, E-mail address: zhongkai1984@gmail.com*

The trivalent Neodymium ion (Nd^{3+}) doped garnet crystals (for example, Nd:YAG) have been regarded as the most excellent laser materials, because of their good physical characteristics and laser performance. With the development of laser diodes, compact and high-efficiency Nd^{3+}-doped garnet lasers have been developing rapidly with the convenience of pumping around 808 nm. Besides the well-investigated red, green and blue lasers generated by frequency doubling of their 1.3x μm, 1.06x μm and 0.9 x μm laser lines, most fundamental lasers used in frequency conversion to the deep-violet to far-infrared, even the terahertz region are Nd:YAG lasers. The other Nd^{3+}-doped garnet crystals, such as Nd:GGG[1], Nd:YGG[2], Nd:GSGG[3], Nd:GSAG[4], Nd:YSGG[5], etc, are also very good laser materials, with some of their properties even better than Nd:YAG. Replacing part of the Yb^{3+} ions with Gd^{3+} in Nd:YSGG, another kind of garnet material -- Nd,Gd:YSGG can be obtained. Its structural formula can be written as $Nd:Gd_{3x}Y_{3(1-x)}Sc_2Ga_{3(1+\delta)}O_{12}$ ($x=0\sim1$, $\delta=-0.2\sim0.2$), or Nd:GYSGG for short[6]. The segregation coefficient of Nd:GYSGG crystal is larger than that of Nd:YAG and high-quality, highly-doped, large size crystals are much easier to grow than Nd:YAG crystals. It is also found the luminescence performance of the Nd:GYSGG crystal can be enhanced under gamma irradiation, which lead to better laser performance. Therefore, it is a promising laser crystal for space uses. The Nd:GYSGG laser is efficient and convenient to be pumped at 808 nm, with the absorption cross section of about 5.844×10^{-20} cm^3. Another interesting characteristic of Nd:GYSGG is that it has comparable emission cross sections around 1060 nm, indicating the possibility of generating coherent terahertz (THz) wave using the difference frequency generation (DFG) method. In this letter, we report a diode-end-pumped high-efficiency continuous-wave (cw) dual-wavelength Nd:GYSGG laser operating at 1058.4 nm and 1061.5 nm, with the maximum output power of over 10 W and the slope

efficiency of about 60%. The experimental results show Nd:GYSGG crystal is an excellent laser material with the potitential applications for generating THz wave at 0.83 THz.

The Nd:GYSGG crystal was grown by the Czochralski method with the Nd^{3+} concentration of 1.1at%. Cutting along the <111> direction into small pieces of $3\times3\times6mm^3$, both end faces are polished and anti-reflection (AR) coated at 808 nm and 1060 nm for diode-end-pumping. The experimental setup for a continuous wave Nd:GYSGG laser is shown in Figure 1.

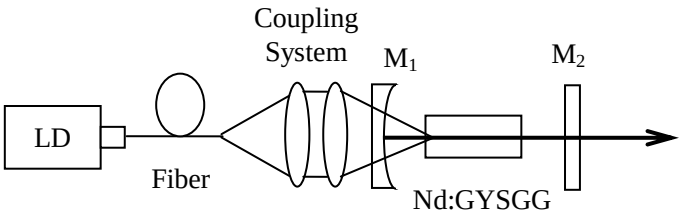

Figure 1 Experimental scheme of the Nd:GYSGG laser

The optimized output coupler has a transmittance of 12.4% around 1060 nm, and the laser cavity length is about 18 mm. The output power versus absorbed pump power is shown in Figure 2. The pump threshold is about 0.6 W and 10.1 W output power was obtained when the absorbed pumped power is 18.45 W, with the conversion efficiency of 54.74% and the slope efficiency of 59.33%. The output spectrum is measured by an Agilent 86142B spectrum analyzer, as shown in Figure 3. Two laser lines are found simultaneously at 1058.4 nm and 1061.5 nm.

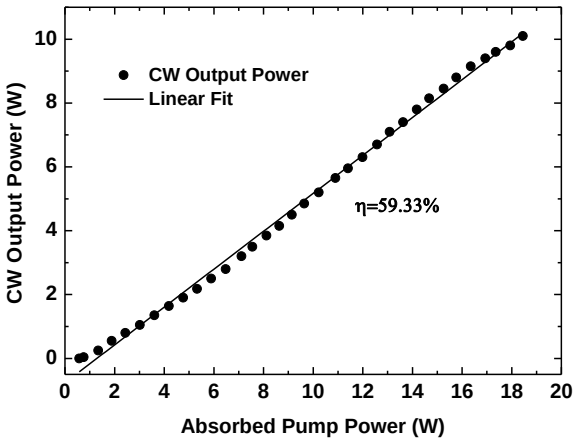

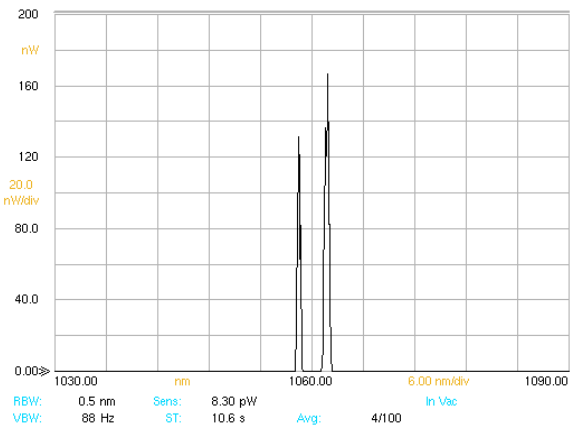

Figure 2 CW operation of the Nd:GYSGG laser Figure 3 Output spectrum of the Nd:GYSGG laser

With an A-O Q-switch inside the laser cavity, the total cavity length is 82 mm. The maximum average output power of the A-O Q-switched Nd:GYSGG laser is 2.77 W at 10 kHz when the absorbed pump power is 11.4 W, corresponding to the conversion efficiency of

24.3% and the single pulse energy of 277 μJ (Figure 4). The temporal pulse shape is shown in Figure 5.

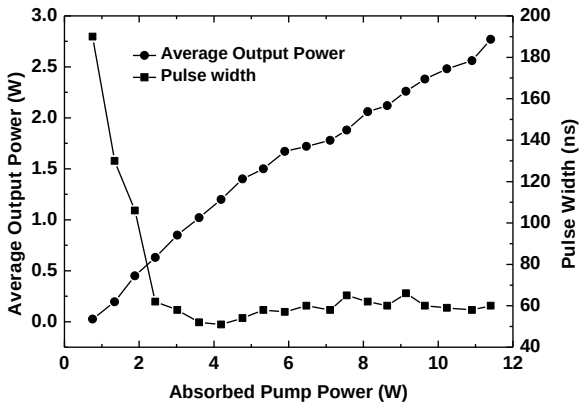

Figure 4 Average output power and pulse width of the A-O Q-switched Nd:GYSGG laser

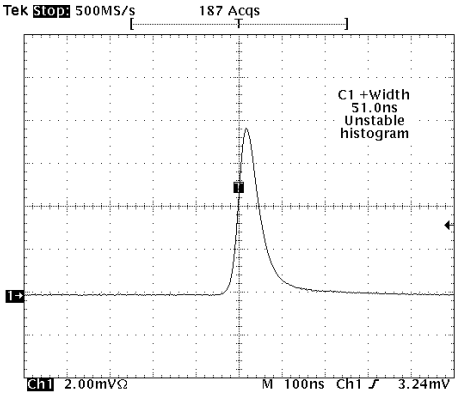

Figure 5 A typical temporal pulse shape of the A-O Q-switched Nd:GYSGG laser

As a result of the long cavity length, the pulse width cannot be reduced effectively, leading to limited peak power. If passively Q-switched by a Cr:YAG absorber, the pulse width can be narrowed to a few nanoseconds, therefore the peak power will be enhanced by at least an order.

In summary, we have presented an efficient dual-wavelength laser based on a new garnet crystal -- Nd:GYSGG. This material has the merits of highly-doping, high quality, large size, antiradiation, etc, and demonstrates excellent laser performance, which provides a promising candidate for extremely high power laser oscillators and amplifiers. Similar to the Nd:YAG crystal, 1.3x μm and 0.9x μm lasers can also be realized by the Nd:GYSGG crystal, which is what we are preparing to do for the next step.

Reference:

1. K. Yoshida, H. Yoshida, and Y. Kato, IEEE J. Qutantum Electron. **24,** 1188 (1988).

2. H. Yu, K. Wu, B. Yao, H. Zhang, et al, Opt. Lett. **35,** 1801 (2010).

3. C. Pfistner, R. Weber, H. P. Weber, et al, IEEE J. Quantum Electron. **30,** 1605 (1994).

4. S. G. P. Strohmaier, H. J. Eichler, C. Czeranowsky, et al, Opt. Commun. **275,** 170 (2007).

5. C. Pfistner, P. Albers, H. P. Weber, et al, Opt. Materials **1,** 101 (1992).

6. J. Q. Luo, Ph.D thesis, Anhui Institute of Optics and Fine Mechanics, CAS (2009).

PULSED NANOSECOND LASER WITH INJECTION OF A SINGLE-FREQUENCY RADIATION

Dmitriy Bordzilovskiy, Alexandr Mayorov, Evgeniy Lonshakov, Sergey Struz, Vladimir Tarasov

Institute of Laser Physics SB RAS, Novosibirsk, Russia
Poster presentation on "New Directions in solid-state lasers"

The effect of the injected radiation on parameters of generation Q-swich Nd:YAG laser with flat resonator are observed.

Nowadays powerful lasers running in single frequency mode are interesting. This lasers used for create a sensitive analytical instruments as an intense narrow band radiation source. Narrowband near-infrared emitters is interesting because lot of the tested substances have absorption bands in this spectral region also the nonlinear conversions of near-infrared radiation can get through the generation of visible and UV range. Creating a powerful narrowband near-infrared emitters can be realized by single-frequency radiation with injection into the laser cavity with a flat-mode and Q-switching.

The main difficulty in designing such a narrow-band transmitter with catch frequency is the matching modes of single-frequency oscillator and a laser with linear resonator and Q-switched, as well as matching caustic of both emissions.

To generate radiation at 1064 nm, we used the crystal YAG: Nd3 +.Giant pulse mode was realized with using an electro-optical switch. The conversion efficiency of pump energy into the energy of the radiation of nanosecond duration is 1.5%.

This paper presents the results of research of the emitter, a mode of a giant pulse with the catching signal of single-frequency continuous oscillator with a wavelength of 1064 nm, designed to work in the complex for the spectroscopy of sodium at a wavelength of 589 nm. To obtain generation 589 nm will be used scheme for the sum frequency (1319 nm is added to 1064 nm) in a nonlinear crystal. The implementation of the scheme imposes high demands stability of the generation for a good combination of spatial beams in a volume nonlinear element. Single-frequency master oscillator was developed at the Institute of Laser Physics SB RAS (Novosibirsk) and has the following characteristics: the lasing wavelength of 1064 nm, 0.55 nm tuning range, mode composition TEMooq, the line width of 2.5 GHz,output power $\geq$ 200mW.

Resonator scheme was realized, it is shown in Fig. 1.

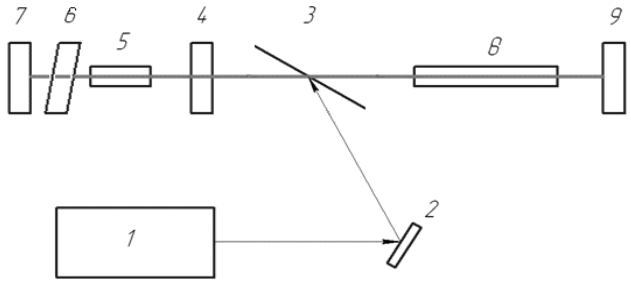

Fig. 1. 1-master oscillator, 2-rotating mirror, 3-polarizer, 4-quarter-plate, 5-electro-optic element DKDP, 6-compensator, 7-HR mirror, 8-active element, 9-VRM mirror.

This scheme provides a minimum length of the resonator, it is necessary to meet the conditions for the duration of the Q-switch pulse.

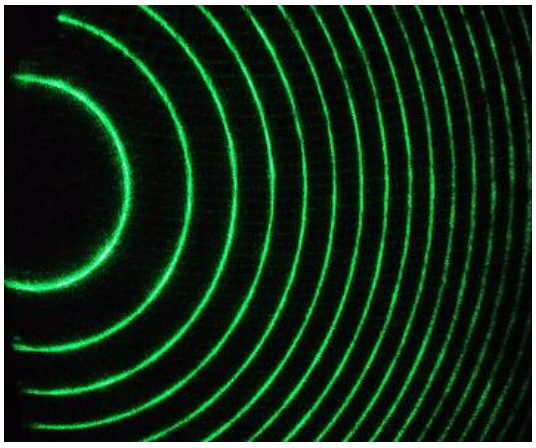

Fig. 2. The emission spectrum of master oscillator

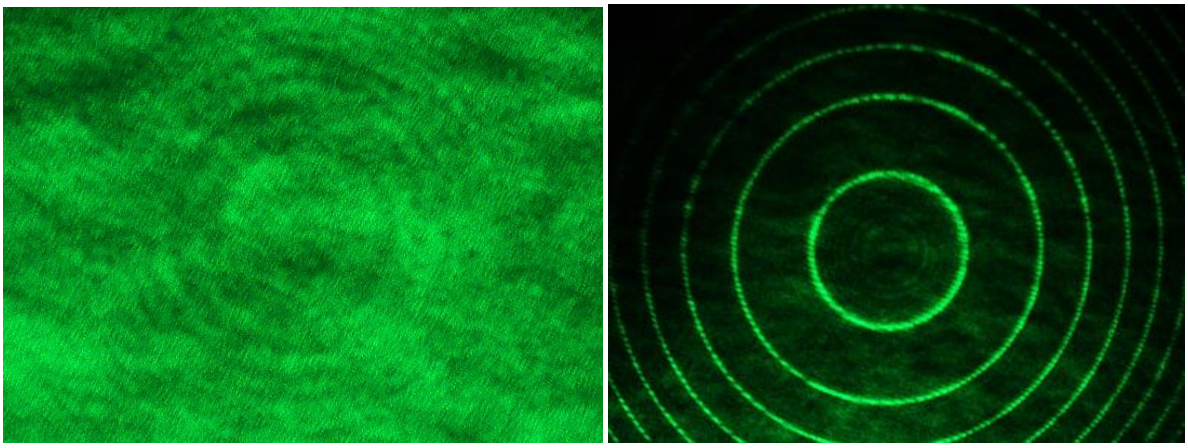

Fig. 3. The emission spectrum of Q-switched laser a) no injection signal, and b) with injection signal

Well as conducted research characteristics: electro-optical switch pulse parameters, pulse parameters of free generation and pulse parameters with a Q-switching, investigated dependence catching signal on the the cavity length, output power with the catching signal and without catching signal.

1. O. Zvelto, Principles of Lasers, 2008
2. N. Hodgson, H. Weber, Laser resonator and beam propagation,2007
3. GG Gurzadyan, VG Dmitriev, DN Nikoghosyan, NonlinearOptical Crystals, 2010

UPCONVERSION GREEN LIGHT EMITTING MACROPOROUS LN:ER RANDOM LASER

Fan Shi, Xinzheng Zhang*, Qiang Wu, Xuanyi Yu, Yongfa Kong, and Jingjun Xu

The MOE Key Laboratory of Weak-Light Nonlinear Photonics, TEDA Applied Physics School and School of Physic, Nankai University, Tianjin 300457, China

Romano A. Rupp

Institut für Experimentalphysik, Universität Wien, Boltzmanngasse 5, A-1090 Wien, Austria
**Corresponding author: +86 22 23501743, zxz@nankai.edu.cn*

The optical cavity of conventional lasers consists of mirrors in the feedback mechanism. In recent years, random lasers have attracted much interest and attention [1-3]. Their cavity results from multiple scattering and light localization in a disordered gain medium. Since random lasers were first proposed by Letokhov [4], they have been widely studied by a number of groups because one can learn more about important scientific concepts such as transport and localization in active random media and because there are highly interesting technological applications such as micro/nano lasers, laser paint, light emitting devices, and display technology. Random lasing action has been demonstrated in the infrared [5], yellow [6], blue [7] and ultraviolet spectral range [1, 8]. So far we cannot find report on random lasers emitting in the green region. Since green is one of the primary colors, developing random laser in the green spectral region is vital for practical applications. Moreover, an upconversion emission mechanism can significantly improve the capabilities of random lasers [9-12]. One advantage of upconversion random lasers is that the threshold in this case is decreased, so upconversion mechanism supplies an idea to achieve green light emitting random laser at relatively low pump intensities. Furthermore, it permits to reduce the cost of green light emitting random laser using a 980 nm diode laser as a pump one which is commercially available and usually cheaper than blue and ultraviolet pulsed ones. These advantages make upconversion green light emitting random lasers attractive.

A LN single crystal doped with 0.2 mol% Er^{3+} was grown by Czochralski method and ground to small particles by a planetary ball mill. The LN:Er particles passed through a 220 nm membrane filter and were dispersed in deionized water. Then the suspension was dried up in a glass beaker at 333 K. The thickness of the resulting sample was about 2.0 mm. The average size of the LN:Er particles was several hundred nanometer evaluated with an atomic force microscope (AFM) (the inset of Fig. 1). The scattering mean free path was esti-

mated to be 981 nm by coherent backscattering measurements, in which the wavelength of the probe beam was 532 nm.

For the study of random lasing behaviors, the macroporous LN:Er sample was optically excited by a 980 nm CW laser impinging perpendicularly to the sample surface and being focused by a lens to a spot with a diameter of 0.10 mm. To avoid heating by the pump laser, the sample was put in a temperature controller set at 298 K and the irradiation (not the intensity) was reduced by a chopper (200 μs pulse duration, 67 Hz repetition rate) placed before it. Emission spectra were collected by a spectrometer in a direction 30° from the sample surface.

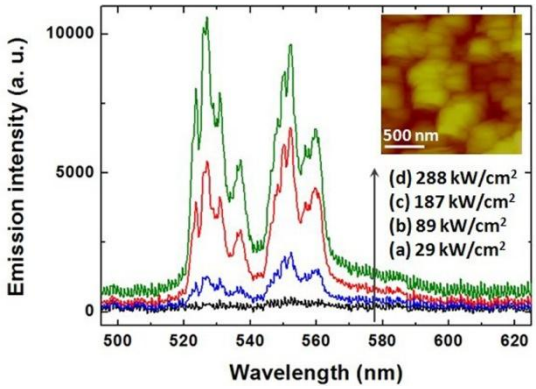

Fig. 1. Emission spectra of the macroporous LN:Er sample at different excitation intensities. The inset is an AFM image of the sample.

Fig. 1 shows the evolution of the photoexcited upconversion emission spectra with increasing pump intensity. At low intensity, only a broad emission band at about 550 nm can be observed (Fig. 1(a)). When the pump intensity increased, several narrow emission peaks arose. As can clearly be seen in Fig. 1(c) and (d), the sharp peaks can be classified into two bands centered at 550 and 527 nm, respectively. The integrated green light emission intensity of the macroporous LN:Er random laser was shown in Fig. 2(a) for both emission bands as a function of excitation power. Lasing thresholds were estimated to be 53 and 39 kW/cm^2 for the 527 and 550 nm bands, respectively. The slope efficiencies above their own thresholds were larger than below. Below thresholds the intensity of the 527 nm emission band was much lower than that of the 550 nm emission band and the intensities of both bands increase slowly. Above thresholds the former one increased more sharply. These can also been seen in Fig. 1. At a pump intensity of about 257 kW/cm^2, their emission intensities became equal to each other. With further increase of the excitation intensity, the intensity of 527 nm emission band exceeded the other one.

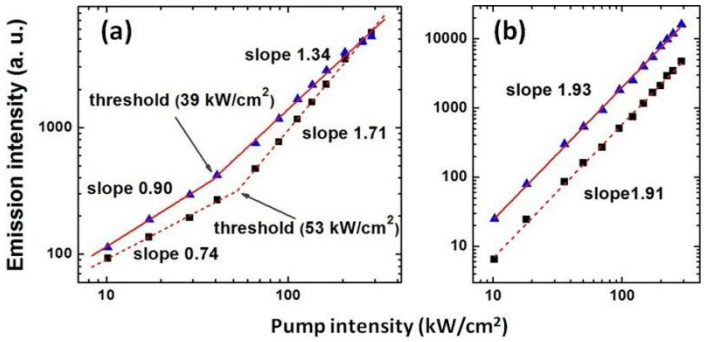

Fig. 2. Integrated emission intensity as a function of excitation intensity on a log-log scale for (a) macroporous and (b) bulk LN:Er. The intensities were integrated from 520 to 540 nm (527 nm emission band) and from 540 to 560 nm (550 nm emission band). Triangle and square dots are experimental results for the 550 and 527 nm emission bands, respectively. Solid and dashed lines are the pertinent linear fits.

For comparison, we pumped bulk LN:Er for the same experimental configuration. In contrast to random lasing actions, no laser threshold was observed at increasing pump intensity (Fig. 2 (b)). Furthermore, the emission intensity of the 550 nm band was always much stronger than that of the 527 nm band even at an excitation intensity of 288 kW/cm2 (Fig. 2(b)).

To our knowledge, we report for the first time on a green-light-emitting random laser in macroporous LN:Er basing on an upconversion mechanism. The lasing action from two emission bands centred at 527 and 550 nm was induced by a 980 nm excitation laser in macroporous LN:Er, which was quite different from the fluorescent behaviors in bulk LN:Er. Their thresholds were determined to be as low as 53 and 39 kW/cm^2 with a pump spot size of 0.10 mm in diameter for the 527 and 550 nm emission bands, respectively. The lasing slope efficiency of the 527 nm band was larger than that of the 550 nm band. Moreover, the thresholds in macroporous LN:Er were much lower than most previously reported in other disordered gain media. These phenomena demonstrated the indeed occurrence of the random lasing actions, and were attributed to the combined effect of upconversion emission and a multiple scattering feedback mechanism.

Acknowledgement

Supported by National Natural Science Foundation of China (11174161, 10804055), National Basic Research Program of China (2010CB934101) and Program for NCET.

References

1. H. Cao, Y. G. Zhao, S. T. Ho, E. W. Seelig, Q. H. Wang, , and R. P. H. Chang, Phys. Rev. Lett. 82, 2278-2281 (1999).

2. D. S. Wiersma, Nat. Phys. 4, 359-367 (2008).

3. N. M. Lawandy, Nat. Phys. 6, 246-248 (2010).

4. V. S. Letokhov, JETP Lett. 5, 212-215 (1967).

5. T. Nakamura, T. Takahashi, and S. Adachi, Phy. Rev. B 81, 125324(2010).

6. E. Pecoraro, S. García-Revilla, R. A. S. Ferreira, R. Balda, L. D. Carlos, and J. Fernández, Opt. Express, 18, 7470-7478 (2010).

7. T. Takahashi, T. Nakamura, and S. Adachi, Opt. Lett. 34, 3923-3925 (2009).

8. H. K. Liang, S. F. Yu, and H.Y. Yang, Appl. Phys. Lett. 96, 101116 (2010).

9. G. Zacharakis, N. A. Papadogiannis, and T. G. Papazoglou, Appl. Phys. Lett. 81, 2511-2513 (2002)

10. H. Fujiwara, and K. Sasaki, Jpn. J. Appl. Phys. 43, L1337-L1339 (2004).

11. G. Zhu, C. E. Small, and M. A. Noginov, Opt. Lett. 33, 920-922 (2008).

12. M. A. S. de Oliveira, C. B. de Araújo, and Y. Messaddeq, Opt. Express 19, 5620-5626 (2011).

EXPERIMENTAL STUDY ON GENERATION OF COHERENT, TUNABLE THZ RADIATION FROM SURFACE-EMITTED PARAMETRIC OSCILLATOR BY LIN-BO_3-TPG/TPO*

Jianquan Yao, Zhongyang Li , Degang Xu, Bo Sun, Kai Zhong

Institute of Laser & Opto-electronics, Key Laboratory of Opto-electronics Information Science and Technology, Ministry of Education, Tianjin University, Tianjin 300072, China
Phone No:-86-22-27402416, Email: jqyao@tju.edu.cn

Recently THz-wave generation technique has attracted great attention for its uniquely potential applications in material diagnostics, molecular analysis, remote atmospheric sensing and monitoring, real-time imaging and communication [1, 2]. However, despite significant progress recently, the methods of generation of THz radiation are still less developed than in the visible and near-infrared region, so the search for efficient, high-power, inexpensive, compact and room-temperature methods of generation of coherent THz radiation is one of the main topics in modern optoelectronics and photonics [3].

Among many electronic and optical methods for THz generation, THz-wave parametric oscillator (TPO) has many advantages, such as compactness, narrow linewidth, coherent, wide tuning range, high-power output and room temperature operation. For efficient generation of THz-wave using TPO, MgO:$LiNbO_3$ crystal is one of the most suitable crystals due to its large nonlinear coefficient and its wide transparency range. Surface-emitted TPO allows THz-wave to emit out perpendicularly to the surface of MgO:$LiNbO_3$ crystal without any output coupler, so the beam quality of THz-wave is improved [3]. Moreover, the interaction area lies just under the exit surface of THz-wave, which means that the propagation length of THz-wave in crystal is short and the absorption loss will be low. Due to non-collinear phase matching in TPO, the interaction length is vital to the energy conversion efficiency. We will show that larger pump beam radius can increase the interaction length and, consequently, reduce threshold pump power density, since the threshold pump power density of TPO is high.

In this paper, we deduce the expression of TPO threshold pump power density, and under different factors the expression has been theoretically analyzed. The effective interaction length between pump wave and Stokes wave has been calculated, and particular attention is paid to the coupling efficiency of pump wave and Stokes wave. The measured values of THz-wave frequency agree well with the theoretical curve calculated from the non-collinear phase matching condition. We gain high THz-wave energy output with a surface emission

* The project Supported by The National Basic Research Program (973 Program) (Grant No. 2007CB310403), the National Natural Science Foundation of China (Grant No. 60671036)

configuration. When pump power density is large enough the TPO could radiate third-order Stokes wave.

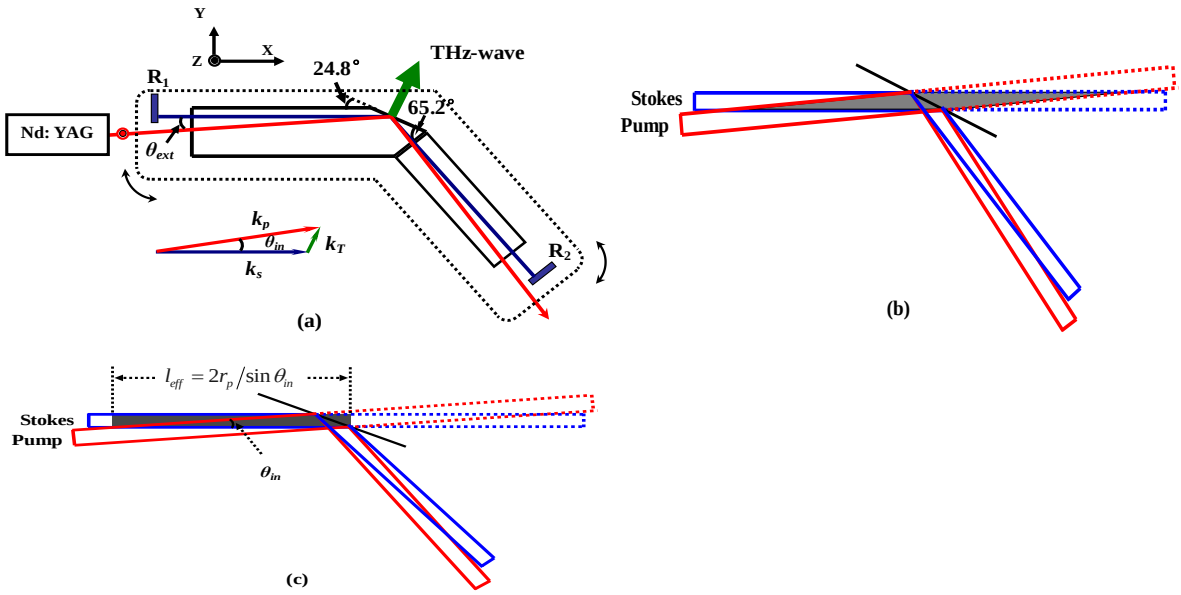

Fig.1 (a) Experimental setup of the MgO:$LiNbO_3$-TPO. (b) Propagation characteristics of pump wave and Stokes wave in MgO:$LiNbO_3$ crystal, the shadow zone is the area where pump wave and Stokes wave interact. (c) Equivalent length of the shadow area

The pump wave and Stokes wave interacted in MgO:$LiNbO_3$ crystal which was symmetrical with the length of 115 mm. Changing the angle θ_{ext} between Stokes wave and pump wave at the external side of crystal could obtain the tuning THz-wave output. We measured the frequency of output THz-wave at different incident angle θ_{ext}, as shown in Fig. 2. The THz-wave frequency was figured out exactly by the energy conservation equation since we have measured the wavelength of Stokes wave. The experimental results agreed well with the values calculated from the non-collinear phase matching condition.

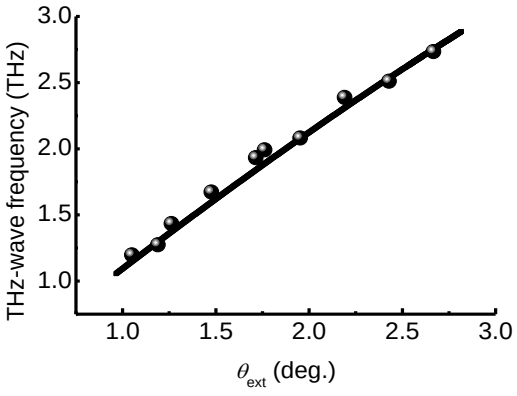

Fig.2

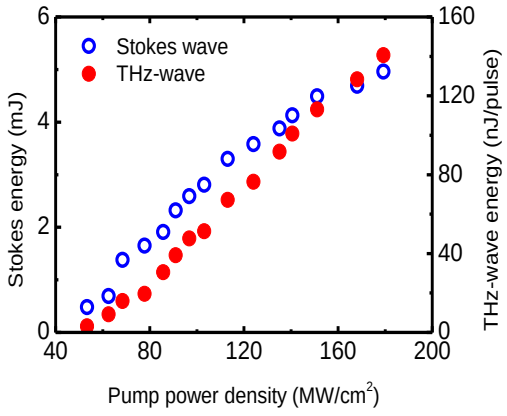

Fig.3

Fig.2 indicates tuning characteristics of the THz-wave. θ_{ext} is the angle between Stokes wave and pump wave at the external side of crystal. The solid curve indicates the values calculated from the non-collinear phase matching condition. Experimental results were showed at Fig. 3 which indicate output energy of the THz-wave and Stokes wave as a function of pump power density.

The expression of threshold pump power density for surface-emitted TPO using MgO:$LiNbO_3$ crystal has been given. Analyses indicate that larger pump wave radius can increase the interaction length between the pump wave and Stokes wave, and therefore reduce threshold pump power density. We analyze the tuning characteristics of surface-emitted TPO. By changing the phase-matching angle θ_{in}, wide range tunability from 0.95 to 2.94 THz was obtained. When pump power density was 179.3 MW/cm^2, the maximum THz-wave output was 140.6 nJ/pulse at 1.85 THz and energy conversion efficiency is about 1.69×10^{-6}. With the phase-matching angle θ_{in} of 0.79° and pump power density of 150 MW/cm^2 we observed the radiation of first-order, second-order and third-order Stokes waves. However, the depletion of first-order Stokes wave energy restricted the enhancement of THz-wave output.

References and links

1. P. H. Siegel, "Terahertz technology," IEEE Trans. Microwave Theory Tech. **50**, 910-928 (2002).

2. K. Kawase, Y. Ogawa, Y. Watanabe, and H. Inoue, "Non-destructive terahertz imaging of illicit drugs using spectral fingerprints," Opt. Express **11**, 2549-2254 (2003).

http://www.opticsinfobase.org/abstract.cfm?URI=oe-11-20-2549

3. E. Kuznetsova, Y, Rostovtsev, N. G. Kalugin, R. Kolesov, O. Kocharovskaya, M. O. Scully, "Generation of coherent terahertz pulses in ruby at room temperature," Phys. Rev. A **74**, 023819 (2006).

EXPLORING THE BRIGHT FUTURE FORWARDS ORGANIC LASER DIODES

Wen-Yong Lai, Wei Huang

Key Laboratory for Organic Electronics & Information Displays (KLOEID) and Institute of Advanced Materials (IAM), Nanjing University of Posts & Telecommunications, 9 Wenyuan Road, Nanjing 210046, China
Email: iamwhuang@njupt.edu.cn

The development of organic semiconductors for organic optoelectronic applications has been growing rapidly in the past two decades. They have shown enormous potential in applications such as organic displays and light-emitting sources. It has been demonstrated that organic semiconductors also have properties that make them as gain materials suitable for solid-state lasers. Amplified spontaneous emission (ASE) and optically pumped organic lasing have been observed in various semiconducting organic molecules. However, the fabrication of an organic laser diode is still challenging. It has been demonstrated that electrically pumped lasing should be possible in amorphous materials. Furthermore, lowing the lasing thresholds is one of the key prerequisites towards organic laser diodes. Research efforts in the past decade have focused attention on small-molecule or polymer semiconductors as gain materials. We present here our recent advances on the development of low-threshold lasing from well-defined nanomolecular semiconductors that combine precise chemical structures with good solution processibility and amorphous morphological stability.

A series of four-armed starburst molecules P1-P3 based on pyrene core and four oligofluorene arms were explored. With 1-D gratings coated with P2 (138 nm film thickness) as the gain medium we were able to attain a very low lasing threshold of 38 ± 7 W/cm2 (i.e. 50 ± 10 pJ/pulse or 0.15 ± 0.03 μJ/cm2) for laser emission at 501 nm. The straight-line fit at higher energies corresponds to a laser slope efficiency of 3.9 ± 0.5%. To examine the effect of increasing the molecular complexity and dimensionality, a series of six-arm monodisperse starburst macromolecules Tr1-Tr4 have also been explored. With simple 1-D DFB gratings, a minimum lasing threshold, Ethlaser ≈ 0.4 nJ/pulse (1.3 μJ/cm2) with high slope efficiency of 5.4% was achieved at a lasing wavelength of 437 nm for the moderate starburst molecule Tr3. This threshold represents one of the lowest reported for an organic semiconductor laser irrespective of cavity design. The findings suggest a novel starburst design strategy for improved organic lasers that show low losses and therefore enhanced lasing characteristics.

Acknowledgments. We acknowledge financial support from the National Basic Research Program of China (973 Program, no. 2009CB930601), the National Natural Science Foundation of China (no. 20904024, 61136003, 51173081), the Doctoral Fund of Ministry of

Education of China (Grant 20093223120004), the NUPT Scientific Foundation (Grant NY210016), and the Qing Lan Project of Jiangsu Province.

INVESTIGATION OF TITANIUM THIN FILMS PRODUCED BY FEMTOSECOND LASER ABLATION

M.N. Gerke, K.S. Khorkov, V.G. Prokoshev, S.M. Arakelian

Vladimir State University, Gorky St., 87, P.C. 600000 Vladimir, Russia
e-mail: freeod@mail.ru

The given work is devoted to experimental researching of the nanostructures arising at laser ablation of titanium targets and deposition ablation's products on a substrate. The optical scheme of our experiment is similar to the scheme offered in work [1].

In our experiments we used two different laser systems. The femtosecond Ti:Sapphire laser system providing following parametres: pulse repetition frequency of 1 kHz, pulse duration of 50 fs, average radiation power of 1 W and spot diameter of the focused radiation 250 μm. And the femtosecond Yb:KGW laser system: pulse repetition rate of 10 kHz, pulse duration of 300 fs, average radiation power of 1.5 W and focused spot diameter 50 μm.

The focused laser radiation gets on the target located under an angle 45^0 to it. The sprayed material of the target scatters in volume of the vacuum chamber and deposits on the cold substrate. The chamber was pumped out by the turbo-molecular pump station to pressure 10^{-4} Torr. Depending on adjustable parametres of experiment sufficiently compound structures are formed.

First of all it would be desirable to concentrate on properties of films produced by Ti:Sapphire laser system. After withdrawal the substrate with the raised dust film from the vacuum chamber, in the central zone occurs an interaction of active nanoparticles with atmospheric oxygen. Quasiperiodic structures reminding folds are formed (Fig. 1, a).

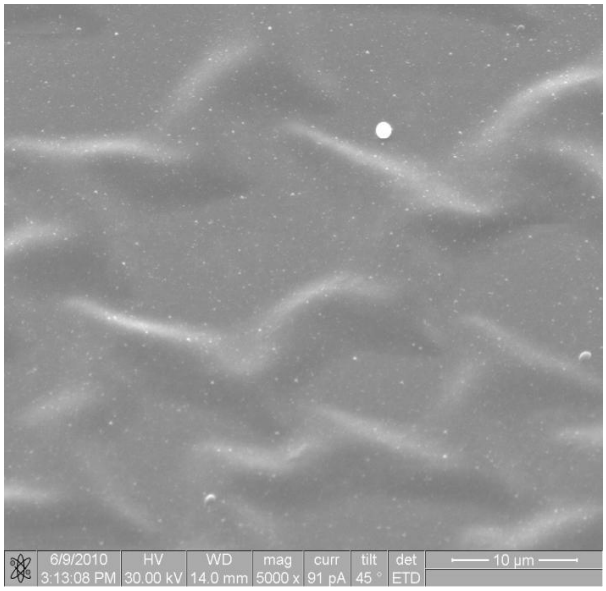

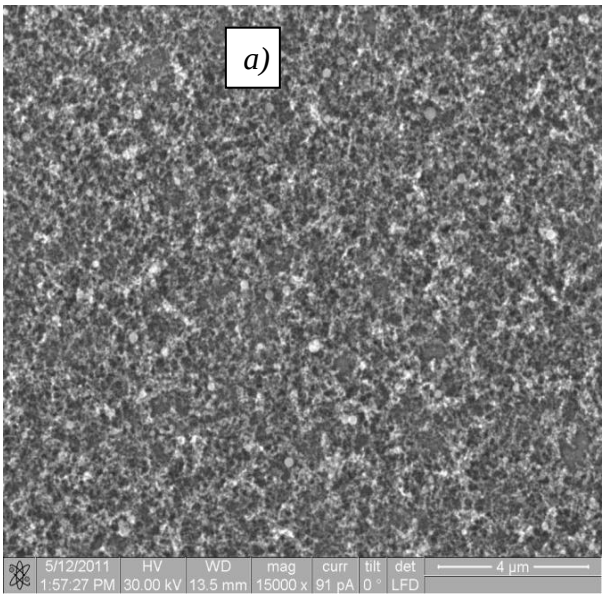

Fig. 1. SEM images of titanium deposition: *a)* thin film produced by Ti:Sapphire laser system in vacuum; *b)* thin film produced by Yb:KGW laser system in air.

Formation of zigzag structures occurs more intensively in the central area of the dusting. Topological parametres of structures change at removal from the central area. The period of a separate strip in the central area corresponds an order 10 μm, the height averages 600 nm. Distance between two strips 5 μm. Dependence of character of structures on conditions of laser influence gives the chance selection of a necessary set of parametres for research area. And the analysis of raman spectrums (Fig. 2, a) has shown the crystal form of titan`s oxide rutile [2]. For rutile the expressed peaks on 447, 611 cm^{-1} and weaker on 244 and 145 cm^{-1} coincide with experimental results.

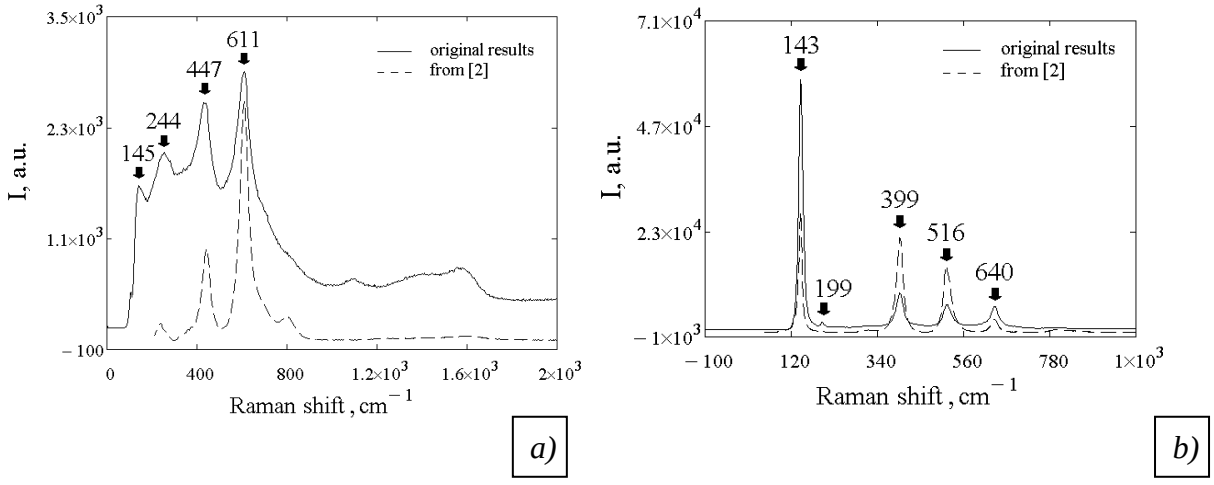

Fig. 2. Raman spectra of titanium deposition: *a)* thin film produced by Ti:Sapphire laser system in vacuum; *b)* thin film produced by Yb:KGW laser system in air.

At the dusting of films with Yb:KGW laser system uniform distribution of nanoparticles without formation of oxides is formed. The dusting occurred at various parametres, such

as speed of movement of the laser beam on the sample, number of passes and distance from the sample to the substrate. Basically the uniform layer, with the characteristic size of particles 100-300 nm turns out There is no swelling and changes of the film surface relief. But at experiments in air also it is formed other crystal form of titanium oxide – anatase (Fig. 1, b), to which completely there correspond the received spectra (Fig. 2, b).

References:

1. S. Eliezer, N. Eliaz, E. Grossman, D. Fisher, I. Gouzman, Z. Henis, S. Pecker, Y. Horovitz, M. Fraenkel, S. Maman, V. Ezersky, and D. Eliezar, "Nanoparticles and nanotubes induced by femtosecond lasers", Laser and Particle Beams, 15-19 (2005)

2. Romanian database of raman spectroscopy: www.rdrs.uaic.ro

NEW OPPORTUNITIES OF LASER-INDUCED METAL DEPOSITION

Yu.S.Tver'yanovich

Chemical Department of St. Petersburg State University, St Petersburg, Russia
+78124287479, tys@bk.ru

Laser-assisted methods are now the main manufacturing platform of modern microelectronic technology. This is why the creation of new laser sources is inevitably followed by the search for novel application fields and the development of advanced techniques. As the microelectronic industry continuously demands further miniaturization, it is forced to solve the problems associated with the creation of microchips, small integrated elements or ultra large-scale integrated devices with a high density of elements. Generally, the localized (the micrometer or sometimes sub-micrometer range) metallization of insulators or dielectrics can be achieved only through laser-assisted techniques. Among laser-assisted techniques, laser-induced chemical liquid phase deposition (LCLD) is considered to be the most efficient, and the least expensive and dangerous. It is based on the localized laser irradiation of the interface of the substrate and the liquid electrolyte. Under the influence of the laser the chemical reducing reaction is thermally or photolytically initiated resulting in a high adhesive metal precipitation onto the surface of the material to be coated. The chemical reducing agents (components of the electrolyte solution: formaldehyde (HCOH), ethanol (C2H5OH), and so on) and laser-broken chemical bonds act as the electron donors in the process of metal complexes to metal reduction. The LCLD method can be used for the deposition of different metals onto several types of substrate. Lengthy continuous metal structures and micro-patterns are created by scanning of a laser beam onto a substrate surface. The morphology and properties of the resulting metal deposits are found to be considerably dependent on the applied parameters (the laser power, the scan velocity, the number of scans). It has been demonstrated that the temperature of the electrolyte solution greatly influences the deposition process. Namely, by increasing the temperature of the solution one can reduce the threshold laser power required to initiate the metal deposition. The deposition process is significantly affected by a salt precursor, chemical reducing agents, a complex agents. A gases babbles formation in liquid media under laser irradiation produces the significant problems for metal deposition.

The lecture is devoted to the discussion of problems and prospects for the method of laser-induced metal deposition from liquid solutions on dielectric substrate and the possible ways of it development. The list of main publications of the team can be delivered from V. A. Kochemirovsky, L. G. Menchikov, S. V. Safonov, M. D. Bal'makov, I. I. Tumkin, Yu. S.

Tver'yanovich, "Laser-induced chemical liquid phase deposition of metals: chemical reactions in solution and activation of dielectric surfaces", *RUSS CHEM REV*, 2011, **80** (9), *in press*.

ELECTRIC FIELD EFFECTS ON QUANTUM WELL TO QUANTUM DOT TUNNELING

Abramov A.A.

Kuang-Chi Institute of Advanced Technology, China, Shenzhen,
arnold.abramov@kuang-chi.org

Agafonov A.G.

Gottfried Wilhelm Leibniz Universitaet Hannover, Germany, Hannover
agafonov@nano.uni-hannover.de

The interaction between the quantum dot (QD) level and 2D continuum of a quantum well (QW) in the presence of electric field investigated theoretically. Influence of the electric field and barrier distance between QW and QD on the free-electron energy band of QW is studied. Tunneling time for QW to QD transition as a function of the electric field calculated for various barrier distances.

We consider a structure where the quantum well and the quantum dot are in a vicinity of each other; a so-called QW-QD structure. It has been shown that the quantum well coupled to the quantum dots via a thin barrier much improves the characteristics of a QD laser and detector [1-4]. Moreover, the advantage of using quantum dots built in a superlattice has been also discussed in [5,6] and was shown to increase a feasibility of this type of structure for infrared source applications. Even though that these structures have been already theoretically investigated in [7,8] no particular attention, however, has been paid so far to the properties of QD-QW as a function of spatial separation between them. In this work we study influence both of electric field and barrier distance on the 2D QW band structure, as well as the QW to QD tunneling time.

We consider a simple QW-QD structure (Fig.1) in the presence of longitudinal electric field. QW and QD are separated by a thin barrier of thickness L_b, and the *z*-axis corresponds to the direction of structure growth. In such a system the electron wave function satisfies the Schrödinger equation

$$H\psi_k = E_k\psi_k \qquad (1)$$

with Hamiltonian

$$H = -\frac{\hbar^2}{2m^*}\nabla^2 + V_w(z) + V_d(\vec{r}) + |e|Fz$$

where $V_w(z)$ and $V_d(\vec{r})$ are confinement potentials of QW and OD, respectively, both satisfying the following boundary conditions: $V_w(z) = V_1$, $V_d(\vec{r}) = V_2$ for z inside the well/dot, and $V_w(z) = 0$, $V_d(\vec{r}) = 0$ for z outside the well/dot, F – electric field.

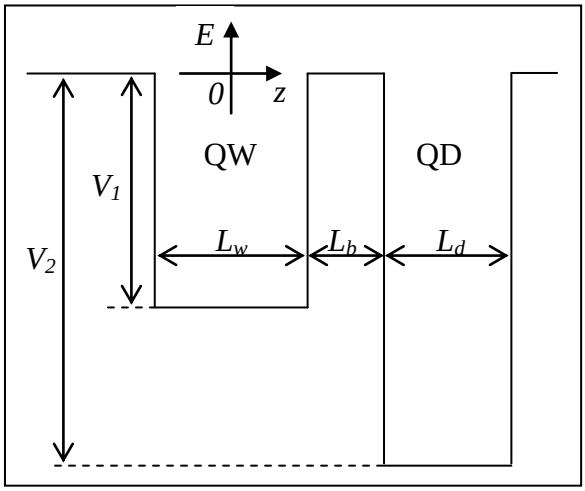

Fig.1. Potential profile of QW-QD

We examine the case when the QDs energy level E_d is buried under the background of the energy spectrum of the subband E_{wk} of the QW. Here we are interested in solution of Eq. (1) particularly in the energy region corresponding to the E_d - level of QD.

The method for solution of equation (1) is described in [9].

For calculation of the tunneling time we chose the same set of parameters that have been used in [10], given that the depths of the QW and the QD are V_1 = 200 *meV* and V_2 = 500 *meV*, respectively, width (L_w) of the QW and the height of the QD is 20 Å and 40 Å, the radius (R_d) of the QD is 80 Å, and the effective mass of electron is $m^* = 0.1\ m_0$. Also we used given in [10] expression for wave functions of QW and QD states. Next, we consider transition of the electron from the state in QW (for the present set of parameters, there is only one level in QW) to that in QD *(q,m,n)*=(2,0,1), where *(q,m,n)* - quantum numbers describing a QD states (according to [10]). The corresponding potential profile is shown in Fig.1.

Now let's consider the tunneling from QW to QD. We plotted the probability of this transition as a function of the distance L_b in Fig. 4. For both cases tunneling time monotonous decreases with increasing electric field. This can be explained by an increased overlap of QW and QD wave functions. The fact that the tunneling time is inversely proportional to the overlap factor between QW and QD wave functions

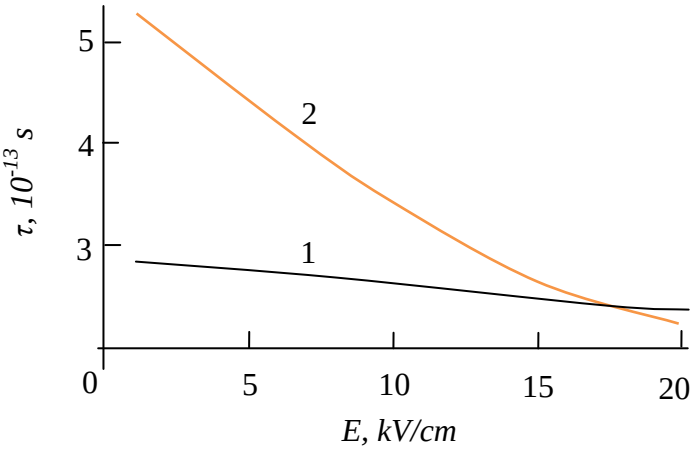

Fig. 4. QW to QD tunneling time as a function of the electric field for various barrier distance L_b(*nm*): 1 - 10, 2 - 50.

and the broadening of resonant level. At shorter distances broadening is greater and respectively tunneling time for case L_b=0.1 is less than for case L_b=*0.5*.

Thus, we are driven to acknowledge the importance of taking into account the effect of influence of electric field and QD potential on changing the free electron energy band of QW whenever we consider the tunneling transition between them. This effect of significantly affect the transport and optical characteristics of QW-QD system.

1. G.Walter, N. Holonyak, J. H. Ryou and R. D. Dupuis *Appl. Phys. Lett*. **79** 1956, 3215 (2001)

2. D. R. Matthews, H. D. Summers and P. M. Smowton, *Appl. Phys. Lett*. **81** 4904 (2002)

3. L. Chu, A. Zrenner, G. Bohm and G. Abstreiter *Appl. Phys. Lett*. **76** 1944 (2000), Appl. Phys. Lett. 79, 2249 (2001), *Appl. Phys.Lett.* **76**, N14, 1944-1946 (2000)

4. Hsu B-C, Lin C-H, Kuo P-S, Chang S T, Chen P S, Liu C W, Lu J-H and Kuan C H *IEEE Electron Device Letters* **25** 544-546 (2004)

5. F. F. Schrey, L. Rebohle, T. Müller, G. Strasser, and K. Unterrainer, D. P. Nguyen, N. Regnault, R. Ferreira, and G. Bastard *Phys. Rev. B* **72**, 155310 (2005)

6. D. P. Nguyen, N. Regnault, R. Ferreira, and G. Bastard *Phys. Rev. B* **71**, 245329 (2005)

7. R. V. Melnik and M. Willatzen *Nanotechnology* **15**, 1 (2004)

8 T. R. Nielsen, P. Gartner and F. Jahnkel *Phys. Rev. B* **69**, 235314 (2004)

9. A.A.Abramov, C.-H. Lin, C.W. Liu Int. J. of Nanoscience, **7**, 181, 2008

10 S. L. Chuang and N. Holonyak, *Appl. Phys. Lett*. **80** 1270 (2002)

LASER TREATMENT OF PLASMA COATINGS

Mitrofanov A.A., Caschin Ye. A, Balashova S.A.

Federal state budgetary educational institution of the higher vocational training «Kovrov state technological academy of a name of V.A.Degtjareva», Vladimir region, Kovrov +7(49232)32062, kanircha@list.ru

Resource of machine parts operation can be successfully increased by applying plasma coating [1,2]. In spite of the progress in the development of plasma sprayed coatings, there exists a problem of stability and quality of obtained plasma coatings. This problem can be solved using laser emission for thermal action on coating. Heating by laser radiation in pulse mode has been used as a method of high temperature treatment of gas spray coatings aimed to obtain coatings with higher working characteristics. A principal possibility of this approach has been shown in previous works [3,4]. Determination of laser treatment parameters is based on determining temperature on surface of coating and its in-depth distribution. If we regard laser beam as distributed surface heating source, location of temperature fields can be reduced to solving classical heat transfer equation:

$$\frac{\partial^2 T(z,t)}{\partial z^2} - \frac{1}{a}\frac{\partial T(z,t)}{\partial t} = -\frac{q_n(z,t)}{\lambda}, \quad (1)$$

where a - is thermal diffusion coefficient; λ - is heat conductivity coefficient; $T(z, t)$ - is a temperature field distributed by penetration depth z; and $q_n(z, t)$ - is intensity of heat generation at radiated surface.

At equal distribution of heat along laser spot using short pulses lasting $\tau_i \le r_n / a$ thermal conductivity problem may be regarded in one-dimensional approach at the surface of semi-infinite solid.

General solution of linear differential equation shall be the following expression:

$$T(z,t) = \frac{2q_n\sqrt{at}}{\lambda} ierfc\left(z/2\sqrt{at}\right) + T_0, \quad (2)$$

where $ierfc(x) = \int_x^\infty (1 - erf(y))dy$ - probability integral function; $erf(y)$ - error function;

T_0 – starting temperature of treated surface.

For small values of time $0 < t < \tau_i$ temperature on surface of radiated material may be approximately determined from expression:

$$T(0,t) = 2q_n / \lambda\sqrt{at/\pi} + T_0, \quad (3)$$

Fig.1 shows dependence of coated surface temperature when heated by laser radiation with varying energy spectral density. Obtained results allow one to determine interval of laser heating modes. Lower boundary of laser emission energy density corresponds to condition of ceramic coating Al_20_3 melting temperature ($t_{melting}$) formation. Upper boundary corresponds to boiling temperature ($t_{boiling}$). Treatment by energy with density surpassing this value leads to evaporation of surface layers of coating.

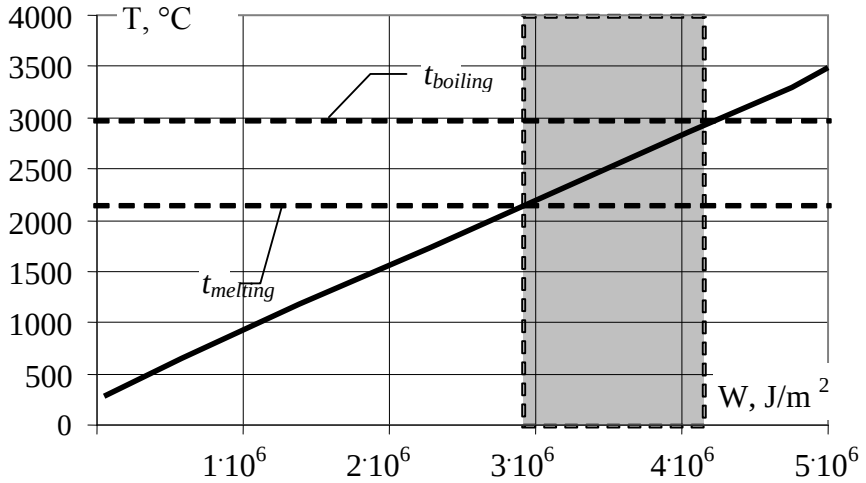

Fig.1. Dependence of coating surface temperature on density of laser emission energy.

Determining distribution of temperature fields along surface layer depth during laser treatment through pulse emission is of practical interest. It is difficult to use expression (1) for this purpose due to large volume of calculations. In this case, it is convenient to use the expression for the calculation of temperatures implicitly, obtained if we admit that $r_n >> \sqrt{at}$

$$T(z,t) = q_n / \lambda \left(2\sqrt{at/\pi} - z\right), \quad (4)$$

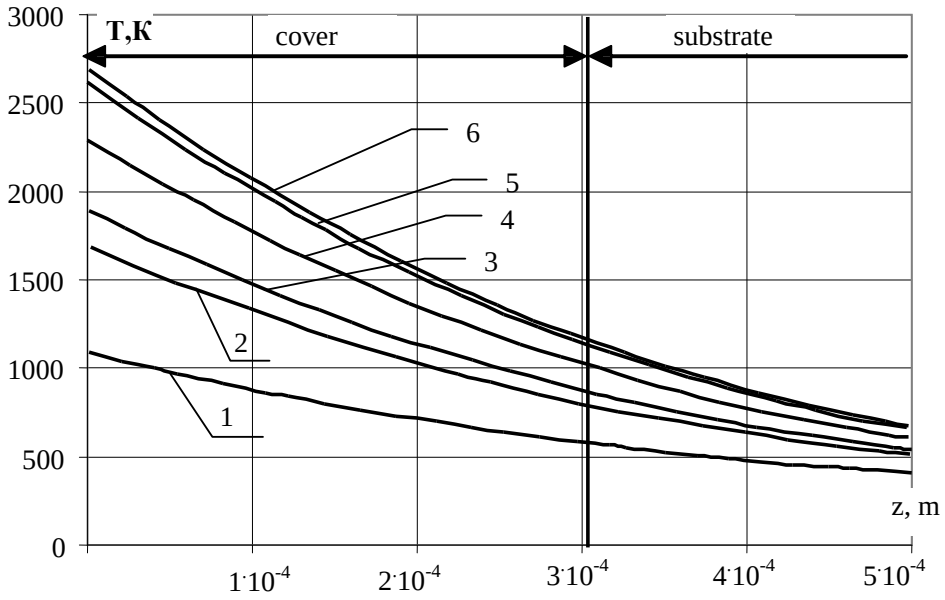

Fig. 2. Graph showing distribution of temperature fields for different values of energy pulse:
1 - $W_i = 20J$; 2 - $W_i = 35J$; 3 - $W_i = 40J$; 4 - $W_i = 50J$; 5 - $W_i = 58J$ and 6 - $W_i = 60J$.

From (4) it is possible to obtain dependence for the determination of melted layer depth at laser heating by pulse length τ_i

$$Z_{melted} = 2\sqrt{a\tau_i/\pi} - T\lambda/q_n , \quad (5)$$

Calculation results (see Fig.2) make it possible to evaluate temperature not only at coating surface but also at undercoat-coating border.

Thus, a problem of choosing coating thickness is solved, where coating surface temperature will not rise above melting temperature while temperature of undercoat at undercoat-coating border reaches melting temperature. If this requirement is met, adhesion strength will be increased due to diffusion processes at undercoat-coating border.

Bibliographic list.

Kudinov, V.V. Plasma coatings. M. Nauka, 1977

Puzryakov, A.F. Theotetical Basis of Plasma Spray Technology: A Textbook of Methodics for course in Metallocomposite Constructions Technology. –M.: N.E.Bauman MGTU Publishers, 2003. – p.360

Chaschin, Ye.A. Increasing Operational Properties of Laser- Sprayed Plasma Coatings / Chaschin, Ye.A , Balashova, S.A./ Motor Driven Machines/ / 2009,-№ 3. - p. 37-41.

Mitrofanov, A.A. /Treatment of Gas-Thermal Coatings using Laser Emission/ Mitrofanov, A.A., Chaschin, Ye.A , Balashova, S.A / Vestnik IGEU, -2011-pp.103-106.

SAFE SPECTRAL RANGE RAMAN LASER FOR ENVIRONMENTAL MONITORING AND LASER LOCATION

Gavrilov A.V., Ershkov M.N., Smetanin S.N., Solokhin S.A., Fedin A.V.

The Kovrov State Technological Academy named after V.A.Degtyarev

Development of compact lasers oscillating at 1.5-micron wavelength and more is a more actual physical task as this radiation is safe for eyes, has minimum atmospheric losses and can be applied in optical location systems, laser ranging, environmental monitoring systems. Stimulated Raman scattering (SRS) of Nd^{3+}:YAG lasers is one of methods of radiation generation in this spectral region. The use of barium tungstate $BaWO_4$ crystal as Raman converter is promising as this crystal possesses optimal thermo-optical characteristics together with high Raman gain coefficient.

In this paper we give the investigation results of radiation generation with high average power at 1.53-micron wavelength with single-stage intracavity SRS conversion of Nd^{3+}:YAG radiation at 1.34-micron wavelength.

As a result of experimental investigations we got the dependences of the average power of SRS radiation at 1.53-micron wavelength from the repetition rate of pumping pulses. For passive Q-switch at 1.34-micron wavelength it was established that the lasing regime with passive Q switch and initial transmittance of about 59% is optimal. We received Raman radiation with average power of 0.28 W in the form of train of 5 pulses with the duration of 20 ns and individual pulse energy of 4mJ under the condition of maximum pumping repetition rate of 15Hz. For passive Q switch with initial transmittance of 47% and 74% the average power of radiation turned to be considerably less and was 0.15W and 0.1W respectively. For electro-optical modulation the thermal distortions influence proved to be less significant, so the repetition rate of pulses was increased up to 30 Hz. When $LiNbO_3$ crystal was used the average power of SRS radiation made up 0.44W, and using $LiTaO_3$ crystal it was 0.85W. The pulse duration of SRS radiation was about 20ns. It is established the dependence of Raman radiation average power from pumping repetition rate in the range 1-30Hz is practically linear. This allows us to conclude that in the given laser circuit configuration the increase of Raman radiation average power is possible if pumping repetition rate is further increased.

SYNTHESIS OF METAL-CARBON NANOSTRUCTURED MATERIALS BY CONTOLED LASER DEPOSITION

Arakelyan S.M., Antipov A.A., Kutrovskaya S.V., Kucherik A.O., Nogtev D.S., Osipov A.V., Prokoshev V.G.

Department of Physics and Applied Mathematics, Vladimir State University,
Gorky st. 87, Vladimir, Russia
Phone: (4922) 479621
Fax: (4922) 333369
E-mail: kstella@vlsu.ru

Laser ablation is widely used for obtaining of nanoparticles and nanoclusters in a cloud of ablation products. It is well controllable and perspective process for many technological applications, the numerical decision for rectangular initial structures of density and pressure is resulted in, shown, that initial structures of distributions of density and pressure in a vapour cloud of material render essential influence on function of distribution formed of nanoclusters.

The carried out experiments of laser deposition show an opportunity of control formation of complex nanostructurized coverings on a substrate surface at used of a target as a mix metals nanopowder and carbon nanotubes. The most perspective appears on a laser method of action on a carbon nanotubes massive at the presence of growth catalysts of the given structures. As shown in work nanoparticles can be such catalysts for growth nanotubes. The question on the mechanism of nanostructures formation on a surface of a cold substrate up to the end is not clear, as during action there can be a reorganization carbon nanotubes at the expense of action of nanoparticles catalysts. In this case the sold scheme of nanostructures formation corresponds to an open reactor with speed of particles evaporation about sound speed. To research of a target surface after laser action show, that during interaction of laser radiation with carbon nanotubes, mixed with metal nanopowder, there is a local profusion. In this case, at active evaporation of substance (visually above area of laser action on a target the intensive plasma torch is fixed), nanotubes appeared on a surface of melting materials can be fond from a surface and be deposited on a substrate. In such system carbon - metal, as shown in work, the formation of fractal structures is possible at self-organizing carbon on metal during thermal laseraction. Simultaneously with it, during distribution of two-componental plasma probably formation of fractal clusters.

The offered method of obtaining of metal-carbon nanostructures has perspective for various applications, photonics and optoelectronics as allows to action on carbon nanotubes

and to change their morphological and physical chemical properties at temperatures considerably smaller then temperatures of fusion of an initial material.

METHOD OF THE CONTROL BY PHASE-LOCKING OF MULTICHANNEL LASER SYSTEM

A.V. Fedin, A.V. Gavrilov, M.N. Ershkov, S.N. Smetanin, S.A. Solokhin

The Kovrov State Technological Academy named after V.A.Degtyarev

New method of control by phase-locking and the optical block diagram of architecture of multichannel laser system with diffraction connected loop laser cavities at the gain gratings are proposed. In them the passive laser Q-switch, which is inserted in one of laser channels, synchronously starts the generation of all laser channels as trains of high powerful nanosecond phase-locked pulses of radiation.

We prove an opportunity of use неодимовых of neodymium laser medium generating as on the basic laser transition (wave length of radiation is 1.06 micrometer), and on the not basic transition (wave length of 1.3 micrometer), having essentially smaller amplification. We also prove the optical block diagrams of multiwave generation in a spectral range from 0.5 till 1.54 micrometer.

The phase-locked generation of Nd:YAG laser system with the passive Q-switch on a basis of a phototropic LiF:F_2^--crystal, demonstrating an identical spatial-temporary picture of radiation as trains of nanosecond pulses both in the channel with the Q-switch, and in the channel without the Q-switch with accuracy of phasing of laser channels is no worse 0.8 is experimentally received.

The radiation of such laser systems for far distance distribution of an atmosphere and other special laser systems can be successfully used.

SYNTHESIS OF MULTYLAERS NANOSTRUCTURED FILMS BY METHOD OF LASER DEPOSITION NANOPARTICLES FROM COLLOIDAL SOLUTIONS

Antipov A.A., Arakelian S.M., Kutrovskaya S.V., Kucherik A.O., Nogtev D.S., Prokoshev V.G.

Department of Physics and Applied Mathematics, Vladimir State University,
Gorky st. 87, Vladimir, Russia
Phone: (4922) 479621
Fax: (4922) 333369
E-mail: aantipov@vlsu.ru

Volumetric or multilayered materials consisting from micro- and nano fractal clusters кластеров, - the separate class of materials possessing a number of unique properties. Physicomechanical properties of such materials depend on their morphological properties and from fractal dimensions. Various experimental setup to synthesis similar clusters structures are applied. One of the perspective directions, allowing to obtain extended massive of nanostructures with controlled morphology, is laser deposition of metals from solutions. Methods of deposition of metal particles at laser action for electrolits applied to tasks formation of thin metal coverings. Synthesis nanostructures from colloidal systems, - now one of perspective technologies, however an opportunity of excitation in a laser field fractal structures has as fundamental value in aspect of obtain of new materials with controlled physical and chemical properties, and applied in aspect of creation of new devices of nanophotonics.

In the given work on the basis of a method of laser deposition metal (and-or oxide) nanoparticles from коллоидных systems (LDPCS), experiments on obtaining of samples nanostrucutres multilayered materials with controlled topology besieged fractal clusters structures are carried out.

MATHEMATICAL MODELING OF THERMAL AND OPTICAL PARAMETERS OF THE ZONE OF LASER ACTION FOR DETERMINATION OF FEEDBACK PARAMETERS OF THE SYSTEM OF ADAPTIVE PRECISION LASER PROCESSING OF MATERIALS

Shilov I.V., Fedin A.V., Gavrilov A.V.

The Kovrov State Technological Academy named after V.A. Degtyarev

The change sequence of spatial and phase parameters of a laser beam penetration in a solid material can be characterized by external, instrumentally measured parameters of the laser influence action: by temperature, optical and electro physical properties of the erosion flow and by properties of the directly irradiated surface. Simultaneously, the energy efficiency of the regime of laser drilling and the final profile of a formed cavity will be also determined by a concrete interrelation of the parameters of laser radiation with the parameters of the formed channel: depths, diameter, form (profile) of the channel, distribution of equivalent thermal sources formed in the channel. As while drilling it's rather difficult to receive the direct information on parameters of the growing channel, so the task of mathematical modeling is the receiving of all possible "scenarios" of the channel form evolution with the change of the equivalent thermal sources distribution, mass flows of the erosion products and the temperature distributions in the channel. Temperature, the mass flows and ionization degree can be measured indirectly or directly, so it gives an opportunity to mark out the attributes indicating the qualitative changes of parameters of the growing channel in the flow of measured data. It also gives an opportunity to correlate these changes with the parameters of laser radiation, to apply these attributes of qualitative changes for temporary calibration of algorithms of parameters management of laser radiation, i.e. for realization of effective adaptive modes of laser drilling, including maximum possible suppression of the plasma action.

To make numerical experiments allowing to estimate the correlation of laser radiation parameters with the parameters of the forming channel, with temperature and optical parameters of the irradiated surface and the erosion flow, the mathematical model of the channel formation in a vaporizing mode in an initial non-stationary growth phase is offered. Non stationary two-dimensional axially symmetric thermal task solution is involved on the computational grid with changing outer boundary coordinated with the task solution of evaporation front displacement determination. The mathematical model of the flow formation of steam and low density plasma in the channel and above the irradiated surface is also coordinated with parameters of the evaporation front.

HETEROSTRUCTURES BASED ON ZINC OXIDE AND THEIR APPLICATION IN DEVICES

Lotin A.A., Novodvorsky O.A., Zuev D.A.

Institute on Laser and Information Technologies, Russian Academy of Sciences (ILIT RAS), Moscow Region, Shatura, (496) 452 5995
e-mail: Lotin_82@mail.ru

ZnO is one of the most promising materials for shortwavelength light-emitting diode (LED) and laser diode applications because it is direct semiconductor with band gap 3.37 eV and it has highest exciton binding energy 60 meV. The band gap control of semiconductors is major problem of optoelectronics. To increase ZnO band gap apply binary composition MgO and to decrease – CdO.

The $Mg_xZn_{x-1}O$ and $Cd_yZn_{y-1}O$ films have been grown on α-sapphire substrates by pulsed laser deposition method. The optical and structural characteristics of the ternary solutions $Mg_xZn_{x-1}O$ and $Cd_yZn_{y-1}O$ have been investigated. The X-ray analysis results of $Mg_xZn_{1-x}O$ and $Cd_yZn_{1-y}O$ films have shown that they possess wurzite crystal structure in range x=(0-0.35) and y=(0-0.3) respectively. The lattice mismatch of ZnO and $Mg_{0.35}Zn_{0.65}O$ films did not exceed 1 %, and their band discontinuity ΔE_g=0.92 eV. The growth orientation of $Mg_{0.45}Zn_{0.55}O$ film was (10.1). The band gap of $Cd_yZn_{y-1}O$ films was decreased from 3.29 eV (y=0) to 2.51 eV (y=0.3). The lattice mismatch of $Cd_yZn_{y-1}O$ and ZnO films was 0.2% for y=0-0.2 and 7.8% for $Cd_{0.3}Zn_{0.6}O$.

The multiple quantum wells (MQW) $Mg_{0.27}Zn_{0.73}O$/ZnO have been grown by the pulsed laser deposition method with different well widths L_w. The interface roughness of quantum wells was inherited from the bottom one and did not exceed 1 nm. We observed the quantum confinement effect showing up in the blue shift of exciton peak in the low temperature (8 K) photoluminescence and absorption spectra at well width reduction. The exciton binding energy of the two-dimensional structures $Mg_{0.27}Zn_{0.73}O$/ZnO was two times higher in comparison with the bulk ZnO. It has been established that Einstein's characteristic temperature Θ_E sharp increase with reduction of well width L_w up to L_w=2.6 nm. It has been revealed that the discontinuity ratio of conduction and valence bands in the heterostructure $Mg_{0.27}Zn_{0.73}O$/ZnO is 0.65/0.35. We demonstrated the abrupt increase in quantum efficiency at reduction of the well width that allowed to observe the optically excited stimulated emission in ZnO quantum wells with the excitation threshold of ~210 kW/cm^2.

Unfortunately, the creation of ZnO homojunction diodes is limited due to the difficulties of *p*-ZnO film fabrication. As an alternative approach to utilize ZnO for optoelectronic applications, a *n*-ZnO/*p*-GaN heterojunction structure has been suggested. In our work the *n*-ZnO/*p*-GaN, *n*-ZnO/*i*-ZnO/*p*-GaN and *n*-ZnO/*n*-$Mg_{0.2}Zn_{0.8}O$/*i*-$Cd_{0.2}Zn_{0.8}O$/*p*-GaN heterostructure LEDs on *c*-Al_2O_3 have been grown and investigated.

The *p*-GaN films were produced by MOCVD and the *n*-ZnO and *i*-ZnO films were grown by PLD. The LEDs showed I-V characteristics confirming a rectifying diode behavior. RT wide electroluminescence peaked at about 490 nm was observed in the *p*-GaN/*n*-ZnO heterojunction and the ultraviolet EL of *n*-ZnO/*i*-ZnO/*p*-GaN peaked at about 380 nm. The *n*-ZnO/*n*-$Mg_{0.2}Zn_{0.8}O$/*i*-$Cd_{0.2}Zn_{0.8}O$/*p*-GaN heterostructure LED exhibited a blue EL with peak about 460 nm. The EL intensity of HS LED was higher than those of *p*-GaN/*n*-ZnO and *n*-ZnO/*i*-ZnO/*p*-GaN LEDs.

4D VISUALIZATION OF SPECTRAL DATA WITH ACCOUNT OF HUMAN EYE OPTICAL SENSITIVITY SPECIFICS.

Zemskov I., Skurihin A.,

NT-MDT

The purpose of scientific visualization is to render the results of a scientific research into visual patterns, which facilitates perception and data processing and allows to make many physical processes, which are invisible to a human eye, perceptible and illustrative. Spectral analysis, which is one of the most common experimental techniques of identification of the object's chemical composition, makes it possible to study the characteristics of physical entities, basing on how the object emits, or interacts with light.

This work is devoted to the implementation of computer 4D Raman spectrum visualization with allowance for spectral properties of human eye sensitivity. The model of the space described has three space axes as well as a wave-length axis. The purpose of spectral visualization is to represent graphically the Raman spectrum data and facilitate considerably it's perception and analysis. [1]

The objective is to develop a visualization technique which allows to create visual images of a spectrum, determined at all points of the sample in a spatial domain given. In this case, a spectrum is a relation between the integral intensity of the emission and the wavelength. This application can be useful in chemistry, medicine, biology, materials science and etc.

During the testing the recieved data was rendered in order to be easily perceptible and processible in the future. Color coding was used for general visualization of the received optical spectrum. RGB color coding method, which is most common method in digital technology, was taken as a model. [2]

Spectral data was rendered according to this method, with account of RGB-sensitivity of an average observer. The eye sensitivity curve was apprised by the Gauss contour, [4] the coefficients of approximation were matched experimentally and were further adjusted for a specific output equipment. The ray tracing method with the use of Phong illumination model [2] was used for data visualization.

Список литературы

А. Е. Бондарев, В. М. Чечеткин Анализ развития концепций и методов визуального представления данных в научных исследованиях задач вычислительной физи-

ки. 19-я Международная Конференция по Компьютерной Графике и Зрению ГрафиКон’2009 Москва, Россия Труды Конференции.

Френсис Хилл. OpenGL Программирование компьютерной графики. Второе издание. Питер, 2002 г.

Пугачев В.С. Теория вероятности и математическая статистика, 2-е изд., исправл. и дополн. - М.: Физматлит, 2002.— 496 с.

Long D.A.(Derek Albert) The Raman Effect: a unified treatment of the theory of Raman scattering by the molecules.

GENERATION OF ENTANGLED POLARITONS IN DOPED WAVEGUIDES

I.O. Barinov, A.V. Prokhorov, A.P. Alodjants, S.M. Arakelian

Vladimir State University named after Alexander and Nikolay Stoletovs,, Vladimir, Russia
(4922) 479947, alodjants@vlsu.ru, *avprokhorov@vpti.vladimir.ru*

Theory of formation of entangled polaritons for probe field in the case of Raman interaction scheme in Y_2SiO_5 crystal doped by ^{59}Pr atoms is analyzed. The opportunity of dynamical amplification of entangled polaritons in such a system is shown.

Figure 1a shows the scheme of atom-optical interaction. Two fields – a classical flat pump wave with frequency ω_p and wave vector $\vec{k}_p$, and weak (quantum) probe (Stokes) field with the frequency ω_s and wave vector $\vec{k}_s$ interact with atomic system with Λ-configuration of energy levels . These field take part in stimulated Raman scattering under interaction with ^{59}Pr atoms doped in Y_2SiO_5 crystal and placed between two mirrors of Fabry-Perot resonator (Fig.1b). Probe field falls onto the waveguide and as a result of mixing of its photons with atomic excitations at the transition $|a\rangle \to |b\rangle$, the formation of (*Raman*) polaritons with wave vector $\vec{k}_{pol} = \vec{k}_p - \vec{k}_s$ takes place. In this geometry, the wave vector component $k_\perp$ perpendicular to the plane of the mirror forms a standing wave; the parallel wave vector component $k_\parallel$ determines the dispersion characteristics and correlation effects for the Raman polaritons, which is the subject of study in this paper.

Assuming that initially most of the atoms are in the ground state $|a\rangle$, we introduce the boson annihilation operators for polaritons:

$$\Phi_{1,k} = \mu f_k + \nu a_k b_k^+, \ \Phi_{2,k} = \nu f_k^+ + \mu a_k^+ b_k, \quad (1a,b)$$

where f_k, f_k^+; a_k, a_k^+; b_k, b_k^+ are annihilation and creation operators of photons of the probe field and atoms at the levels $|a\rangle$ and $|b\rangle$. Operators (1) satisfy the commutation relation $\left[\Phi_{i,k};\Phi_{j,k}^+\right] = \delta_{ij}$, $(i,j=1,2)$ provided $\mu^2 - \nu^2 = 1$. To study quantum correlation properties of two types of polaritons (1) we introduce the parameters:

$$V_k^0 \equiv V_k^\theta\big|_{\theta=0} = \frac{1}{4}\left\{\Delta^2\left(X_{1,k} + X_{2,k}\right) + \Delta^2\left(Y_{1,k} - Y_{2,k}\right)\right\}, \quad (2a)$$

$$V_k^{\pi/2} \equiv V_k^\theta\big|_{\theta=\pi/2} = \frac{1}{4}\left\{\Delta^2\left(Y_{1,k} + Y_{2,k}\right) + \Delta^2\left(X_{1,k} - X_{2,k}\right)\right\}, \quad (2b)$$

where $X_{1,k} = \Phi_{1,k} + \Phi_{1,k}^{+}$, $Y_{1,k} = -i\left(\Phi_{1,k} - \Phi_{1,k}^{+}\right)$, $X_{2,k} = \Phi_{2,k} + \Phi_{2,k}^{+}$, $Y_{2,k} = -i\left(\Phi_{2,k} - \Phi_{2,k}^{+}\right)$ define

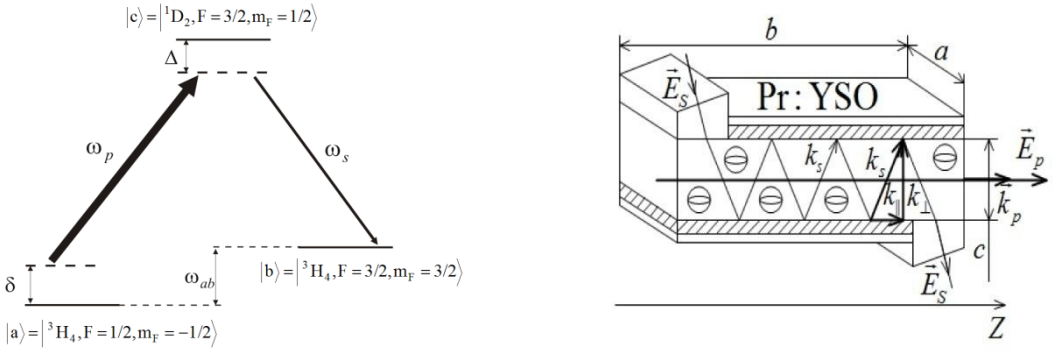

(a) (б)

Fig. 1. (a) Λ - scheme of atomic-optical interaction for atoms ^{59}Pr ; (b) polariton waveguide model based on doped crystal.

Hermitian operators for amplitude and phase quadrature [1]; $\Delta^2 A$ determines the dispersion of values A. The criterion of entanglement of polaritons (1) characterized by inequalities $V_k^0 < 1$, $V_k^{\pi/2} < 1$. In the weak field approximation ($N_{ph} << N$) for Λ - scheme ($\Delta > \gamma_a$) atom-field interaction we obtain the following equations for eigen-frequencies of real $\Omega_{1,2}^{(R)}$ and imaginary $\Omega_{1,2}^{(I)}$ components of the atom-optical system:

$$\Omega_{1,2}^{(R)} = \frac{1}{2}\left(\omega_+ + \frac{k^2\Delta}{\Delta^2+\gamma_c^2} \pm \sqrt{D^2 - \Gamma_-^2 - 4\lambda^2}\right), \qquad \Omega_{1,2}^{(I)} = \frac{1}{2}\left(\Gamma_+ \pm \frac{D\Gamma_-}{\sqrt{D^2 - \Gamma_-^2 - 4\lambda^2}}\right),$$

(3a,b)

where $\Gamma_\pm = \Gamma_{at} \pm \gamma_{ph}$, $\Gamma_{at} = \gamma_a + \gamma_b + \frac{\kappa^2\gamma_c}{\Delta^2+\gamma_c^2}$, $D = \omega_- + \frac{\kappa^2\Delta}{\Delta^2+\gamma_c^2}$, $\lambda = \frac{\kappa g}{\Delta}$,

$\omega_\pm = \omega_{ba} \pm \omega_{ph}$, $\omega_{ph} = \omega_p - \omega_s$; γ_{ph} and γ_i characterize the relaxation processes for the probe field and atoms, respectively. In the paraxial approximation for the probe field the group velocity of the two-dimensional polariton wave packet spreading along z–axis is

$$\upsilon_{1,2,tr} = \frac{1}{2}\hbar k_{||}\left(\frac{u}{m_{at}} - \frac{1}{m_{ph}} \pm \frac{\Delta_0}{\sqrt{\Delta_0^2 - \Gamma_-^2 - 4\lambda^2}}\left(\frac{u}{m_{at}} + \frac{1}{m_{ph}}\right)\right), \qquad (4)$$

where $u = 1 - \hbar k_p \cos\theta / c m_{ph}$, $\Delta_0 = \delta + k^2\Delta\Big/\left(\Delta^2+\gamma_c^2\right)$, $\delta = \omega_{ba}^0 - \omega_p + ck_\perp$, δ is detuning (Fig.1a), $m_{ph} = \hbar k_z / c$ is photon mass in the resonator.

The effect of induced trapping of Raman polaritons of the upper branch (3a) is observed in the strong coupling regime ($\Gamma_- < \lambda$). This effect leads to zeroing of polariton group velocity in the case of the absence of absorption in the system ($\Omega_1^{(I)} = 0$ for point A in Fig.2a). Actually, this conditions determines the threshold of amplification of probe field polaritons and corresponds to the intensity of pump field $I_p = 0.96$ W/cm^2. In the case of exceeding the

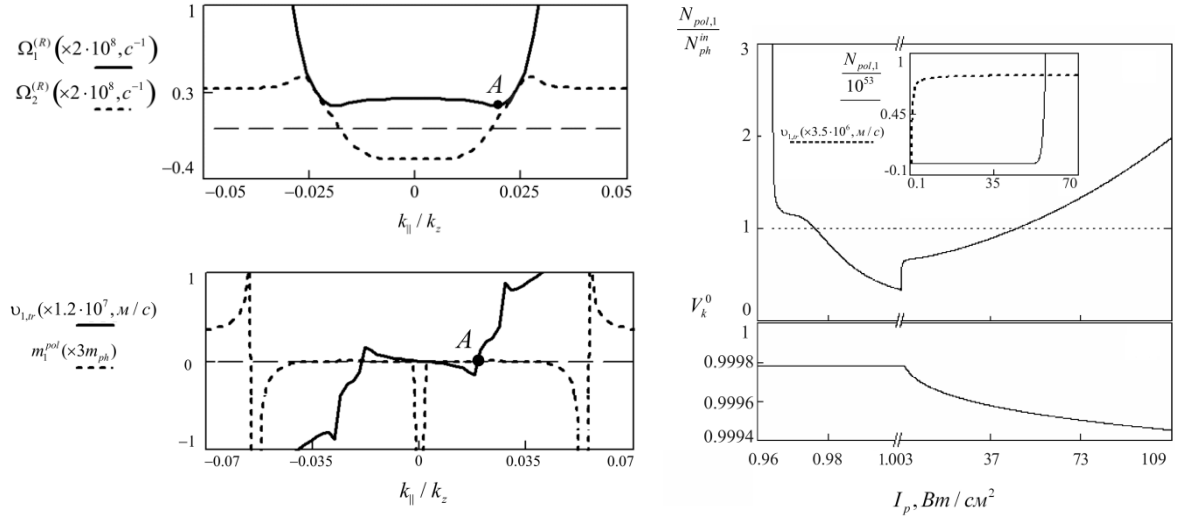

(a) (b)

Fig.2 (a) The dispersion relations $\Omega_{1(2)}^{(R)}$, group velocity $\upsilon_{1,tr}$ and mass of polaritons m_1^{pol} in z-direction; (b) dependences of average number of polaritons $N_{pol,1} = \left|\Phi_{1,k}\right|^2$, normalized to the initial number of photons N_{ph}^{in} and correlation parameter V_k^0 at the output waveguide on the intensity of the pump field. The parameters of interaction are $\Gamma_{at} \approx \gamma_c = 1.47\cdot 10^7 s^{-1}$, $I_p = 0.96$ W/cm^2, $\Delta = 6\cdot 10^4$ c^{-1}; number of atoms in the interaction region $N = 3\cdot 10^4$, number of photons at the input $N_{ph}^{in} = 100$.

threshold of amplification the group velocity of polaritons becomes positive; sharp parametric growth of the polariton number occurs within the intensities $0.96 \div 0.975$ W/cm^2 – see Fig.2b. Further increasing of pump power leads to a decreasing of average number of polaritons at the output of the medium, and within the range of $0.975 \div 47$ W/cm^2 polariton amplification stops. This behavior is in good agreement with experimentally observed transition from the giant polariton luminescence signal obtained from diode [2] to "gap" of generation with increasing pump power. The given phenomenon is accounted for group velocity of polaritons which growth faster as compared with the growth rate of polaritons mean number (see inset in Fig.2b). With further increasing of pump intensity growth of the group velocity is slowed down while increasing of the speed of polaritons amplification and their average

number begins to grow Fig.2b. This regime is accompanied with generation of entangled polaritons in doped waveguide when condition $V_k^0 < 1$ is fulfilled.

1. K. Dechoum, P.D. Drummond, S. Chaturvedi, M.D. Reid, *Phys. Rev. A.*, 70, 053807-053831 (2004).

2. R. Butte, M. S. Skolnick, D.M. Whittaker, D. Bajoni, J.S. Roberts, Phys. Rev. B. **68,** 115325-115330 (2003).

PASSIVE MODE LOCKING ON BASE OF SINGLE-WALL CARBON NANOTUBES FOR Yb:LYSO LASER

A. A. Burtsev[1], D. N. Antonov[1], M. N. Gerke[1], O. Ya. Butkovsky[1], D. V. Khudyakov[2], A. S. Lobach[2]

[1]Vladimir State University, Gorky St., 87, P.C. 600000 Vladimir, Russia
[2]Institute of Problems of Chemical Physics, Russian Academy of Science, Chernogolovka 123182, Russia
e-mail address: murrkiss2009@yandex.ru

Rapidly developing optical technologies need new media with fast optical responses for devices governing optical radiation. The composite materials containing a nonlinear optical element in a polymer matrix are now more widely used as such media due to their technological effectiveness and process ability. Recently, several groups proposed and demonstrated the nonlinear optical materials using single-wall carbon nanotubes (CNTs) as saturable absorbers for mode locking in various laser systems. The advantages of such devices with CNTs are subpicosecond recovery times, a wide IR range, and chemical stability. Optical devices with CNTs can easily be prepared as thin polymer films, which makes them promising as compared with existing passive mode lockers based on semiconductor saturable absorber mirrors, which require complex and expensive techniques.

In order to be able to build a bulk laser in a similar configuration to a SESAM (semiconductor saturable absorber mirror) based cavity we developed reflective type saturable absorbers based on the above-mentioned CNT-polymer composite materials (Fig.1). Our current absorbers consist of commercially available dielectric mirrors based on TiO_2/SiO_2 on a fused silica substrate with a broad reflectivity bandwidth. These mirrors were coated with a thin layer (a few microns thick) of the CNT-polymer composite material by spin coating. For the polymers polyimide and carboxymethyl cellulose (CMC) is used.

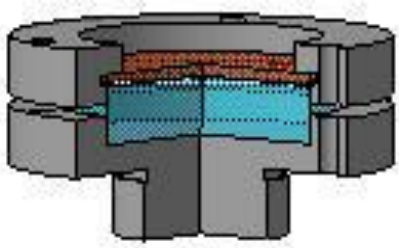

Fig.1. Construction of SAINT (saturable absorber injected nanotubes).

To achieve efficient saturation of the CNTs, the wavelength of the CNT absorption should coincide with the emission wavelength of the laser. Because the wavelength of the

CNT absorption is a function of tube diameter, two types of CNT materials with different diameter distributions are adopted. For 1.5 μm use, CNTs can be prepared by the laser ablation method. For our experiments (λ = 1 μm) CNTs were prepared by HIPCO-method.

Figure 2 shows the absorption spectra of film with nanotubes. The amount of saturable absorption of each sample was controlled by the concentration of CNTs in the polymers and by the rotation speed of the spin coater. Figure 3 shows experimental setup of the Yb:LYSO laser.

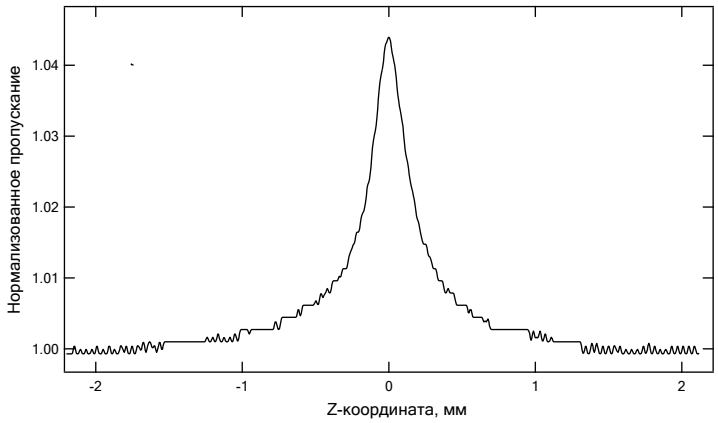

Fig. 2. Absorption spectra of the CNT-polymer composite films.

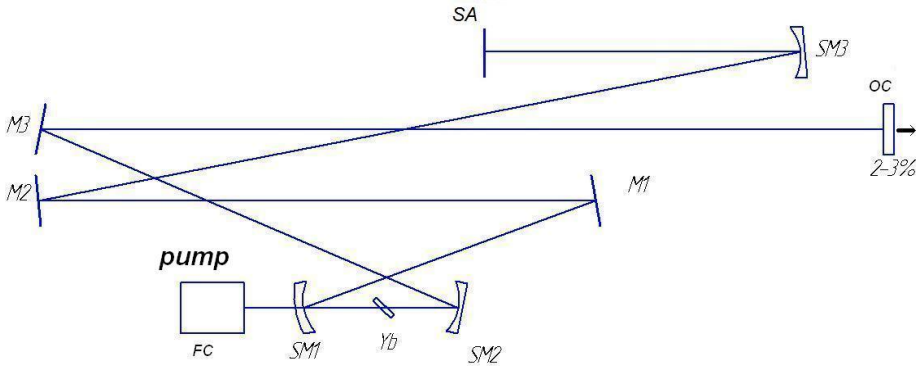

Fig. 3. Experimental setup of the Yb:LYSO laser. OC: output coupler; M1-M3: standard Bragg-mirrors; SM1-SM3: spherical mirrors; SA: Saturable absorber mirror based on semiconductors (in the 1st experiment) and on carbon nanotubes (in the 2nd experiment).

In this work we demonstrate the parameters of non-linear absorption of the CNT/CMC polymer film and the use of the saturable CNT/CMC thin-film absorber for passive mode locking in a solid-state laser at λ= 1050 nm (Yb:LYSO laser).

Literature:

1. Claude Rulliere. Femtosecond laser pulses: principles and experiments. p. cm. – (Advanced texts in physics, ISSN 1439-2674).- 2005, 438 p.

2. Keller U., Weingarten K. J., Kärtner F. X., Kopf D., Braun B. and others. Semiconductor Saturable Absorber Mirrors (SESAM's) for Femtosecond to Nanosecond Pulse Generation in Solid-State Lasers. Article from JSTQE Vol. 2, No. 3, Sept 1996.

3. D. V. Khudyakov, A. S. Lobach, and V. A. Nadtochenko Nonlinear optical absorption of single-wall carbon nanotubes in carboxymethylcellulose thin polymer film and its application as a saturable absorber for mode-locking in pulsed Nd:glass laser. Published 2009

4. S. Y. Set, H. Yaguchi, Y. Tanaka, M. Jablonski, Y. Sakakibara, A. Rozhin, M. Tokumoto, H. Kataura, Y. Achiba, and K.Kikuchi,"Mode-locked fiber lasers based on a saturable absorber in corporating carbon nanotubes," in Optical Fiber Communication Conference, OSA Trends in Optics and Photonics (Optical Society of America, 2003), Vol. 87, paper PD44.

5. T. R. Schibli, K. Minoshima, H. Kataura, E. Itoga, N. Minami, S. Kazaoui, K. Miyashita, M. Tokumoto, Y. Sakakibara Ultrashort pulse-generation by saturable absorber mirrors based on polymer-embedded carbon nanotubes. Published 2005

LASER-ASSISTED AU-CU AND AU-AG NANOPARTICLES DEPOSITION FROM LIQUID METALLOORGANIC COMPLEXES

Povolotskaya A.V., Povolotskiy A.V., Manshina A.A.

Saint-Petersburg State University, Department of Physics, Saint-Petersburg, Russia
avpovolotskaya@yandex.ru

Since the very beginning the laser-assisted methods have become of critical importance for the metal deposition. Various laser techniques allow metal precipitation on the different kinds of the materials. One of them is the Laser-induced chemical liquid phase deposition (LCLD), which is considered among the others to be the most promising and efficient. Indeed, the LCLD method offers convenient way of the metal precipitation with rather high uniformity of the morphology and good electrical properties of the deposits. In spite of the achieved high quality of the metal structures the ongoing attempts are undertaken for the improving of the deposition efficiency and the quality.

In the LCLD method the laser initiates the chemical reducing reaction and the laser focal volume determines the volume of this reaction what results in the localized submicron metal deposition. Also this method permits controling width, morphology and resistance of metal structure as a result of variation laser power, temperature of solution and other parametrs of deposition. The laser-assisted photochemical reaction yields deposition of the structures on the substrate with high degree of adhesion. This method is characterized by technological efficiency, chemical safety and low-price equipment.

Up to now the LCLD method was successfully realized for precipitation of such metals as Cu, Ni, Pd, Ag on several kinds of semiconductors and insulators such as Si, Ge, GaAs, polymers and so on. But a question about nano-alloys deposition using this method has been never risen.

In the present work the possibility of nano-alloy precipitation was investigated. The deposition process was carried out from metalloorganic complexes witch consist of the $[Au_6Cu_6]$ and $[Au_8Ag_{10}]$ clusters 'wrapped' in the $[Au_3(diphosphine)_3]^{3+}$ triangles [1,2]. Possibility to change Au-Cu and Au-Ag ratio in the initial solution allow controling composition of the deposited metal structure.

This technology for creation nanoparticles can be successfully used in Surface Enhanced Raman Spectroscopy (SERS) [1-3] and Localized Surface Plasmon Resonance spectroscopy (LSPR).

References:

[1] I.O. Koshevoy, A.J. Karttunen, S.P. Tunik, M. Haukka, S.I. Selivanov, A.S. Melnikov, P.Y.Serdobintsev, M.A. Khodorskiy, T.A. Pakkanen, " Supramolecular Luminescent Gold(I)-Copper(I) Complexes: Self-Assembly of the Au_xCu_y Clusters inside the $[Au_3(diphospine)_3]^{3+}$ Triangles," Inorg. Chem. 47, 9478 (2008).

[2] I.O. Koshevoy, Y.-C. Lin, A.J. Karttunen, M. Haukka, P.-T. Chou, S.P. Tunik, T.A. Pakkanen, "An intensely and oxygen independent phosphorescent gold(I)-silver(I) complex: "trapping" an Au_8Ag_{10} oligomer by two gaold-alkynyl-deiphosphine molecules", Chem. Commun., 20, 2860-2862 (2009).

SYNTHESIS OF MULTI-WALLED CARBON NANOTUBES OVER MgO-SUPPORTED CATALYSTS

Romantsova I.V., Melezhyk A.V., Tkachev A.G.

Tambov State Technical University, Tambov
8 (4752) 63-92-93, iris_tamb68@mail.ru

Carbon nanotubes (CNTs) are allotropes of carbon with a cylindrical nanostructure. These cylindrical carbon molecules have novel properties, making them potentially useful in many applications in nanotechnology, electronics, optics, water and gas purification, and other fields of materials science, as well as potential uses in architectural fields. At present moment there are many methods of carbon nanotubes synthesis, such as arc discharge, laser ablation, high pressure carbon monoxide (HiPco), and chemical vapor deposition (CVD) [1]. CVD is a common method for the commercial production of carbon nanotubes. During CVD, a substrate is prepared with a layer of metal catalyst particles, most commonly nickel, cobalt, iron, or a combination [2].

Catalyst is the key factor and powerful instrument determining the quality of CNTs. Numerous methods of synthesis of catalysts are known, for instance, co-precipitation, thermal decomposition. However, the best homogeneity of a catalyst is provided by sol-gel technology, due to uniform distribution of components in starting solution.

The goal of the present work is creation of highly effective catalytic systems for multi-walled CNTs (MWCNTs) production by citrate sol-gel method, as well as evaluation of influence of the catalysts chemical composition and working parameters on yield and quality of carbon nanotubes.

In order to study influence of catalyst chemical composition on CVD MWCNTs production process following systems were investigated: Ni-Co/MgO, Ni-Y/MgO, Ni-Mo/MgO, Ni-Fe-Co/MgO, Ni-MgO, Fe-Co/MgO.

The Ni-Co/MgO catalyst was prepared by a citrate sol-gel method. Typically, $Ni(NO_3)_2 \cdot 6H_2O$ was added into appropriate amount of distilled water under stirring until a transparent solution was obtained, then $Mg(NO_3)_2 \cdot 6H_2O$ and $Co(NO_3)_2 \cdot 6H_2O$ was added into the solution under stirring followed by introducing ethylene glycol $(CH_2OH)_2$ and Citric acid $HOC(CH_2COOH)_2 \cdot COOH$ into the solution. The solution was then heated at 80 ^{0}C for 3 h until it became a sheer of green foamy materials and then was heated at 140 ^{0}C for 1 h the foamy materials were ground into powder. The powder was placed into muffle furnace in air at 550 ^{0}C for 1 h to burn the organics. To grow the MWCNTs, the catalyst powder was sprayed on the metal disk located at the center of a reactor of periodic CVD process of CNTs

production. The temperature of process was 650 ^{0}C. A mixed gas consisting of propane-butane. The time of process was 30 min.

The catalysts and the as-grown MWCNTs were characterized by scanning electron microscopy (SEM) (Carl Zeiss, Neon 40), transmission electron microscopy (TEM) (JEOL, JEM-200CX), high resolution transmission electron microscopy (HRTEM) (JEOL, JEM-2010).

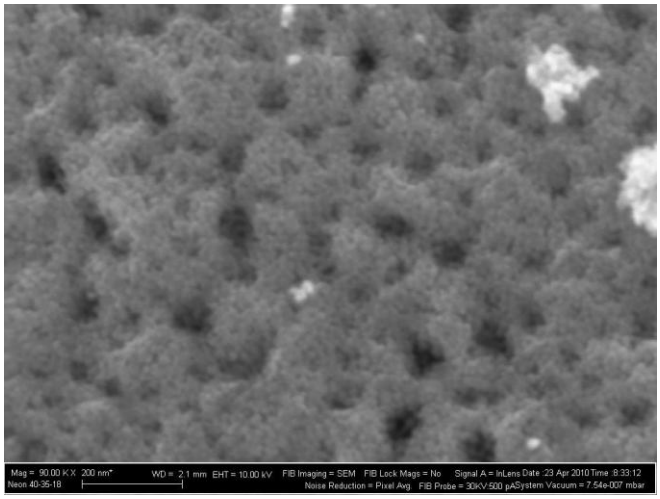

Fig. 1. SEM images of the Ni-Co/MgO catalyst structure

Fig. 1 gave the SEM images of the catalysts structure. The size of the catalyst is in the range of 10–25 nm.

In the present work structural and texture parameters of catalyst were studied. Among the most valuable characteristic of a catalyst there are surface area, pore volume and pore size distribution. These parameters were measured with using SORBTOMETR-M surface analyzer. Typically the catalysts studied were characterized by following values of parameters: specific surface area 3.2-133 m^2/g, area of mesopores 4.4-138 m^2/g, micropore volume 0.001-0.062 cm^3/g.

Catalyst particle size distribution was determined with MicroSizer 201 laser analyzer. The compositions and properties of the catalysts are summarized in Table 1.

Table 1. The main characteristics of the catalytic systems.

Catalyst chemical composition	Yields, g/g	Surface area, m^2/g	Particle size, mcm	Bulk density, kg/m^3	Real density, kg/m^3
Ni-Co-MgO	38.4	61	49.7-57.1	640	3306
Ni-Y-MgO	26.5	46	39.9-47.1	410	2749
Ni-Mo-MgO	20.9	50	39.1-47.1	800	2794
Ni-Fe-Co-MgO	15.4	41	39.1-47.1	590	2059
Ni-MgO	1.96	34	33.8-39.9	390	2136
Fe-Co-MgO	1.83	62	39.1-47.1	370	2012

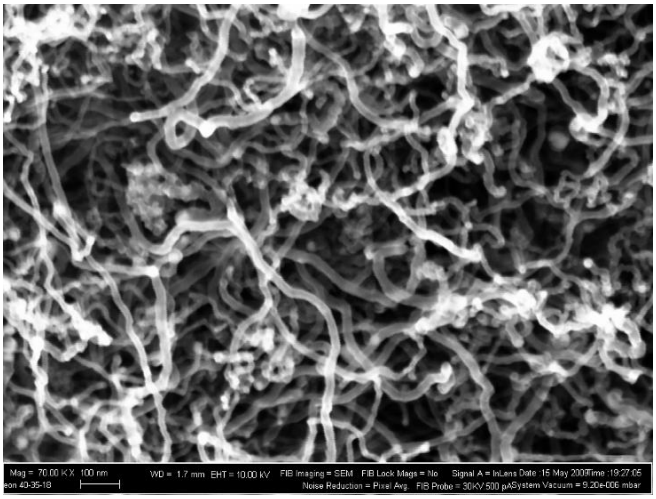

Fig. 2. MWCNTs grown on Ni-Co/MgO catalyst

Fig. 2 represent the typical SEM images which showed that the MWCNTs synthesized using propane-butane as carbon source and Ni-Co/MgO as catalyst are MWCNTs with the diameter of the nanotubes is in the range of 5–30 nm. High resolution TEM observation showed that the MWCNTs have well-graphitized structure with conical walls (Fig. 3). Conic nanotubes are most subject to connection of various functional groups and show increased adsorptive characteristics and these nanotubes can be successfully used for purification of liquids and gases.

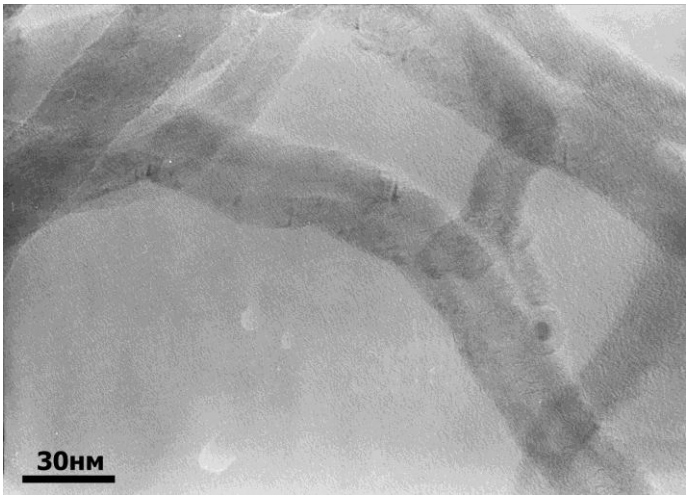

Fig. 3. HRTEM images of an individual MWCNTs

In the present work demonstrated that MgO-supported catalysts synthesized by citrate sol-gel method can be used for the growth of MWCNTs with high yields and high purity (surface area, diameter, length and so on).

BIBLIOGRAPHY

1. Harris P. F. Carbon Nanotubes and Related Structures: New Materials for the Twenty-first Century, Cambridge University Press, 279 (1999).

2. Dupuis A.C. The catalyst in the CCVD of carbon nanotubes a review // Progress in Materials Science, Vol. 50, pp. 929-961 (2005).

EFFICIENCY OF RECORD OF THE QUANTUM INFORMATION IN THREE LEVELS

Nefediev L.A., Rusanova I.A.

Tatar state humanitarian-pedagogical university, Kazan, RUSSIA
8(843)2925373, irusanova@yandex.ru

Investigation of quantum information processes in the three-level systems in the optical echo-holography. The effectiveness of recording and copying the previously shown distribution of quantum gates within the inhomogeneously broadened resonance lines of the number of elements of the message the first object pulse and the magnitude of the inhomogeneously broadened line, the length of the time interval between the object and copying the pulse and medium parameters, as well as power laser pulses. We consider the temporal evolution of quantum information in the light of relaxation times. It is shown that the time between the pulses are close to the relaxation time, is more rapid destruction of the superposition states.

We investigate the recording conditions in three-level quantum information systems with phase memory. Resonant medium consisting of multilevel atoms interacting with a sequence of laser pulses of different frequencies, can behave as multi-level quantum gates that perform logic operations. Methods of optical holography, the echo can store, transform and manipulate information stored in the object laser impulsah1 импульсах[1,2]. Study the effectiveness of the process of recording and conversion information contained in the encoding of the object pulse, based on previously developed information theory method for the study of quantum information processes in the three-level resonant media with phase memory. After the interaction with laser pulses selected quantum states of the subsystems are entangled with different frequencies. This entanglement of states can lead to copying the distribution of q-bits on different lines inhomogeneously[3-5].

The bearer of structural information in a resonant medium is transient dynamic lattice described by a density matrix. If there are only two quantum states of a system $|1\rangle$ and $|2\rangle$, and the general state is a linear superposition $|\psi\rangle = \alpha|1\rangle + \beta|2\rangle$ (where α and β - the complex numbers). The corresponding density matrix operator

$$\rho = |\psi\rangle\langle\psi| = |\alpha|^2|1\rangle\langle 1| + |\beta|^2|2\rangle\langle 2| + \alpha\beta^*|1\rangle\langle 2| + \alpha^*\beta|2\rangle\langle 1|,$$

where are the active part of the last two terms. Determine the amount of quantum information systems in the q-bits. Consider the transformation of information J_C contained in

the object laser pulse (OR) for its impact on the system of three-level atoms with a state $|1\rangle,|2\rangle,|3\rangle$. Object momentum can be represented as a sequence (train) of pulses under the condition $n\partial t << T_1, T_2$, where T_1 and T_2 - the longitudinal and transverse irreversible relaxation of the system, ∂t - the duration of message element. After the interaction with laser pulses selected quantum states of the subsystems become entangled at different frequencies. This entanglement of states and can lead to copying the distribution of q-bits on different lines inhomogeneously. Consequently, the efficiency of copying quantum information J_q depends on the type of entanglement of states. The final result will look like:

$$J_q(Q) = \int_{-\infty}^{\infty} g(\Delta_1) d\Delta_1 \int_{-\infty}^{\infty} g(\Delta_2) J_q(Q(\Delta_1, \Delta_2)) d\Delta_2,$$

$$J_q(Q_1) = \int_{-\infty}^{\infty} g(\Delta_1) d\Delta_1 \int_{-\infty}^{\infty} g(\Delta_2) J_q(Q_1(\Delta_1, \Delta_2)) d\Delta_2,$$

$$J_q(Q_2) = \int_{-\infty}^{\infty} (1-\rho_{22}) g(\Delta_1) d\Delta_1 \int_{-\infty}^{\infty} g(\Delta_2) J_q(Q_2(\Delta_1, \Delta_2)) d\Delta_2,$$

$$J_q(Q_2|Q_1) = J_q(Q) - J_q(Q_1) \approx J_q(Q_2),$$

where $g(\Delta_1), g(\Delta_2)$ - the distribution function of q-bits in frequency.

Optimal conditions for copying quantum information J_q depends on the type of entanglement of states. The effectiveness of recording, copying and converting quantum information depends largely on the power of momentum, and copying the characteristics of the acting laser pulse code. The influence of the recording and copying of quantum information elements of the communication object first pulse, the duration of the time interval between the object and copying the pulses and the medium. We consider the time evolution of quantum information, based on relaxation times. It is shown that the time between the pulses close to the relaxation time, a more rapid destruction of the superposition states[6,7].

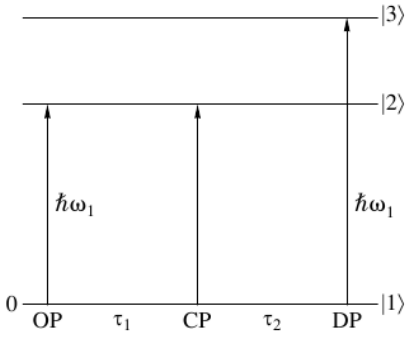

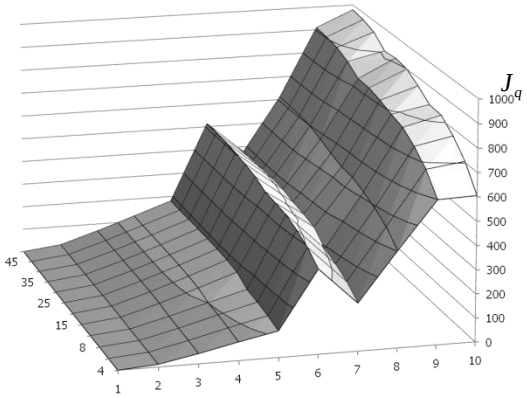

A σ B n

Pic.1. A) Scheme to record and copy information. OP - object pulse, CP – copying pulse, DP - showing impulse, τ_1, τ_2 - the time intervals between pulses; B) dependence of the quantum information of the resonant medium J_q on the number of elements of the message n object pulse and the magnitude of the inhomogeneously broadened line σ.

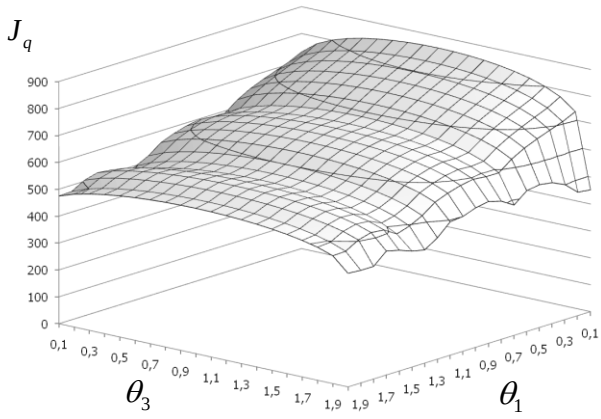

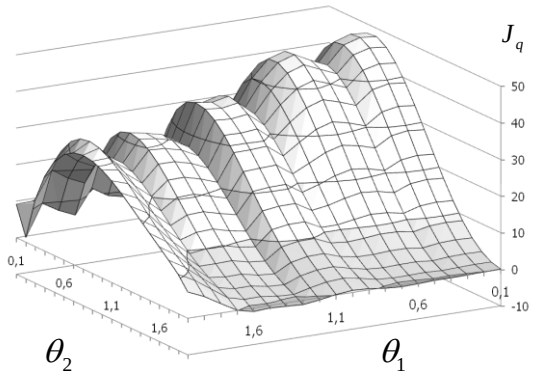

Pic.2. The dependence of quantum information of the resonant medium J_q the power of the object Θ_1, copying Θ_2 the developing Θ_3 pulses.

1. Л.А.Нефедьев, В.В.Самарцев, *ЖПС*. **47** №4, 640 (1987).

2 L.A.Nefediev, V.V.Samartsev, *Phys.Stat.Sol*. **88 (a)** 631 (1985).

3. N.J. Cerf, C. Adami *Phys.Rev.Lett.* **79,** 5194 (1997).

4. L.A. Nefed'ev, I.A. Rusanova, *Опт. и спектр.*, **90**, 1001 (2001).

5. L.A. Nefed'ev, I.A. Rusanova, *Laser Physics*, 3, 1 (2002).

6. L.A. Nefed’ev, I.A. Rusanova, Fourteenth International Youth Science School "Coherent Optics and Optical Spectroscopy", 18 - 21 October 2010, Kazan.

7. L.A. Nefed’ev, I.A. Rusanova, Multilevel quantum gates in the echo-holography, VI International Conference "Fundamental Problems of Optics - 2010" October 18-22, 2010, St. Petersburg.

PHOTOELECTRICAL PROPERTIES OF GRANULAR METAL FILMS

Gladskikh I.A.

Saint-Petersburg state university ITMO
Phone number - +79043333403, e-mail – 138020@mail.ru

Vashchenko E.V.

Saint-Petersburg state university ITMO
Phone number - +79111352029, e-mail – ev.vaschenko@gmail.com

In recent decades, researchs in the physics of low-dimensional structures are rapidly evolving. Nanostructured materials are the subject of increasing interest for fundamental and applied science [1,2] because, with a decrease of the characteristic sizes of their structural units to the nanoscale, they often acquire new properties due to quantum size effects and the increasing role of surface atoms and interactions.

Among the nanoparticles of simple materials, metal nanoparticles and their ensembles occupy a special place [3]. Close attention to them is due to the peculiarities of their electronic structure, on the one hand, and on the other, to the relative simplicity of their preparation for experimental studies. Delocalized electrons in metallic nanoparticles determine the nature of their behavior during interaction with external fields. In these processes, the most interesting feature is strong collective effects in the electronic system, determining the response of nanoparticles to an external perturbation.

In this study we investigated the electrical and photoelectrical properties of granular metal films supported on the surface of sapphire. Despite of the fact that the crystalline structure of the discrete islands comprising the granular film of a typical metal in most cases is similar to bulk, electrical properties of the granular metal films on an insulating substrate is radically different from the properties of the bulk metal, their properties being closer to that of semiconductors. The electrical resistivity of such systems is many orders of magnitude higher than that of the bulk metal, being determined, primarily, by the thickness of the film.

We measured the current-voltage characteristics of the deposited metal films both in vacuum and in air. Surface resistivity of the film in air was found to be $\rho = 2{,}5 \cdot 10^{14}$ Ω/□ , two times larger than in vacuum, $\rho = 1{,}25 \cdot 10^{14}$ Ω/□. To determine the nature of the dark conductivity of granular silver films on sapphire the temperature dependence of the dark current in the temperature range from 0° C (273 K) to +80° C (353 K) was measured With increasing temperature the dark current increases, hence, the conductivity of the films is non-

metallic. The activation energy of the conductivity of the granular silver films on sapphire substrate was found to be 0.48 eV in vacuum, and 0.2 eV in air.

We obtained the dependence of the photocurrent on the radiation wavelength in vacuum. Extinction spectrum and photoconductivity spectrum of the investigated film is shown in Figure 1. As can be seen, the plasmon resonance at 2.82 eV is obseved in the photoconductivity spectrum. It turned out that at the photon energies between 2.6 eV and 2.7 eV the photocurrent changes its sign.

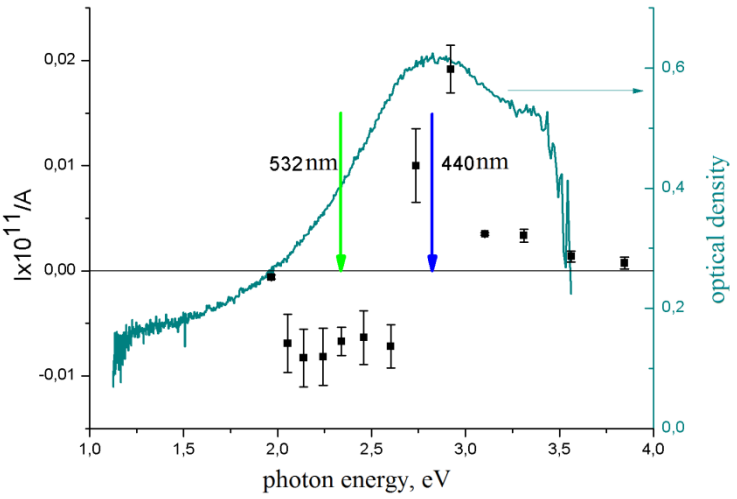

Fig. 1. Extinction spectrum of an the granular silver film on the sapphire substrate in vacuum (solid line, the corresponding y-axis is shown by the arrow); the photoconductivity spectrum of an ensemble of silver nanoparticles on sapphire in vacuum at room temperature. Negative values correspond to the decrease of the current under illumination.

We see that the short-wavelength radiation increases the conductivity of the film, while the long-wavelength radiation reduces the current flowing through the film. In this photoconductivity spectrum y-axis corresponds to the difference between the current measured under illumination during and without it (in darkness).

For a more detailed study of this effect, we measured the temperature dependence of the photocurrent at different wavelengths of illumination. This dependence was measured using a cw diode lasers with a wavelength of 440 nm (laser power 20 mW), in which case it is close to the maximum of the extinction spectrum, and with a wavelength of 532 nm (laser power 20 mW). Lasers were used to increase the signals. It was found that under illumination by photons with the energy of 2.33 eV in vacuum, with increasing temperature the photocurrent changes sign. In air the sign change of the photocurrent during the heating was not observed.

The coincidence of the bands and the closeness the maxima of the photoconductivity spectra and that of extinction are obvious. These experimental findings indicate that the collective electronic excitations localized in the metallic nanoparticles play an important role in the mechanism of the photoconductivity of granular metal films.

The experimental results are well described by a model based on the assumption that the conductivity occurs inside a dielectric substrate through the traps. The electrons from the metal granules move on the traps in the substrate, located near the Fermi level of silver. The activation energy obtained from the temperature dependence of dark conductivity for island metal films shows that the carrier transport is carried with a threshold of about 0.48 eV for silver films on sapphire. I.e., in these areas, the concentration of traps is sufficient for hopping conduction. For granular silver films on sapphire in vacuum, the photons with the energies larger than 2.7 eV throw the electrons in the conduction band of sapphire. Thus, the depth of the conduction band relative to the vacuum level in the band structure of sapphire is 1.58 eV. The photons with the energies less than 2.7 eV transfer electrons to the traps below the conduction band of the dielectric, where their mobility is lower than in the channel of dark conductivity. This leads to the decrease of the current under illumination of the film.

In the future we plan to make similar measurements for an island silver film on quartz.

Bibliographic list

1. Bohren C.F., Haffman D.R. Absorption and scattering of light by small particles. // Wiley 1998.
2. Kreibig U., Vollmer M. Optical Properties of Metal Clusters // Springer, Berlin, 1995.
3. Nepiiko S.A. Fizicheskie svoistva malykh metallicheskikh chastits. (In Russian, Kiev, 1985.)

SILVER HALIDE CRYSTALS FOR OPTICAL FIBERS USED IN INFRARED LASER SYSTEMS

Zaramenskikh K.S., Golovanov V.F., Lisitskiy I.S., Polyakova G.V., Kouznetsov M.S.

"GIREDMET", Moscow, Russia
(495) 981-30-10 (125), e-mail: gradan@mail.ru

Silver halide single crystals are transparent in a wide range of visible and infrared spectrum (from 0.35 to 30 microns), have low absorption of laser radiation ($3–5 \cdot 10^{-4}$ cm^{-1}), slightly soluble ($< 1 \cdot 10^{-4}$ g / 100g H_2O) and not toxic.

Interest to silver halides as an optical material appeared with the development of production technologies of optical fibers based on these compounds used in laser surgery as an element of the delivery of infrared radiation from the generator to the processing object. Theoretically, the estimated minimum of optical losses in laser crystals of KRS-13 (75% AgCl - 25% AgBr) is $1 \cdot 10^{-4}$ dB/km (in 4-5 μ wavelength range).

However, in practice, the crystals and fibers produced from them usually have the level of optical losses of about 1000 dB / km, which is also accompanied by the material degradation. This is explained by photolysis of silver halides, which is catalyzed by impurities and products of decomposition enhance the process that leads to instability of optical characteristics – reducing of light transmission and increasing of light scattering and absorption.

While obtaining silver halide materials for laser fiber optics the first aim is connected with deep purification of the initial salts for further crystals growth.

The analysis of pollution sources and the composition of impurities allows us to divide them into three groups:

1. Impurities coming from the reagents: cation impurities associated with metal (Cu, Al, Fe, Zn, Pb, Sn, etc.) and anionic impurities obtained from the reagents (NO3-, OH-, various sulfur compounds, water).

2. Impurities introduced into the material during the technological operations (organics, sulfur, cationic impurities)

3. Products of silver halides decomposition by photolysis, thermal dissociation, interaction of halides with anionic impurities.

The classification of impurities and their sources allows us to evaluate different methods of initial salts obtaining and purification and to choose the ways that provide the most optimized production of salt, suitable for laser crystals growing.

After analysis and testing of silver halides producing methods offered in literature (hydrochemical methods and direct synthesis from the elements), we choose a traditional deposition of individual chloride and bromide from nitrate solutions followed by the precipitate washing. Moreover, we applied know-how techniques at all stages of the process, what gave the opportunity to minimize the pollution of salts and to avoid photolysis.

Methods of deep purification of silver halides must satisfy the following requirements:

- provide removing of both cationic and anionic impurities,
- minimize the number of material transfers in order to avoid secondary contamination of salts,
- create conditions for conversion of decomposition products into the halide form.

The solution to these problems was provided by a complex of two apparatus units allowing combining several steps of purification in one process (filtration, vacuum distillation and directional crystallization), following one another without intermediate material transfers.

The resulting salts were analyzed using spark mass spectrometer JEOL JMS-01-BM. The total content of cationic impurities was less than $1 \cdot 10^{-4}$ wt.%, of halogens - $5 \cdot 10^{-4}$ wt.%. The content of anionic impurities (SO_4^{2-}, NO_3^-, OH^- and H_2O), estimated by infrared spectroscopy, was less than $1 \cdot 10^{-4}$ wt.% for each compound.

The crystals with diameter of 18 mm and length of 100-120 mm used for the extrusion of fibers were grown by the Bridgman-Stockbarger method. Quality control of these crystals showed that over 80% of the samples have laser radiation absorption coefficient $\leq 3 \cdot 10^{-4}$ cm^{-1}.

In order to create a double-layer optical fibers with different optical characteristics, in particular with different numerical aperture, we have to grow crystals with different refractive indices. These crystals must be chemically and optically homogeneous along the length and diameter.

It is known from literary data that AgCl-AgBr system form a continuous order of solid solutions with the minimum point, which is located in the range of 64-78% AgBr according to different sources. To determine the composition of the minimum point we have investigated AgCl-AgBr system in the whole concentration range by differential thermal analysis using derivatograph OD-103. To define more exactly the minimum point position the method of vertical directional crystallization of the melts with the composition in the range of 70-80% AgBr (with step of 1%) was used. The process was conducted at a speed of 1 mm/h, i.e. close

to equilibrium. In each case by means of chemical analysis of the beginning and end of the crystal phase separation of components along the length of the ingot was estimated. Additional growth processes of crystals with step in composition of 0.5% in the range of 73-77% AgBr with the rate of 0.5 mm/h allowed to determine finally that the system minimum point corresponds to 25 wt.% AgCl - 75 wt.% AgBr.

After a series of experiments the growth conditions providing obtaining the crystals with non-minimum point composition with a minimum phase separation of components along the length were chosen. Studies of double-layer fibers extruded from samples with different composition showed that crystals KRS-11 (50% AgCl - 50% AgBr), KRS-36 (35% AgCl - 65% AgBr) and KRS-63 (65% AgCl - 35% AgBr) are suitable for the extrusion of high optical quality fibers. Varying the core and shell composition the fibers with a required aperture of coming out beam were produced. The optical losses of the best waveguides extruded from the obtained crystals were 130 dB/km for single-layer and 250 dB/km for double layer ones.

The work was financially supported by the Department of Education and Science of RF in the frame of the project "Development of production methods of optical crystals based on high purity silver-containing compounds for IR-devices", the state contract № 16.513.12.3001.

NEW NONLINEAR OPTICAL CRYSTALS BASED ON THALLIUM, LEAD AND MERCURY HALIDES

Zaramenskikh K.S., Lisitskiy I.S., Golovanov V.F., Polyakova G.V., Kouznetsov M. S.

"GIREDMET", Moscow, Russia
(495) 981-30-10 (125), e-mail: gradan@mail.ru

The development of nonlinear laser optics and applying of effects revealed in the case of high-power light beams requires the creation of a new class of materials that not only transmit or refract the light, but also convert it. A special place is occupied by a parametric conversion of the optical signal with its frequency increasing, with the delivery of information of the original IR signal what allows using photo detectors and analyzers in the visible range, as they significantly exceed the medium- and long-wavelength ones by their sensitivity and resolution, and do not require cooling and background radiation screening.

Parametric conversion is used not only for the detection of the received signal, but also for the creation of IR spectra analyzers, highly sensitive thermal imaging systems for real time hot objects recognition. Such systems with the simultaneous use of single crystals and crystalline fibers of nonlinear optical materials provide the creation of compact multifunction IR and microwave photo detecting systems with full protection from the influence of a strong electromagnetic influences and flows of high-energy charged particles and gamma - photon and operate at room temperature.

Parametric conversion takes place while mixing infrared radiation with auxiliary radiation in a nonlinear medium. As a result, the radiation with the sum or differential frequency generates, containing the same information from the original IR signal. This effect has the most importance for mid-IR range (5 - 10 μ) in which atmospheric «transparency window», black-body radiation maximum at room temperature, and the working range of the most powerful of CO and CO_2 lasers are concentrated.

The creation of a nonlinear media requires the transition from elementary substances and double bond materials to the more complex compounds (triple and quadruple). This is accompanied by the complication of structure: the inversion center disappears, the ionic component of chemical bond caused by connecting the 2 or 3 kinds of atoms appears. At the same time, crystals suitable for a parametric conversion devices, must possess the transparency in wide spectral range of all the interacting wavelengths, good optical quality, resistance to the bulk and surface radiation damage (high beam strength) as well as large geometric size (a few cm^3).

We point out the compounds in TlCl-PbCl2, TlBr-PbBr2, TlJ-HgJ2 systems as promising nonlinear optical materials because the crystals on the basis of them can significantly extend the range of spectral transparency (from 0.4 to 45 μ). The halides of thallium, lead and mercury, previously deeply purified (content of 80 cationic impurities was 10^{-4} - 10^{-6} wt.% for each component), were used in this work.

In $PbCl_2$-TlCl, $PbBr_2$-TlBr and HgJ_2-TlJ systems the formation of several compounds promising for use in nonlinear optics is possible. The analysis of native and foreign literature has shown that the data about the composition of the melting points of these compounds given by different authors differs significantly. Therefore, the definition of phase diagrams using the methods of thermal analysis (derivatograph Q 1500D) and X-ray diffraction (DRON-4) was carried out.

At present stage of the work compounds Tl_3PbCl_5, Tl_4PbCl_6 and Tl_4HgJ_6 for new nonlinear crystals were synthesized. The synthesis was carried out in sealed ampoules in a halogenating atmosphere at the "rotating container" setup choosing the composition of the initial blend in accordance with the phase diagrams features. After melting of the mixture the ampoule was rotated around the axis for 3 hours in order to receive the complete homogenization of the melt.

The crystals were grown by the Bridgman-Stockbarger method. All Tl_3PbCl_5, Tl_4PbCl_6 Tl_4HgJ_6 crystals were visually transparent. The plates were cut from the crystals, polished and used for testing of optical characteristics. Transmission spectra of single crystal samples were measured using spectrophotometer (Specord 75IR) and Fourier spectrometer.

The phase diagrams of TlCl-$PbCl_2$, TlBr-$PbBr_2$, TlJ-HgJ_2 systems improved using the obtained data, as well as the results of structure X-ray studies and transmission spectra of the obtained crystals will be presented in the report.

The work was supported by the State Corporation "Rosatom" in the frame of the project "Development of production technology of new optical materials based on silver and thallium halide ", the state contract № H.4f.45.90.11.1041.

APPLICATION OF LASER IN SOLAR CELLS TECHNOLOGIES

Zuev D.A., Lotin A.A., Novodvorsky O.A.

Institute on Laser and Information Technologies, Russian Academy of Sciences (ILIT RAS), Moscow Region, Shatura, (496) 452 5995
e-mail: zuewda@yandex.ru

Laser technologies are widely used in industry and microelectronics. The replacement of expensive technologies for laser ones is the current trend in industry. For example, the use of laser patterning of ITO (tin-doped indium oxide) thin films instead of "wet" etching technology gives strong cost advantage in the flat panel industry [1]. The main task of PV is to reduce the cost of electricity produced by solar panels. The most obvious trend in the manufacture of solar cells is to substitute some of the most expensive technologies for new one. Currently investigations are being carried out to use the laser technologies for fabrication of contact structures (laser scribing for buried contacts, laser-fired contacts, depth-selective laser ablation, thin-film selective removal), surface texturing to reduce reflection, deposition of transparent conductive oxides (TCO) and laser doping, etc. [2-5].

In the case of mc-Si solar cells the problem of reflective losses is very acute as the conventional methods of chemical surface texturing do not yield the desired result because of the randomized crystallographic orientation of multicrystalline silicon grains. We have conducted the experiments to apply the laser technologies for mc-Si surface texturing. Texturing was performed in the vacuum chamber by the beam of the second harmonic Q-switched Nd:YAG laser with the pulse repetition frequency of 10 Hz, energy of 250 mJ, pulse duration of 10 ns and spot diameter about 2.5 mm. The optimal regimes for uniform texturing of a multicrystalline silicon (mc-Si) surface by pulsed laser radiation have been determined. The morphology and reflectance spectra of the texturized mc-Si have been studied. The laser texturized mc-Si samples with reflectance of 2-3% over a wide spectral region have been produced. The influence of subsequent chemical etching on the reflective properties of the texturized surface has been analyzed. It is important that the method of mc-Si surface texturing enables obtaining the texturized samples of large area. The size of the produced samples is sufficient for solar cell fabrication and characterization.

Investigation of low-temperature methods of (TCO) films production, which do not require subsequent heat treatment and produces films of good quality, is also important problem. TCO (transparent conductive oxides) have been widely used in thin-film solar cells, organic solar cells, optoelectronic devices, light emitting diodes, sensors, etc. Tin-doped indium

oxide (ITO) is one of the most used in this class of materials due to its high transparency in the visible region and good conductivity. We have performed experiments to study the optical, electrical, morphological and structural properties of films of ITO, obtained by the method of pulsed laser deposition. ITO thin films have been deposited by PLD on quartz substrates. The experimental setup has been described elsewhere [6]. The targets have been prepared of powders In_2O_3 and SnO_2. The set of ceramic targets ITO containing Sn in ratio of 2,5,8,11 at%. has been used. During deposition, the substrate temperature has been varied within (25 ÷ 400) C°. The pressure of Oxygen background gas introduced into the chamber during deposition has been ranged within (5 ÷ 20) mTorr after the initial evacuation to 10^{-7} Torr. The growth rate of ITO films has been determined by optical interferometer MII-4 (λ = 543 nm), surface morphology has been studied by atomic force microscopy (AFM) DME DualScope 2401. Optical properties (T%) have been measured by spectrophotometer Cary-1950 (Varian), the electrical properties have been investigated by Hall technique using an automated setup HSM 3000, the structural characteristics of the films were studied by X-ray diffractometer DRON-3M. The conditions of ITO films deposition have been defined, which allowed smooth films with a surface roughness of less than 3 nm. having a good conductivity ($1\text{-}2 \times 10^{-4}$ Ohm • cm) and high transparency in the visible region (>90%).

References

1. Matt H., Photonics Spectra, Vol. 42, I.3, March (2008)

2. L. Pirozzi, G. Arabito, F. Artuso, V. Barbarossa, U. Besi-Vetrella, S. Loreti, P. Mangiapane, E. Salza, Solar Energy Materials & Solar Cells, 65, 287-295 (2001)

3. V.V. Iyengar, B.K. Nayak, M.C. Gupta, Solar Energy Materials and Solar Cells 94(12), 2251 (2010)

4. Konstantinos A. Sierros, Darran R. Cairns, J. Stuart Abell, Stephen N. Kukureka, Thin Solid Films, 518, 2623–2627 (2010)

5. Jong Hoon Kim, Kyung Ah Jeon, Gun Hee Kim, Sang Yeol Lee, Applied Surface Science, 252, 4834–4837 (2006)

6. A.A. Lotin, O.A. Novodvorsky, V.Ya. Panchenko, L.S. Parshina, E.V. Khaydukov, D.A. Zuev, V.V. Rocheva, O.D. Khramova, K.D. Sherbachev, Physics of the Solid State, 53(3), 438 – 442 (2011)

TRAVELLING PLASMONIC MOD IN 1D SPASERS ARRAY

Andrianov E.S.,[1,2] Pukhov A.A.,[1,2] Dorofeenko A.V.,[1,2] Vinogradov A.P.[1,2]

[1] Moscow Institute of Physics and Technologies
[2] Institute of Theoretical and Applied Electromagnetics RAS

The collective interaction of self-oscillations spasers above the spasing threshold is studied theoretically. It is considered the simplest example of spasers array – the chain of spasers with equal distance between them. Spaser consists of a metal nanoparticle with plasmonic resonance coupled with quantum dot which population inversion caused by an external source. Above the threshold inversion spaser begins to generate a coherent near-field, localized at metal nanoparticle. However, for the development of metaplasmonics, it is of great interest to consider not a single spaser, but nanoscale structures composed of ordered lines and planes of spasers. In this case, the collective near-field interaction between spasers can significantly change the threshold of the generation and even lead in these structures to new phenomena and instabilities. It turns out that this chain of spasers generates not uniformly along its length, but by entirely different way. The generation process is carried out in a chain by the propagation of the steady harmonic autowave. This wave have a given wavelength four times more than the distance between spasers, and a given frequency equals the spasing frequency of an autonomic spaser. Because this harmonic wave is considerably nonlinear, then its amplitude is also unambiguously defined. Thus, the seemingly plausible assumption that the chain of spacers generates uniformly along its length is incorrect. It turns out this state of the spasing chain is unstable with respect to small perturbations. The development of the instability leads to arising travelling spasing autowave described above. From a general point of view such harmonic autowave of spasing interesting because it gives us, apparently, the first example of a nonlinear wave in the dissipative medium having a fixed frequency and wavelength, i.e. having the form of a harmonic wave.

PRINCIPALS OF LASER HOLE DRILLING VIA ADAPTIVE CONTROL BY THE REPETITIVELY PULSED LASER RADIATION CHARACTERISTICS

S.A. Solokhin, S.N. Smetanin, A.V. Gavrilov, M.N. Ershkov, A.V. Fedin

Kovrov State Technological Academy, ul. Mayakovskogo 19, Kovrov, 601910, Russia
E-mail: SolokhinS@gmail.com

In this paper principals of laser drilling of deep microholes via adaptive control by the repetitively pulsed laser radiation characteristics are presented. An optimum diagram of the laser radiation control during the laser hole drilling is defined. Possibilities to increase the hole depth and drilling rate at controllable Q-switching and active mode locking of the powerful Nd:YAG laser are proved in good accordance with experimental results.

LOCAL FIELDS AND RENORMALIZATION OF CHARACTERISTIC INTERACTION PARAMETERS FOR LIGHT EMITTERS IN A DIELECTRIC MEDIUM

Gladush M.G.[1], Kuznetsov D.V.[2]

[1]*Institute for Spectroscopy of the Russian Academy of Sciences (ISAN)*
Fizicheskaya Str., 5, Troitsk, Moscow region, 142190 Russia
[2]*Troitsk Institute for Innovation and Fusion Research (TRINITI)*
Pushkovykh str., vlad. 12, Moscow reg., Troitsk, 141190 Russia
Phone: +7 (495) 978 26 50
Fax: +7 (496) 751 08 86
E-mail: mglad@isan.troitsk.ru

We study the influence of macroscopic parameters of the host material on optical characteristics of impurity particles. A generalized master equation is derived for two-level emitters which form an ensemble of optical centers in a dielectric medium. The equation contains the effective values of the acting pump field, Lorentz shift and the radiation relaxation rate of on an optical center. The formalism represents a fully microscopic approach and is based on a BBGKY hierarchy for reduced density matrices and correlation operators of material particles and field modes. The method is free of phenomenological procedures when taking into account the effects of individual and collective behavior of the emitters associated with the presence of intermediate environment. The analytical expressions for the excitation lifetime of an optical center are shown to be in agreement with several experiments.

ROLE OF THE MULTIPHOTON IONIZATION IN GENERATION OF BROAD-BAND TERAHERTZ RADIATION FROM OPTICAL BREAKDOWN PLASMA

M. N. Esaulkov[1], A. V. Borodin[1], I.I. Kuricyn[1], I.A. Kotelnikov[2], A.P. Shkurinov[1]

[1]Moscow State University, Moscow, Russia, esaulkov_mich@mail.ru
[2]Budker Institute of Nuclear Physics, Novosibirsk, Russia

Generation of Terahertz pulses in laser-induced plasma still raises theoretical and practical interest since it offers the most broadband spectrum and high peak electric field (up to hundreds kV/cm). The most efficient THz generation occurs under two-color plasma excitation using both first and second harmonics of optical pulse.

One of the widely used model for generation of THz pulses based on the concept of microscopic photocurrent was proposed in 2007 by Kim [1]. In this work, we pay special attention on the role of two-color photoionization process in emission of low-frequency radiation through generation of photocurrent.

We apply a semi-classical Imaginary Time Method (ITM) approach to calculate the ionization probability and the electron momentum acquired in a two-color ionization process. We investigate the ω to 2ω phase and polarization dependences for the multiphoton ionization (MPI) regime.

It is found that the second harmonics field plays two different roles in formation of photocurrent. First, it modulates the probability of photionization according to the cosine law:

$$P_{mpi} \sim \exp[I/4\ \varepsilon^2\gamma^2(\cos(2\psi))]. \quad (1)$$

Second, it results in formation of a nonzero average momentum acquired by the electron during the optical pulse, including the initial momentum it receives while leaving the parent atom or molecule. The momentum also has the dependence on ω to 2ω phase ψ and angle between polarizations θ:

$$\alpha_x \sim \varepsilon\gamma^2 \sin(\psi)\cos(\theta)/2\ln(2\gamma). \quad (2)$$

This approach allows for the ability of accurate coherent polarization control and for modulation of ionization probability (thus the plasma density), through variation of ω to 2ω phase. Both of these effects are observed experimentally (See fig. 1 and 2).

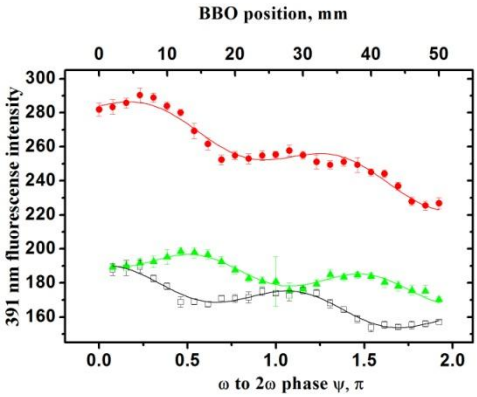

Fig. 1. Fluorescence intensity of the first negative band of N_2^+ (proportional to plasma density) at different points of plasma column vs phase shift between ω and 2ω

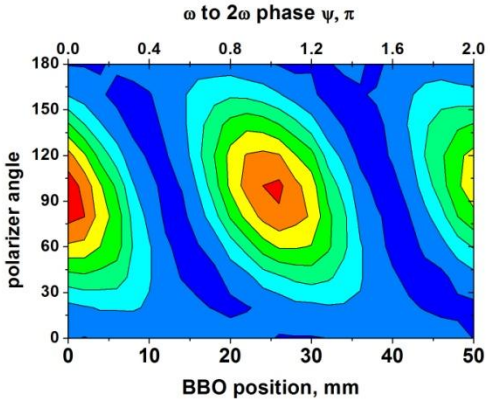

Fig. 2. Measured THz radiation intensity as a function of polarizer angle and ω to 2ω phase

We also claim the direct observation of the conical space profile of terahertz emission from laser-induced plasma. A 320x240 microbolometer detector array [2] is used to obtain the spatial profile of terahertz radiation intensity. The THz radiation after the generator was collimated and then focused with two off-axis parabolas. The radiation formed a ring structure when the detector plane was moved before and after its focus (see fig. 3).

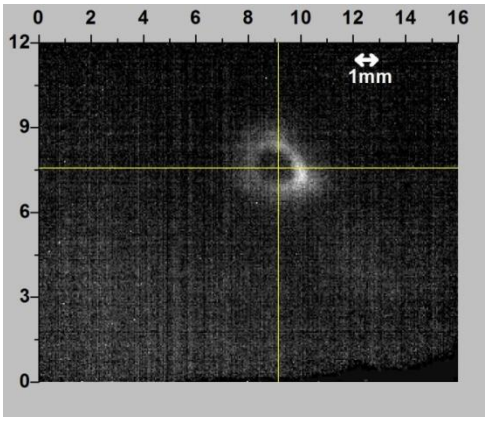

Fig. 3. Ring-shaped spatial profile of THz radiation observed with a microbolometer array

References

1. *Kim, K. Y., et al.* Terahertz emission from ultrafast ionizing air in symmetry-broken laser fields // Opt. Express. 2007. V. 15, No. 8. P. 4577–4584.

2. *Demyanenko, M. A., et al.* Microbolometer detector arrays for the infrared and terahertz ranges // *J. Opt. Technol.* 2009. V. 76, No. 12. P. 739–743.

STEADY-STATE FLUORESCENCE INTENSITY OF TWO IDENTICAL ATOMS WITH DIPOLE-DIPOLE INTERACTION

D.V. Kuznetsov,[1,3] M.G. Gladush,[2,3] Vl.K. Roerich[1]

[1]State research center of Russian Federation Troitsk Institute for Innovation and Fusion Research, Pushkovykh Str., vlad. 12,
Troitsk, Moscow region, 142190 Russia
[2]Institute for Spectroscopy of the Russian Academy of Sciences, Fizicheskaya Str. 5,
Troitsk, Moscow region, 142190 Russia
[3]Vladimir State University, Gorkogo Str. 87,
Vladimir, 600000 Russia

We consider the optical properties of a system consisting of two identical atoms in the laser field with dipole-dipole interaction. The aim of our research is to obtain the analytical description of the full fluorescence intensity as a function of the laser field frequency in the steady state. For this purpose it was used the Dicke basis of the collective states, in which two entangled atoms are presented as a four-level system. The evolution of this system is determined by the Bloch equation for the diatomic density matrix. We show that the problem can be reduced to a simpler two-level and three-level model if the laser field propagates at an angle close to 90 degrees to the line connecting two atoms. In this geometry, the fluorescence intensity on the laser field frequency will have two peaks. The central peak occurs due to the two-photon excitation process when the laser frequency close to the dipole transition frequency of the atoms. The other peak of the fluorescence intensity will be shifted relative to the central peak on the frequency depending on the dipole-dipole interaction energy which arises due to the transition from the symmetric state to the ground state. We obtained the analytical expression for the fluorescence intensity in the entire range of the laser field frequencies. It was shown, that the full intensity curve of the two atoms can be approximated by the sum of two Lorentzians. Each of them can be described by the two and three level model.

BCS – LIKE PHASE TRANSITION FOR STRONGLY LOCALIZED POLARITONS IN A LATTICE

E.S. Sedov, I.O. Barinov , A.P. Alodjants, and S.M. Arakelian

Department of Physics and Applied Mathematics, Vladimir State University named after Alexander and Nikolay Stoletovs, Gorky Street 87, 600000 Vladimir, Russia
alodjants@vlsu.ru

We propose a new type of spatially periodic structure, i.e. polaritonic crystal (PolC), to observe a 'slow'/'stopped' light phenomenon due to coupled atom–field states (polaritons) in a lattice. We have shown that the phase transition to the superfluid Bardeen–Cooper–Schrieffer (BCS) state occurs under the strong coupling condition. Such a transition results in the appearance of a macroscopic polarization of the atomic medium at non-zero frequency. The principal result is that the group velocity of polaritons depends essentially on the order parameter of the system, i.e. on the average photon number in the cavity array.

Nowadays, photonic band-gap micro- and nanostructures are known to be important tools for controlling light propagation properties in media, see e.g. [1]. The important features of such structures are connected with 'slow' light, which can be explored in the design of quantum optical storage devices [2]. The physical reason for reduction of the group velocity of light propagation in a medium is determined by the so-called dark and bright polaritons, bosonic quasi-particles representing a linear superposition of photon states in the external electromagnetic field and the macroscopic (coherent) excitations in the two-level oscillator system. The low branch polaritons can form Bose–Einstein condensation (BEC) due to the phase transition occurring in the cavity [3]. Modern nanofabrication and nanophotonic technologies make it possible to study 'slow' light and phase transitions of polaritons using the array of photonic cavities (or coupled resonator waveguides - CROWs) doped by two-level atoms, see e.g. [4].

In our work we have proposed a spatially periodical structure, the so-called *polaritonic crystal* (PolC), being a lattice of weakly coupled trapped atomic ensembles interacting with the optical field in the cavity [5] – see Fig. 1a. We consider an array of M single-mode microcavities with the nearest-neighbor interactions in the XY-plane. Each of the cavities contains an ensemble of ultracold two-level atoms interacting with quantized electromagnetic fields in the z-direction. One of ways to produce such a system experimentally is based on the confinement of atoms in a special photonic band-gap structure, i.e. photonic crystal or CROW. The overlapping of optical fields and atomic wave functions takes place in the XY-plane.

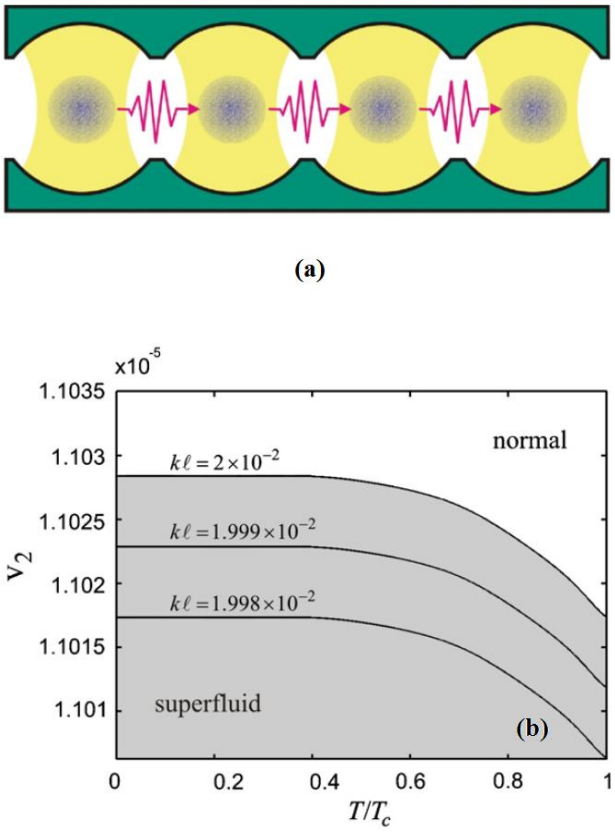

Fig. 1. (a) Model of the polaritonic crystal: an array of the microcavities with macroscopically small number of two-level atoms. (b) The reduced group velocity $v_2 \equiv v_2(k)$ for the lower branch polaritons as a function of the reduced temperature T/T_c (the detuning $\tilde{\delta}/2g = 5$); v_2 is represented in units of the light velocity in vacuum. The shaded region corresponds to the superfluid state for atom-like polaritons with various quasimomentum k.

First, we have got the group velocity for lower and upper branch polaritons:

$$v_{1,2}(k) = \frac{\hbar \sin(k\ell)}{2\ell m_{ph}}\left(1 + \frac{m_{ph}}{m_{at}} \pm \left(1 - \frac{m_{ph}}{m_{at}}\right)\frac{\delta}{\left(\delta^2 + 4g^2\right)^{1/2}}\right),$$

where m_{at} and m_{ph} are atomic and photonic masses, respectively, g is an atom-field coupling coefficient, δ is the phase mismatch depending on the quasi-momentum k, ℓ is a lattice constant. For $k\ell << 1$, the dependence for group velocities $v_{1,2}$ is approximately linear, i.e. $v_{1,2}(k) \approx \hbar k / m_{1,2}$, where $m_{1,2}$ are the masses of the upper and lower polariton branches,

respectively. Thus, the manipulation of group velocity for propagating light in the PolC structure can be realized by varying the polaritonic effective masses $m_{1,2}$ with the help of the atom–field detuning $\tilde{\Delta}$.

Second, we have considered the atomic polariton phase transition from the normal state to the superfluid (condensed) state. The parameter combination $2g\lambda_{\vec{k}}$ plays a role of the frequency gap, as the normalized photon number $\lambda_{\vec{k}}$ represents the order parameter. The normal state of polaritons is obtained for $\lambda_{\vec{k}} = 0$ and occurs for the temperature $T > T_c$ (T_c is the critical temperature of the phase transition). On the other hand, the case of $\lambda_{\vec{k}} \neq 0$ characterizes the superfluid state of polaritons for the temperature $T < T_c$. The critical temperature T_c has been obtained as

$$T_c \approx \frac{\hbar g \Omega_{at}^{(0)}}{2k_B \operatorname{atanh}(-2\rho_{\vec{k}})} \approx \frac{\hbar g(-2\rho_{\vec{k}})^{1/2}}{k_B \ln(2(1-2\rho_{\vec{k}})^{-1})}, \qquad (1)$$

where we have denote $\Omega_{at}^{(0)} = -\delta/2g + \left((\delta/2g)^2 - 2\rho_{\vec{k}}\right)^{1/2}$; $\rho_{\vec{k}}$ is the polariton excitation density. The last expression in equation (1) is true for $\delta = 0$ in the low-temperature limit, when the condition $k_B T << \hbar g$ is satisfied.

Third, we have examined the polariton group velocity behavior versus temperature when the equilibrium state of the system occurs. In Fig. 1b we present the phase boundaries for the group velocities of low branch polaritons versus reduced temperature T/T_c of the atomic system. Figure 1b demonstrates a significant reduction of the group velocity value for atom-like polaritons. There exist some temperature domain and order parameter value region where the polaritons (for the given quasi-momentum $\vec{k}$) fall in the superfluid state. The fact can be useful to determine the superfluid properties of polaritons in the medium.

References

1. Joannopoulos J.D. et al., *Photonic Crystals: Molding the Flow of Light* (Princeton, NJ: Princeton University Press, 2nd edn, 2008).
2. Milonni P.W. *Fast Light, Slow Light and Left-Handed Light* (Bristol: Institute of Physics Publishing, 2005).
3. Averchenko V.A. et al., Russ. J. Quantum Electron. **36** 532 (2006).
4. Aoki T. et al., Nature **443** 671 (2006).

5. Barinov I.O., Alodzhants A.P. and Arakelyan S.M., Russ. J. Quantum Electron. **39** 685 (2009);
6. Alodjants A.P., Barinov I.O., Arakelian S.M., J. Phys. B: At. Mol. Opt. Phys., 43, 095502 (2010)

LOW-FREQUENCY VIBRATIONAL SPECTRA OF ANDROGENS

***O. P. Cherkasova*[1], *M. M. Nazarov*[2], *E. V. Fedulova*[2], *A.P. Shkurinov*[2], *V.A. Volodin*[3,4]**

[1]*Institute of Laser Physics SB RAS, Novosibirsk, Russia, , +7(383)3309922; chrom@laser.nsc.ru*
[2]*Departament of Physics and International Laser Center, M.V.Lomonosov Moscow State University , Moscow*
[3]*Institute of Semiconductor Physics SB RAS, Novosibirsk, 4Novosibirsk State University, Novosibirsk, Russia*

Androgens have key roles in normal physiology and in male sexual differentiation as well as in pathological conditions such as prostate cancer. These hormones have similar general structure and differ only by the position of OH-group in steroid basis. This type of molecular structure has four rings providing conformational flexibility which is expected to have a number of low-frequency motions. The effects of androgens are mediated by the androgen receptor, which is a ligand-dependent transcription factor that belongs to the nuclear receptor superfamily. Upon hormone binding, steroid receptors change conformation and initiate gene transcription. We believe that low-frequency vibrations of corticosteroids are essential in hormone-receptor recognition since they provide librational-vibrational energy transfer and influence other intermolecular interactions. Therefore research of low-frequency vibrations can help with understanding of hormonal action, in a prediction of bioactivity of pharmaceutical products, in attempt of modulation of receptor activity by THz radiations. The aim of this work is THz time-domain spectroscopic study of dehydroepiandrosterone, androstenedione, testosterone, 5α-dihydrotestosterone in the frequency range 0,1 - 3,0 THz and comparison of the data with the Raman ones. The density functional theory (DFT) calculations are used for the qualitative interpretation of the experimental data [1].

We used androgens from Sigma (USA) without further purification. For THz-TDS measurements the cylindrical pellets of various thickness (200-500 μm) (m=2.5-5.0 mg, 5 mm diameter) were formed. The scheme of the terahertz pulsed spectrometer was described in detail in [2]. The Raman spectra were recorded in back-scattering geometry with the 514.5 nm Ar+ laser excitation with the use of Triple spectrometer Horiba Jobin Yvon T64000 in the micro-Raman geometry.

The greatest differences in structure of androgens are observed in the A- and B-rings and in hydroxyl- or keto-group at C^3 and C^{17}. The analysis of vibration spectra indicates that there are some interesting correlations between molecular structure and spectral properties. The THz absorption spectrum of testosterone has intensive absorption maxima at 1,42 and

2,41 THz. The DFT calculation testosterone is predicted three vibrational modes in this region. These modes include twisting of four-ring systems of steroid molecules. 5α-dihydrotestosterone is a biologically active metabolite of the testosterone and is 3 times more biologically active than testosterone. It has restored A-ring and conformation changes from 1α-sofa (testosterone) to chair-conformation. The THz absorption spectrum of 5α-dihydrotestosterone has intensive absorption maxima at 1,44 and 2,42 THz. 5α-dihydrotestosterone and testosterone can form intermolecular hydrogen bonds. Androstenedione has two keto-groups at C^3 and C^{17} and are not able to hydrogen bonding. The THz absorption spectrum of androstenedione has bands at 1,16, 1,44 and 2,42 THz. The conformation A- and B-rings of dehydroepiandrosterone differs from other androgens and it has only one intensive absorption maxima at 1,95THz. Substances under study have several intensive features in the low- frequency Raman spectra, which exceed the intensity of peaks in the region of stretching vibrations.

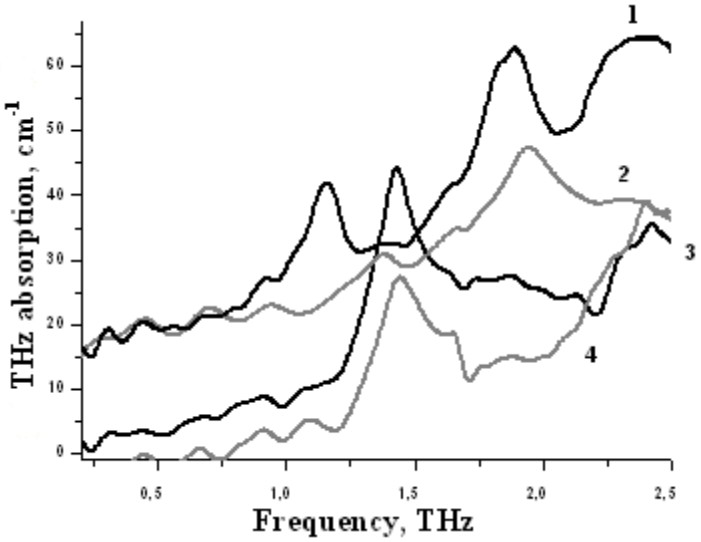

Fig. The THz absorption spectra of androstenedione (1), dehydroepiandrosterone (2), testosterone (3) and 5α-dihydrotestosterone (4). The spectra are shifted along the vertical axis.

Thus, androgens have several intensive low-frequency vibrations that are mainly assigned to the collective skeleton bending motions. The features are uniquely determined by a hormone structure and can be used for diagnostic of these substances in different samples.

The research was supported RFBR grant N 11-02-12248-OFI-M.

References

1. V. A. Minaeva, B. F. Minaev, S. S. Kapinus, “Study of IR spectrum of the testosterone and ethyniltestosterone by quantum-chemical density functional theory”, Biopolymers and Cell, **26**(1), 62-71 (2010).

2. M.M. Nazarov, A.P. Shkurinov, E.A.Kuleshov, and V.V.Tuchin, “Terahertz time-domain spectroscopy of biological tissues”, Quantum. Electron., **38** (7), 647-655 (2008).

LASER PROCESSING OF GOLD-BEARING MINERAL AND TECHNOGENIC MEDIUM

Kuzmenko A.P., Kuzmenko N.A.,Khrapov I.V.
South-West State University, Kursk, 304050

Leonenko N.A.
Mining Institute Mine Matter Far-East Branches RAS, Khabarovsk, 680020

Silutin I.V., Dobromyslov M.B.
Pacific National University, Khabarovsk, 680035

The present paper deals with the effect of laser radiation on mineral gold-bearing media. From the results of comparative structural, elemental, and mineralogical analysis of the initial compounds and the products of laser processing a qualitative physical model has been proposed which appropriately describes chemical and structural changes of those materials in laser processing. In laser agglomeration of noble metal particles of nanoscale sizes to the sizes of practical value has been shown to occur. Several tens of gold-bearing samples from various deposits were chosen for the study. These were the samples of raw materials with gold, depositions of integrated mining-and-concentration plants, as well as model compositions. At the next stage of the study all samples were laser processed, either pulsed processed with the setup SKAT 201 or continuously with the fiber laser LC, 06. As a result the formation of burnt dark spheres with diameters of 500 to 3000 μm was recorded. At those surfaces the formation of melted gold particles the size of 50 to 500 μm of a spherical and drop like shapes was observed, as attested by the typical scanning electron images given below. Attention is attracted by the changes in the surface structure of agglomerated gold particles. Figure 1 shown electron images of the products before – and after laser treatment with element distribution across the surface, which corroborates the dominant compositions precisely in gold on the agglomeration products with a drop like shape.

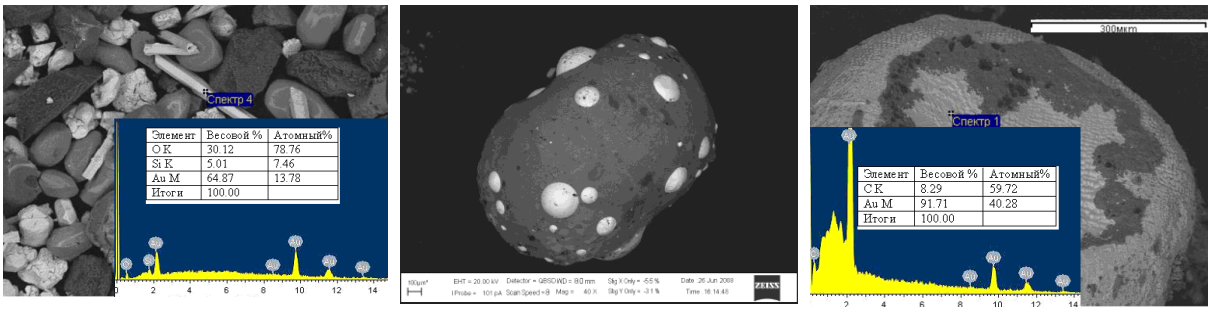

a b c

Fig. 1. Scanning images before- and after laser treatment – a,b; distribution of ele-

ments of the products of laser agglomeration – c

High intensity laser interaction on mineral and technological medium, including containing ultrafine gold, caused by melting, as a result of their high-speed defragmentation, as far followed by crystallization upon cooling, and laser agglomeration [1]. In the area of the melt, in one way or another, are convection, diffusion, capillary and thermocapillary mechanisms [2] that cause structural and phase transformations in the properties of the material. To simplify the analysis we assume that the laser acts as a highly efficient heater. Then the process of heating, melting and evaporation can be written a simple equation of heat balance:

$$I_0 A = V_{ml}\rho(L_{ev} + L_{ml} + C(T_{ml} - T_R)).$$

To estimate the characteristic parameters of the process, all values can be averaged, taking into account the contribution of equity. Here is ρ – density, C – heat capacity, L_{ml}, L_{ev} – heat of fusion and evaporation, T_{ml}, T_R – melting temperature of the environment, I_0 – the power density of incident radiation, A – the thermal environment. From the heat balance equation can be calculated velocity of propagation of melting – V_{ml} and time of processes - t. In the stationary regime of melting for a given thickness of material V_{ml}:

$$V_{ml} = I_0 A/\rho(L_{и} + L_{пл} + C(T_{пл} - T_0)) \sim 10^2 \text{ m/c}$$

For the reality value of this velocity is to several hundred m/s, which corresponds to the composition of the treated medium with strong dispersion. However, with increasing power density (several hundred watts) value V_{ml} can be increased substantially. Given the thickness of the bulk of the layer subjected to laser treatment, we can calculate the time of penetration:

$$t = a\pi((\rho l_{ml} C(T_{ml} - T_R)/(2I_0 L_{ml}))^2 \sim 10^{-8} \div 10^{-6} \text{ c}.$$

Are here a – also averaged thermal diffusivity and l_{ml} – the thickness of the layer of bulk material to be processed. The ratio of the Rayleigh number to the number of Marangoni, the so-called Bond number: $\rho g a h^4/\sigma$ [3] is much smaller than 1. This follows from the fact that the characteristic size of the agglomerates (up to hundreds of microns), the Bond number is determined mainly by the value σ, which for the precious metal is a record high (Pt - 1.82 and Au - 1.1 J/m^2). Are here g – acceleration due to gravity, h – characteristic size of the agglomerate (foil thickness or size such a spherical shape) gold-bearing environment. It is a condition where $\rho g \beta h^4/\sigma < 1$ corresponds, according to [3], the dominant role of the thermocapillary mechanism of laser agglomerating of ultrafine gold (and other noble metals).

As a result of variations in shape, structure, and granulometric compositions of mineral gold-bearing associations after laser processing it is possible to extract gold from these

with traditional methods, which attests to their practical value. On this basis a reasonably efficacious and environmentally friendly technique is proposed for the selection of noble metal micro- and nanosize particles, not extracted by traditional methods, with the use of laser processing which incorporates optical and thermal physical features of noble metals with a view to extracting further by application of traditional techniques [1,2].

References

1. Shevkun E.B., Kuzmenko A. P., Leonenko N.A., Yatlukova N.G., Kuzmenko N.A. Means for laser concentration of mineral associations with noble metals (in Russian). Patent of Russia. №2255995 04.12.03. Publishing 10.07.05. Bul. N19.

2. Kuz'menko A. P., Leonenko N. A., Kharchenko V. I., Kuz'menko N. A., Silyutin I. V., and Khrapov I. V. Thermocapillary Mechanism of Laser Stimulated Agglomeration of Ultradisperse and ColloidalIonic Gold. Technical Physics Letters. 2009. Vol. 35. No. 9. P. 837–840. © Pleiades Publishing, Ltd., 2009.

3. Zuev A.L., K.G. Kostarev K.G. Certain peculiarities of the solutocapillary convection. Uspekhi Fizicheskikh Nauk. 2008. Vol.178 (10). P. 1065 – 1085.

SUPERCONDUCTING SINGLE PHOTON DETECTOR INTEGRATED WITH OPTICAL CAVITY

S. Ryabchun, A. Smirnov, I. Pentin, Yu. Vakhtomin, K. Smirnov, N. Kaurova, B. Voronov, and G. Goltsman

Federal State-financed Educational Institution of Higher Professional Education "Moscow State Pedagogical University", Russia, Moscow
(499)-246-12-02, nadya@rplab.ru

We present advanced superconducting single photon detector (SSPD) designed especially for quantum cryptography, telecom lines. These applications demand fast single photon detectors with high sensitivity at telecom wavelength of 1.55 μm. Commercial available InGaAs APDs with sensibility up to 1.8 μm have count rate about 10MHz [1]. Although some researchers [2] report 2 GHz count rate. Since high level of dark count rate (10^3 s^{-1}) InGaAs APDs are normally gated with only ~ 1 megahertz frequencies with each active gate lasting for a few nanoseconds. This circumstance is inconvenient for many applications. Superconducting detectors became alternative to APD. Transition edge sensor (TES) reaches 90% quantum efficiency at 1.55 μm wavelength [3]. Unfortunately this devices are saturated by background radiation and have low count rate (up to 20kHz). Furthermore they need cooling bellow 100 mK and sophisticated temperature stabilization system. SSPD exhibits ~ 100 MHz count rate, single-photon sensibility up to 5.6 um [4], low dark counts rate (10^{-4} s^{-1}) and 30 ps jitter. Quantum efficiency of the best devices is 30% at 1.3 μm wavelength and 15% at 1.55 μm at 2K. Thanks to their high characteristics SSPDs are already used in solving many scientific problems [5-7], but further expansion of their applications requests increasing of quantum efficiency, especially at telecom wavelength.

SSPD is long (500 μm), narrow (100-120 nm) and thin (3-4 nm) NbN meander-shaped strip, formed on sapphire substrate. Meander covers area of 10 um x 10 um to optimize coupling with optical fiber. SSPD fabrication method is based on direct electron-beam lithography and reactive ion etching [8].Operation principle of SSPD is described by "hot-spot" model [].NbN strip is maintained at a temperature *T* well below the critical temperature *Tc* and biased along its length by the current *Ib* close to critical current *Ic*. According to "hot-spot" model, upon an absorption of a light quantum *hν* by a Cooper pair, the highly excited electron is created. This excited electron extremely rapidly loses its energy via electron-electron scattering and creates an avalanche of secondary excited quasiparticles. Effective electron temperature *Te* increases above the superconducting critical temperature *Tc*. As a result, a single photon can create a local collapse of superconductivity and form a normal state

hot-spot region. The hot-spot diameter is significantly smaller than the strip width. Although in a strip biased close to *Ic* the hot-spot appearance leads to the supercurrent redistribution, i.e. the current is expelled from the hot-spot in the "sidewalks" around it where the current density exceeds critical value and a resistive barrier appears in the entire cross-section of the strip. This resistive barrier gives rise to a voltage signal with the amplitude proportional to *Ib*. After its growth phase, the hotspot decreases due to relaxation and outdiffusion of quasiparticles and finally collapses. The superconductivity restores and the detector is ready to register another photon.

Since small thickness of NbN strip its absorption doesn't exceed 30% [9]. This fact limits quantum efficiency of SSPD. We integrated our SSPD in optical cavity to enhance NbN strip absorption. Our cavity is optimized to wavelength 1.55 μm. It consists of quarter-wavelength dielectric layer and metal mirror deposited above active area of SSPD. We used three types of dielectrics: Si_3N_4, SiO_2 and SiO. SiO_2 and SiO were deposited by electron-beam evaporation in Evatec BAK501; Si_3N_4 layers were formed by the gas-phase deposition technique. Dielectric thicknesses were selected to obtain maximum of NbN strip absorption for given refractive index. The thicknesses of Si3N4, SiO2, and SiO layers were 192, 268, and 221 nm, respectively. The metal mirror was 150–300 nm thick gold films deposited by electron-beam evaporation. In case of SiO and SiO_2 both cavity layers were formed by lift off electron lithography. Si_3N_4 was formed using direct electron lithography that simplified fabrication and enhanced yield. Schematic image of cross-section SSPD integrated with cavity is presented in Figure 1.

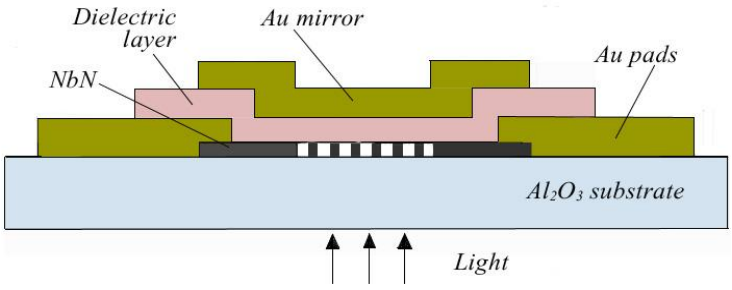

Figure 1. Schematic image of cross-section SSPD integrated with cavity

Quantum efficiency measurement leads to dirtying of SSPD surface and following degradation of cavity characteristics. Therefore we can't measure quantum efficiency before and after cavity fabrication and compare measurement results. Instead we measured spectral sensitivity of SSPD integrated with cavity and compared it with SSPD without the cavity. We researched spectral sensitivity in range 0.7 μm -1.8 μm using grating spectrometer. We used free space coupling spectrometer radiation with SSPD. Spectral sensitivity minimum of SSPD integrated with cavity [See Figure 2 a] can be explained by destructive interference in NbN

strip. We also plotted ratio of SSPD integrated with cavity spectral sensitivity (η_{sspd+c}) to spectral sensitivity of SSPD without cavity (η_{sspd}) [See Figure 2 b]. Using this curves we estimated Q values of the cavity as 2,4; 1,87; 1,7 for SiO, Si_3N_4, SiO_2 respectively. We can conclude that SiO is more perspective to cavity production as having maximum Q values.

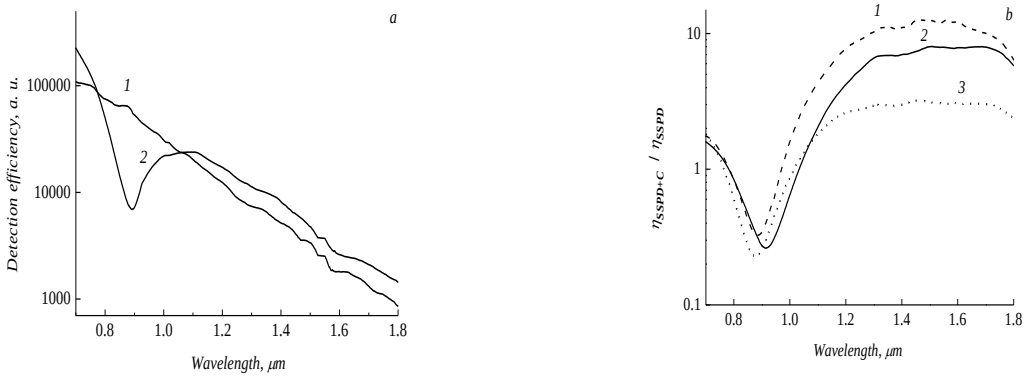

Figure 2. a - Spectrum sensitivity of SSPD (1) and of SSPD integrated with cavity (2); b - ratio of SSPD integrated with cavity spectral sensitivity to spectral sensitivity of SSPD without cavity (dielectric used for cavity fabrication: (1) – SiO, (2) – Si_3N_4, (3) – SiO_2)

Reference.

[1] *Bethnune D.S., Navarro M., Risk W.P.* // Appl. Opt. 2002. V. 41. P. 1640.

[2] *Z. L. Yuan, A. W. Sharpe, J. F. Dynes, A. R. Dixon, A. J. Shields //* Appl. Phys. Lett. 2010. V. 96. P. 071101.

[3] *Lita A., Miller A., Nam S.* // Optics express. 2008. V. 16 (5). P. 3032.

[4] *Tarkov M., et al //* in Proc. of 17th Int. Symp. on Space Terahertz Technol. 2006. P. 119-122.

[5] *M. Stevens, R. Hadfield, R. Schwall, S. W. Nam, R. Mirin, and J. Gupta //* Appl. Phys. Lett.. 2006. V. 89. P. 031109.

[6] *J. Chen, J. Altepeter, M. Medic, K. F. Lee, B. Gokden, R. Hadfield, S. W. Nam, and P. Kumar //* Phys. Rev. Lett.. 2008. V. 100 (13). P. 133603.

[7] *M. Halder, A. Beveratos, N. Gisin, V. Scarani, C. Simon, H. Zbinden //* Nature Physics. 2007. V. 3. P. 692.

[8] *Gol'tsman, G.N., Smirnov, K., Kouminov, P., Voronov, B., Kaurova, N., Drakinsky, V., Zhang, J., Verevkin, A., Sobolewski, R.* // IEEE Trans., on Appl. Supercond.. 2003. V. 13. P. 192.

[9] *M. Born and E. Wolf* // Principals of Optics: Electromagnetic Theory of Propagation, Interference,and Diffraction of Light. 1999. P. 752-758.

NOISE EQUIVALENT POWER AND DYNAMIC RANGE OF NBN HOT-ELECTRON BOLOMETERS

A. Maslennikova, P. Larionov, S. Ryabchun, A. Smirnov, I. Pentin, Yu. Vakhtomin, K. Smirnov, N. Kaurova, B. Voronov, and G. Goltsman

Moscow State Pedagogical University, 29 Malaya Pirogovskaya St., Moscow, Russia 119992
+7 (499) 246-1202, annamaslennikova@rplab.ru

We report on the noise equivalent power and dynamic range measurements of NbN hot-electron bolometers. The measurements performed at frequencies of (0.4-2.5) THz showed an optical NEP of the order of (1.2-4.5)×10^{-13} W/$Hz^{1/2}$ and a response time of 50 ps. The saturation power level of our devices was found to be about 2 μW (at 3-dB compression point). All our measurements were performed at the temperature of the superconducting transition with the use of a 0.4-0.55 THz Backward Wave Oscillator and a gas discharge laser operating on a 2.5-THz H_2O line.

Nowadays the submillimeter (sub-mm) and the terahertz (THz) frequency ranges (0.1 - 10 THz) attract great public attention. The secret of this popularity lies in a variety of useful applications (security systems, imaging, biological sphere, drugs and explosives detection, etc.) and human health safety. The THz range has got not only practical aspect, but also an astronomical one. It has been discovered [1, 2] that about half of all radiation coming down on Earth from space contains information in this part of the spectrum. Also, 98% of the photons emitted since the Big Bang fall into the sub-mm and far infrared. Older galaxies, like our Milky Way, thanks to cool interstellar dust clouds, radiating in this energy range (Fig. 1), can take us back to the early universe. [3]

Choice between the two types of detectors heterodyne and direct that can be used in the THz band depends on the application. But on the establishment of direct detection systems in spectroscopic and technical vision systems of ultraviolet, visible, IR and sub-mm regions of electromagnetic range as reliable detectors, they had begun to be successfully used in the THz region as well. This variant of detectors is so good because they are mostly frequency independent and there is no need for multielement arrays formation conditioned by local oscillator required for a heterodyne detector. [4]

There have been developed several types of such detectors (semiconductors, direct extrinsic photoconductors), [4] but only thermal radiation detectors such as bolometers and nanobolometers [6] have turned out to be successful in the THz spectral range. They can offer extra high sensitivity and an *optical* NEP~10^{-18}-10^{-19} W/$Hz^{1/2}$ under ultra low temperatures (down to 100 mK). [7,8]

Bolometer is a thermal sensor which converts incident power into an electrical signal. The main feature of any bolometer is a weak thermal link between the absorbing element and the thermal reservoir. [9] This can be achieved through varying the material of the detector thus changing the electron energy relaxation time (electron-phonon interaction time) τ_{th}. Due to strong electron-phonon interaction the leading position among different types of bolometers belongs to superconducting hot electron bolometers (HEBs).

We can characterize bolometer operation through the noise equivalent power (NEP) which in general is defined as the incident signal power required to obtain a signal-to-noise ratio of 1 Hz output bandwidth. [10]. Here we present the results of our measurement of the *optical* NEP, that is the *total* NEP for RF power incident on the cryostat window, and also the voltage responsivity 3-dB compression point determining the HEB dynamic range.

Our HEB mixers were patterned from 3.5-nm NbN films deposited onto high-resistivity Si substrates. The deposition of NbN layer was followed by the deposition of a 15-nm Au layer using the *in situ* technique. The dimensions of our bolometric elements typically were 0.1 μm long and 1 μm wide.

The voltage responsivity of an HEB as well as the output signal voltage versus the incident radiation power were measured at 0.4 THz, 0.55 THz, and 2.5 THz. The measures showed that the voltage responsivity is compressed by 3 dB, relative to its value at the lower end of the power scale, at about 2 μW. This value together with the minimum optical NEP of 1.2×10^{-13} W/Hz$^{1/2}$ determined the dynamic range DR of 25 dB. The maximum voltage responsivity S of an HEB was 104 V/W at 100nW-2.5-THz signal.

The research was funded by the Ministry of Science and Education, the Russian Federation (Contract Nos. 14.740.11.0269, 14.740.11.0343, 16.740.11.0378, 14.740.11.1074, 16.740.11.0580, 14.740.11.1249 and П1287). FTP "Scientific and scientific-pedagogical personnel of innovative Russia".

Bibliographic list:

1. A.W.Blain, I.Smail et *al*., Submillimetre galaxies, Phys. Rep. 369, 111-176, 2002.

2. D.Leisawitz et *al*., Scientific motivation and technology requirements for far- infrared/submillimeter space interferometry, Pros. SPIE, vol. 4013, 2000.

3. P.H.Siegel, Terahertz technology, IEEE Trans. on Microw. Theory and Tech., vol. 50, no. 3, 2002.

4. F.Sizov, THz radiation sensors, Opto-electron. Rev., 18, no. 1, 2010.

5. F.S. Goulding, Semiconductor detectors - an introduction, Lawrence Berkeley National Laboratory LBL-7282, 2011.

6. B.S.Karasik et *al*., Development of the nano-HEB array for low-background far-IR applications, the SPIE Symp. on Astr. Telesc. and Instr., San Diego, California, 2010.

7. B.S.Karasik, R.Cantor, Demonstration of high optical sensitivity in far-infrared hot-electron bolometer, App. Phis. Lett. 98, 193503, 2011.

8. K.S.Il'in. M.Lindgren et *al.*, Picosecond hot-electron energy relaxation in NbN super-conducting photodetectors, Appl. Phys. Lett. 76, 2752-2754, 2000.

9. A.Rogalski, Infrared Detectors, Gordon and breach, 2000.

10. P.L.Richards, Bolometers for far infrared and millimeter waves, J. Appl. Phys., 76(1), 1994.

ENHANCEMENT OF RAMAN SIGNAL FROM GRAPHENE FLAKES BY SURFACE PLASMONS IN METALIZED AFM TIP

A. Shchekin, P. Dorozhkin, A. Shelaev, E. Kuznetsov, V. Bykov,

NT-MDT Co., Build. 100, Zelenograd Moscow, 124482 Russia, schokin@ntmdt.com

We demonstrate capabilities of Atomic Force Microscopy (AFM) integrated with Confocal Raman/Fluorescence/Rayleigh microscopy when applied to graphene experimental study attached to Si/SiO2 substrate. Graphene is a single atomic layer of carbon taken from c-face of graphite bulk crystal. First obtained in 2004 [1], graphene has already proven to be unique promising object in different research and application areas.

Previously we reported about combined AFM/Confocal Raman studies of graphene flakes on gold substrate [2]. Here we extend AFM/Raman integration demonstrating near-field graphene Raman signal enhancement by the metalized AFM probe. This technique well-known as Tip-Enhanced Raman Spectroscopy (TERS) first reported in 2000 [3] could be described in terms of light resonant interaction with surface plasmons localized in metal layer covering AFM probe. The interaction causes several orders enhancement of Raman signal and reduction of lateral Raman map resolution down to AFM level well beyond optical diffraction limit [3,4].

Plasmon nature of TERS results in unique behavior of enhancement factor versus different physical parameters of experimental setup: it strongly depends on excitation geometry, wavelength and polarization, tip-to-sample distance and sample dimensionality. Previous TERS experiments were done mainly in inverted geometry [4] when the laser beam was focused from the bottom of the transparent sample and AFM probe was approached from the top.

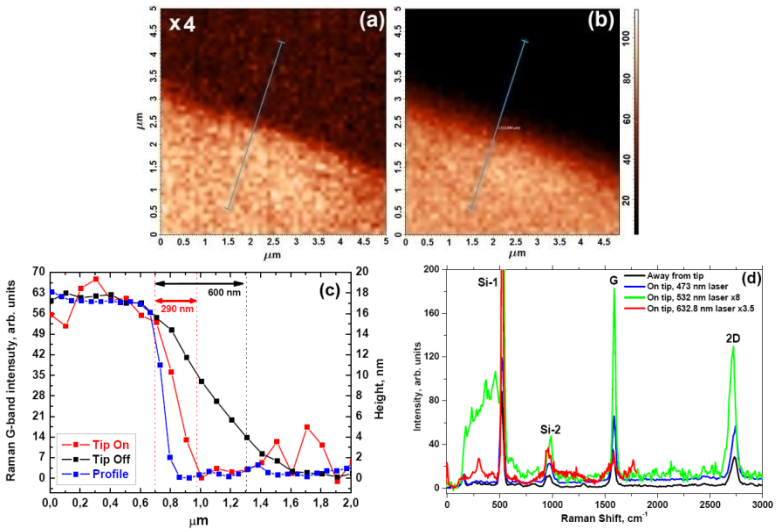

Fig 1. a), b). Graphene G-band intensity maps, obtained in TERS and conventional confocal microscopy mode correspondingly c) AFM profile and G-band intensity map cross sections obtained in TERS and conventional confocal microscopy modes. d) Graphene Raman spectra measured with different excitation lasers with and without metalized AFM probe.

Here we present first results of Tip Enhanced Raman Spectroscopy (TERS) or "nano-Raman" mapping realized in Upright excitation configuration (reflected light configuration suitable for opaque samples) when the probe and the laser beam interact with the sample from the top. Fig 1a,b display graphene G-band intensity maps obtained in TERS and conventional confocal modes and Fig 1c shows the cross sections of these maps together with AFM profile taken from the same sample place. One can see the resolution in TERS mode exceeds diffraction limited confocal resolution more than two times and approaches AFM resolution. Fig 1d shows enhancement factor dependence on excitation wavelength. Actual plasmonic and near field nature of the Raman enhancement was proven by a number of ways: dependence of the enhancement on the excitation wavelength and polarization, enhancement versus tip-sample distance curves, observation of selective enhancement of Raman signal from thin surface layers of the sample etc. Finally, the ultimate performance of TERS was demonstrated by measuring Raman 2D maps with subwavelength lateral resolution – determined not by the wavelength of light, but by the localization area of the surface plasmon electromagnetic field.

[1] K.S. Novoselov and et al., Science, 306, 666, 2004

[2] P. Dorozhkin, E. Kuznetsov, A. Schokin, S. Timofeev, V. Bykov, Microscopy-Today, 18, 06, 2010

[3] R. M. Stöckle, Y. D. Suh, V. Deckert, R. Zenobi, Chem. Phys. Lett., 318, 131, 2000

[4] S.S. Kharintsev, G.G. Hoffmann, P.S. Dorozhkin et al., Nanotechnology, 18, 15502, 2007

RESEARCH OF THE SEMICONDUCTOR LAYERED SYSTEMS OF PHOTONICS

Abramov D.V., Khorkov K.C., Kutrovskaya S.V., Noman M.A.A., Prokoshev V.G.

Vladimir State University, Vladimir, Russia
e-mail: awraam@mail.ru

Semiconductor layered micro- and nanosystems are often used in photonics devices now. One group of such lasers devices is lasers on heterotransitions. Researches of structure of laser diode layers and their geometrical characteristics are necessary for definition of the reasons of disorder of parameters of semiconductor lasers and development of technologies of their manufacture. Modern methods and means of scanning probe microscopy and scanning electron microscopy give such possibilities.

Results of analysis of structure and characteristics of layers of the laser diodes ruler LLD-20 are presented in that report. Experimental researches has been carried out by means system of atom force microscopy and Raman spectroscopy “Nanolaboratory Integra-Spectra” and scanning electron microscope Quanta 200 3D (SEM).

On the basis of SEM images the location of working area of the laser diode is defined and the analysis of its layers is carried out. Experimental results show the possibility of allocation of separate structural layers of the semiconductor laser made of materials which are different only molar concentration Al and alloying degree. For studying laser diode the difference of concentration Al in the next layers of heterostructure made 20 % and concentration of an alloying impurity didn't exceed 1019 sm-3 and differed in the next layers on one order.

Further more precision researches of heterostructure are carried out by a method of Raman spectroscopy (Fig. 1). The buffer layer is identified on the basis of characteristic TO peak of Raman scattering GaAs with frequency of 268 sm-1. Registration of peaks of Raman scattering AlxGa1-xAs shows transition to area p-emitter. There are characteristic AlAs peak on frequency of 360 sm-1 and the peak caused GaAs phonons was displaced on frequency of 263 sm-1. Displacement is caused by occurrence in structure of the semiconductor of aluminum and is depended on it molar concentration x. Transition from the p-emitter to the first dueling layer is registered on occurrence in a spectrum of scattering of a wide strip in the field of frequency of 1000 sm-1 **(Fig. 2).** Occurrence of such peaks and strips is caused by nanometer width of dueling and active layers of the semiconductor laser. Return transition from the second dueling layer to the n-emitter is registered on disappearance of that specified strip of Raman scattering. The all area AlxGa1-xAs is registered till the moment when peak of AlAs phonons disappears and the peak of GaAs comes back to frequency of 268 sm-1. The given

fact shows transition from heterostructure of the semiconductor laser to a buffer layer and further to a substrate.

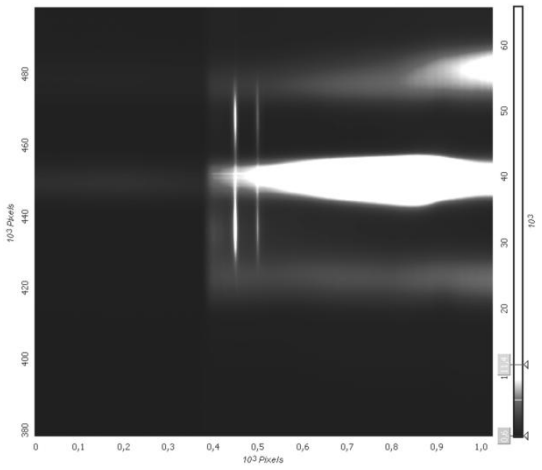

Fig. 1. Map of Raman spectra of studied structure.

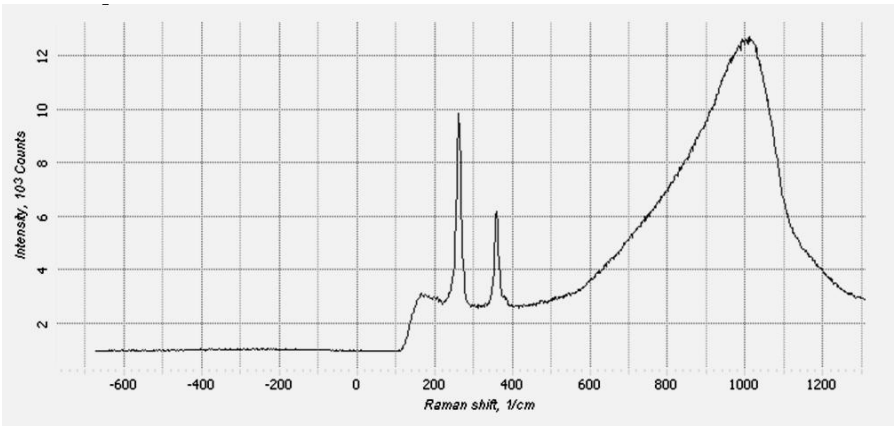

Fig. 2. Raman spectra in area of dueling and active layers of the semiconductor laser.

Results of the experimental researches have shown possibilities of diagnostics of layered systems of photonics by means of a complex of systems of microscopy of the high permission. Systems of the scanning electronic microscopy, scanning probe microscopy and Raman spectroscopy have certain problems and scopes and successfully supplement each other.

COHERENT DARK RESONANCES: HIGH RESOLUTION SPECTROSCOPY AND APPLICATIONS

Victor N. Zadkov

International Laser Center and Department of Physics
M.V.Lomonosov Moscow State University, Moscow 119899, Russia

Spectroscopic investigations of atoms and molecules, including spontaneous emission from excited atoms, being a natural focus of early quantum mechanics, became an especially active area in 70s, after developing of narrow-band tunable lasers. Today, it is again at the forefront of quantum optics research, following the recent advances in the construction of atomic traps and direct observation of emission and absorption of individual quanta from isolated atoms.

It is long known that multilevel atoms interacting with electromagnetic field can display a much broader range of effects than their two-level counterparts as a result of the coherences among the states induced by the radiation and quantum interference. Interference produced by the presence of coherences have been known since the development of quantum mechanics, and their creation has been largely exploited in spectroscopy and quantum optics. However, a macroscopic effect such as the total suppression of fluorescence emission by coherent population trapping is quite unusual.

The talk will be focused on this phenomenon and its applications. Coherent population trapping is most conspicuous in a three-level system with two closely spaced long-lived levels optically coupled to a third distant short-lived level by two laser fields (Λ- or V-system), which being tuned into resonance lead to trapping of the population in a coherent superposition of the closely spaced levels. In Raman absorption spectra it is revealed as an ultranarrow dip in an absorptive profile, whereas in resonance fluorescence spectra it appears as a dark line yielding the name "nonabsorbing (dark) resonance". For a vapor cell of Cs atoms, for example, width of the resonance line in absorptive profile of less than 50Hz can be achieved experimentally.

Several applications of the CPT phenomenon crucial in the modern Physics will be discussed in the talk, as well. In magnetometry, for example, current experimental setups based on the high-precision spectroscopy of the dark resonances allow detect changes in the magnetic flux density of less than 10pT within a measurement time of 1 second, that is about 0.25×10^{-6} of the Earth's magnetic field. The use of coherent dark resonance for the frequency standards could allow the construction of particularly compact frequency standards and atomic clocks. Finally, the velocity-selective coherent population trapping (VSCPT) allows cool down a cloud of atoms in an atomic trap to a temperature much lower than both the Doppler and recoil limits. For example, for helium atoms with Doppler limit of 23 μK and the recoil limit of about 4 μK a record temperature or some 180 nK (that is 22 times below the recoil limit!) was recently reached experimentally.

ALL-OPTICAL CONTROL OF NONCLASSICAL COUPLED ATOM-LIGHT STATES IN A DOPED RESONANCE MEDIUM

M. Yu. Gubin, A.V. Prokhorov, A.Yu. Leksin, S.M. Arakelian

Vladimir State University named after Alexander and Nikolay Stoletovs, Vladimir, Russia
(4922) 479947, avprokhorov@vpti.vladimir.ru

In this work, we investigate multilevel schemes of atom–optical interaction in doped optical mediums for observation of nonclassical coupled atom–field states and realization of quantum computing.

For the first time, we consider the effects of nonlinear interaction for two–mode probe light pulse in an optical matrix doped with optically resonant atoms. In particular, we investigate the mechanism of formation of huge nonlinear cross–interaction for probe pulses by changing the dispersive properties of atomic medium during the M–scheme of atom–field interaction [1]. We focus our attention on the case of formation of squeezed atom–optical states in such a system when the optical losses in the system can be dynamically suppressed.

Second, we considered a new method for coding and processing quantum information based on the control of propagating single–photon light pulses in an doped optical matrix. We have studied M–scheme of interaction with single–photon pulses for efficient manipulation with entangled photon states. These principles can be implemented for development of systems of distributed quantum information processing.

1. G. A. Burmakin, M. Yu. Gubin, A. V. Prokhorov, S. M. Arakelyan, Optics and spectroscopy, 109, # 1, 19 (2010).

CONTENTS

Program **5**

Abstracts **17**

Yb DOPED LuAG LASER CERAMICS

Benxue Jiang ,Shuping Liu， Min Chen , Jiang Li, Wenbin Liu， Yubai Pan **19**

VECTORIAL SELF-DIFFRACTION EFFECT

Gu Bing, Ye Fan, Lou Kai, Chen Jin, Li Yong-Nan, and Wang Hui-Tian **22**

OPTICAL CONFIGURATIONS FOR HIGH AVERAGE POWER FREE ELECTRON LASERS WITH THEORETICAL AND NUMERICAL SIMULATION

Yang Jing, Wang Zhimin, Cui Da Fu, Peng Qinjun, Xu Zuyan, Deng Haixiao, Dai Zhimin, Zhao Zhentang **24**

OPTICAL TOMOGRAPHIC DEMONSTRATION WITH PRE-AMPLIFICATION OF WEAK IMAGES USING A GATED OPTICAL PARAMETRIC AMPLIFIER

Yang Jing, Zhang Jingyuan, Du Shifeng, Cao Dong,Cui Dafu, Peng Qingjun, and Xu Zuyan **27**

DIRECT ADDITIVE MANUFACTURING OF INDIVIDUAL AND CUSTOMIZED METAL PARTS BY SELECTIVE LASER MELTING

Yongqiang Yang, Fuhai Li **30**

ANALYSIS ON POLARIZATION CHARACTERISTIC OF CHERENKOV RADIATION BY OPTICAL RECTIFICATION IN $LINBO_3$

Pengxiang Liu **31**

SYNTHESIS OF CARBON NANOFIBERS AND NANOCLUSTERS BY LASER RADIATION OF A CARBON TARGETS PLACED IN THE EXTERNAL FIELDS

A.A. Antipov, S.M. Arakelyan, S.V. Kutrovskaya, A.O. Kuchrik, A.V. Osipov, V.G. Prokoshev, and A.A. Schekin **34**

THEORETICAL INVESTIGATION ON THE ATMOSPHERIC PROPAGATION OF THZ RADIATION

Ran Wang, Jianquan Yao, Haixia Cui, and Kai Zhong **39**

QUANTITATIVE IMAGING OF TERAHERTZ PHONON POLARITON AND ITS APPLICATIONS

Qiang Wu, Chengliang Yang, Bin Zhang, Jingjun Xu, Christopher A. Werley, and Keith A. Nelson **41**

NANO- AND MICROSCALE STRUCTURES SYNTESIS BY CONTROLLED LASER ACTION

S.M. Arakelian, S.V. Kutrovskaya, A.O. Kucherik, V.G. Prokoshev **45**

ALL-FIBER OPTICAL MODULATOR FOR CONTROL THE OPTICAL PHASE OF LASER RADIATION

Koliada N.A., Nyushkov B.N. **55**

FROM NANO- TO TERA-: APPLICATIONS OF THE TERAHERTZ RADIATION FOR STUDIES OF ARTIFRITIAL MATERIAL NANOSIZE STRUCTURES

Alexander Shkurinov, Maxim Nazarov **58**

CONJUGATED POLYMER COLLOID-BASED SOFT SEMICONDUCTORS TOWARD NEXT-GENERATION ORGANIC OPTOELECTRONIC MATERIALS

Ling-Hai Xie, Wei Huang **59**

POLARIZATION DEPENDENCE OF NONLINEAR OPTICS IN ISOTROPIC MEDIUM

Xiao-Qing Yan, Zhi-Bo Liu, Jian-Guo Tian **60**

AN EFFICIENT DUAL-WAVELENGTH ND,GD:YSGG LASER

Kai Zhong, Jianquan Yao , Chongling Sun, Degang Xu, Qingli Zhang, Dunlu Sun, Shaotang Yin **63**

PULSED NANOSECOND LASER WITH INJECTION OF A SINGLE-FREQUENCY RADIATION

Dmitriy Bordzilovskiy, Alexandr Mayorov, Evgeniy Lonshakov, Sergey Struz, Vladimir Tarasov **66**

UPCONVERSION GREEN LIGHT EMITTING MACROPOROUS LN:ER RANDOM LASER

Fan Shi, Xinzheng Zhang, Qiang Wu, Xuanyi Yu, Yongfa Kong, and Jingjun Xu, Romano A. Rupp **69**

EXPERIMENTAL STUDY ON GENERATION OF COHERENT, TUNABLE THZ RADIATION FROM SURFACE-EMITTED PARAMETRIC OSCILLATOR BY $LINBO_3$-TPG/TPO

Jianquan Yao, Zhongyang Li , Degang Xu, Bo Sun, Kai Zhong **73**

EXPLORING THE BRIGHT FUTURE FORWARDS ORGANIC LASER DIODES

Wen-Yong Lai, Wei Huang **76**

INVESTIGATION OF TITANIUM THIN FILMS PRODUCED BY FEMTOSECOND LASER ABLATION

M.N. Gerke, K.S. Khorkov, V.G. Prokoshev, S.M. Arakelian **78**

NEW OPPORTUNITIES OF LASER-INDUCED METAL DEPOSITION

Yu.S.Tver'yanovich **81**

ELECTRIC FIELD EFFECTS ON QUANTUM WELL TO QUANTUM DOT TUNNELING

Abramov A.A., Agafonov A.G. **83**

LASER TREATMENT OF PLASMA COATINGS

Mitrofanov A.A., Caschin Ye. A, Balashova S.A. **86**

SAFE SPECTRAL RANGE RAMAN LASER FOR ENVIRONMENTAL MONITORING AND LASER LOCATION

Gavrilov A.V., Ershkov M.N., Smetanin S.N., Solokhin S.A., Fedin A.V. **89**

SYNTHESIS OF METAL-CARBON NANOSTRUCTURED MATERIALS BY CONTOLED LASER DEPOSITION

Arakelyan S.M., Antipov A.A., Kutrovskaya S.V., Kucherik A.O., Nogtev D.S., Osipov A.V., Prokoshev V.G. **90**

METHOD OF THE CONTROL BY PHASE-LOCKING OF MULTICHANNEL LASER SYSTEM

A.V. Fedin, A.V. Gavrilov, M.N. Ershkov, S.N. Smetanin, S.A. Solokhin **92**

SYNTHESIS OF MULTYLAERS NANOSTRUCTURED FILMS BY METHOD OF LASER DEPOSITION NANOPARTICLES FROM COLLOIDAL SOLUTIONS

Antipov A.A., Arakelian S.M., Kutrovskaya S.V., Kucherik A.O., Nogtev D.S., Prokoshev V.G. **93**

MATHEMATICAL MODELING OF THERMAL AND OPTICAL PARAMETERS OF THE ZONE OF LASER ACTION FOR DETERMINATION OF FEEDBACK PARAMETERS OF THE SYSTEM OF ADAPTIVE PRECISION LASER PROCESSING OF MATERIALS

Shilov I.V., Fedin A.V., Gavrilov A.V. **94**

HETEROSTRUCTURES BASED ON ZINC OXIDE AND THEIR APPLICATION IN DEVICES

Lotin A.A., Novodvorsky O.A., Zuev D.A. **95**

4D VISUALIZATION OF SPECTRAL DATA WITH ACCOUNT OF HUMAN EYE OPTICAL SENSITIVITY SPECIFICS.

Zemskov I., Skurihin A. **97**

GENERATION OF ENTANGLED POLARITONS IN DOPED WAVEGUIDES

I.O. Barinov, A.V. Prokhorov, A.P. Alodjants, S.M. Arakelian **99**

PASSIVE MODE LOCKING ON BASE OF SINGLE-WALL CARBON NANOTUBES FOR Yb:LYSO LASER

A.A. Burtsev, D.N. Antonov, M.N. Gerke, O.Ya. Butkovsky, D.V. Khudyakov, A. S. Lobach **103**

LASER-ASSISTED AU-CU AND AU-AG NANOPARTICLES DEPOSITION FROM LIQUID METALLOORGANIC COMPLEXES

Povolotskaya A.V., Povolotskiy A.V., Manshina A.A. **106**

SYNTHESIS OF MULTI-WALLED CARBON NANOTUBES OVER MgO-SUPPORTED CATALYSTS

Romantsova I.V., Melezhyk A.V., Tkachev A.G. **108**

EFFICIENCY OF RECORD OF THE QUANTUM INFORMATION IN THREE LEVELS

Nefediev L.A., Rusanova I.A. **112**

PHOTOELECTRICAL PROPERTIES OF GRANULAR METAL FILMS

Gladskikh I.A., Vashchenko E.V. **116**

SILVER HALIDE CRYSTALS FOR OPTICAL FIBERS USED IN INFRARED LASER SYSTEMS

Zaramenskikh K.S., Golovanov V.F., Lisitskiy I.S., Polyakova G.V., Kouznetsov M.S. **119**

NEW NONLINEAR OPTICAL CRYSTALS BASED ON THALLIUM, LEAD AND MERCURY HALIDES

Zaramenskikh K.S., Lisitskiy I.S., Golovanov V.F., Polyakova G.V., Kouznetsov M. S. **122**

APPLICATION OF LASER IN SOLAR CELLS TECHNOLOGIES

Zuev D.A., Lotin A.A., Novodvorsky O.A. **124**

TRAVELLING PLASMONIC MOD IN 1D SPASERS ARRAY

Andrianov E.S., Pukhov A.A., Dorofeenko A.V., Vinogradov A.P. **126**

PRINCIPALS OF LASER HOLE DRILLING VIA ADAPTIVE CONTROL BY THE REPETITIVELY PULSED LASER RADIATION CHARACTERISTICS

S.A. Solokhin, S.N. Smetanin, A.V. Gavrilov, M.N. Ershkov, A.V. Fedin **127**

LOCAL FIELDS AND RENORMALIZATION OF CHARACTERISTIC INTERACTION PARAMETERS FOR LIGHT EMITTERS IN A DIELECTRIC MEDIUM

Gladush M.G., Kuznetsov D.V. **128**

ROLE OF THE MULTIPHOTON IONIZATION IN GENERATION OF BROADBAND TERAHERTZ RADIATION FROM OPTICAL BREAKDOWN PLASMA

M. N. Esaulkov, A. V. Borodin, I.I. Kuricyn, I.A. Kotelnikov, A.P. Shkurinov **129**

STEADY-STATE FLUORESCENCE INTENSITY OF TWO IDENTICAL ATOMS WITH DIPOLE-DIPOLE INTERACTION

D.V. Kuznetsov, M.G. Gladush, Vl.K. Roerich **132**

BCS – LIKE PHASE TRANSITION FOR STRONGLY LOCALIZED POLARITONS IN A LATTICE

E.S. Sedov, I.O. Barinov , A.P. Alodjants, and S.M. Arakelian **133**

LOW-FREQUENCY VIBRATIONAL SPECTRA OF ANDROGENS

O.P. Cherkasova, M.M. Nazarov, E.V. Fedulova, A.P. Shkurinov, V.A. Volodin **137**

LASER PROCESSING OF GOLD-BEARING MINERAL AND TECHNOGENIC MEDIUM

Kuzmenko A.P., Kuzmenko N.A., Khrapov I.V., Leonenko N.A, Silutin I.V., Dobromyslov M.B. **140**

SUPERCONDUCTING SINGLE PHOTON DETECTOR INTEGRATED WITH OPTICAL CAVITY

S. Ryabchun, A. Smirnov, I. Pentin, Yu. Vakhtomin, K. Smirnov, N. Kaurova, B. Voronov, and G. Goltsman **143**

NOISE EQUIVALENT POWER AND DYNAMIC RANGE OF NBN HOT-ELECTRON BOLOMETERS

A. Maslennikova, P. Larionov, S. Ryabchun, A. Smirnov, I. Pentin, Yu. Vakhtomin, K. Smirnov, N. Kaurova, B. Voronov, and G. Goltsman **146**

ENHANCEMENT OF RAMAN SIGNAL FROM GRAPHENE FLAKES BY SURFACE PLASMONS IN METALIZED AFM TIP

A. Shchekin, P. Dorozhkin, A. Shelaev, E. Kuznetsov, V. Bykov **149**

RESEARCH OF THE SEMICONDUCTOR LAYERED SYSTEMS OF PHOTONICS

Abramov D.V., Khorkov K.C., Kutrovskaya S.V., Noman M.A.A., Prokoshev V.G. **151**

COHERENT DARK RESONANCES: HIGH RESOLUTION SPECTROSCOPY AND APPLICATIONS

Victor N. Zadkov **.....153**

ALL-OPTICAL CONTROL OF NONCLASSICAL COUPLED ATOM-LIGHT STATES IN A DOPED RESONANCE MEDIUM

M. Yu. Gubin, A.V. Prokhorov, A.Yu. Leksin, S.M. Arakelian **..... 154**

FOR NOTES

Научное издание

Современные лазерная физика и лазерные информационные технологии для науки и производства

(Modern laser physics and laser-information technologies for science and manufacture)

Программа и тезисы докладов

Первой международной Российско-Китайской конференции / молодёжной школы-семинара

23–28 сентября 2011 г.

Суздаль / Владимир

Печатается в авторской редакции

Подписано в печать 20.09.2011.

Формат 60×84/8. Усл. печ. л. 18,83. Тираж 100 экз.

Заказ 13 – 2011 г.

Издательство

Владимирского государственного университета.

600000, Владимир, ул.Горького,87.

Тел.: (4922) 53-50-98

Факс: (4922) 53-50-98

E-mail: laser@vlsu.ru